UNIVERSITÀ
DEGLI STUDI
DI PADOVA

Università degli Studi di Padova

Dipartimento di Matematica

SCUOLA DI DOTTORATO
DI RICERCA IN SCIENZE MATEMATICHE

INDIRIZZO MATEMATICA

CICLO XXVIII

Controllability and optimization of deformable bodies in fluids: from biology to robotics

Direttore della Scuola: Prof. Pierpaolo Soravia

Coordinatore d'indirizzo: Prof. Franco Cardin

Supervisore: Prof. Franco Cardin

Dottorando: Marta Zoppello

Ringraziamenti

Desidero esprimere la mia più profonda gratitudine al mio relatore Franco Cardin che fin dalla tesi triennale ha seguito e incoraggiato il mio percorso, mi ha sempre sostenuto e aiutato dandomi preziosi consigli sia dal punto di vista dello studio che in ambito accademico. I suoi insegnamenti sono stati fondamentali, grazie a lui ho imparato a non arrendermi di fronte alle difficoltà e ad amare la fisica matematica.

Un grande ringraziamento va al prof. Antonio DeSimone della Scuola Internazionale di Studi Superiori Avanzati (SISSA) che è stato co-relatore, accanto al prof. Franco Cardin, per questa tesi, sebbene non emerga tecnicamente per motivazioni formali di Ateneo. Ho cominciato a lavorare con lui con la tesi magistrale grazie alla quale mi sono avvicinata allo studio dell'auto-propulsione di microrganismi nei fluidi. La nostra collaborazione è continuata nello sviluppo della mia tesi di dottorato e spero continui anche negli anni a venire. Grazie al suo approccio pragmatico e le sue idee innovative siamo riusciti insieme ad ottenere risultati interessanti ed originali.

Insieme a lui devo ringraziare anche il prof. François Alouges dell'École Polytechnique di Parigi con cui ho lavorato durante questi tre anni. Mi ha invitato più volte a Parigi per ultimare i risultati delle nostre collaborazioni e mi ha dato preziosi consigli su come affrontare alcuni scogli matematici. Tramite lui ho conosciuto Laetitia Giraldi, Junior Researcher dell'INRIA presso l'università di Sophia Antipolis. A lei va un sentito ed amichevole ringraziamento per aver lavorato e condiviso con me sia alcuni successi professionali, sia preziosi insegnamenti ma anche per essere non solo una collega ma un'amica.

Voglio anche ringraziare Pierre Martinon ricercatore dell'INRIA presso l'École Polytechnique di Parigi, senza il suo aiuto e le sue conoscenze e il software di ottimizzazione, Bocop, che il suo team ha sviluppato, non sarebbe stato

possibile ottenere numerosi dei risultati numerici presentati nella tesi.

Preziosi sono stati anche il confronto su diversi aspetti dell'applicazione della teoria del controllo al mio lavoro con il professor Franco Rampazzo e anche l chiarimenti fornitimi su specifici argomenti dall'esimio professor Giuseppe De Marco.
Importanti sono stati gli incoraggiamenti ricevuti da tutti i membri del gruppo di fisica matematica dell'università di Padova e l'interesse dimostrato per il mio lavoro dal professor Francesco Fassò.

Devo altresì ringraziare la mia famiglia che dal punto di vista affettivo mi è stata di impareggiabile sostegno.
Infine ma non meno importanti un sentito grazie ai colleghi dottorandi Daniele, Daria, Davide, Federico, Francesco, Gabriele, Laura, Lucio, Luigi, Luisa, Matteo, Valentina e Veronica, che hanno sopportato le mie paturnie durante questi anni e condiviso con me gioie e dolori.

Riassunto

Questa tesi di dottorato prende culturalmente le origini abbastanza lontane nel tempo. La mia tesi 3-nnale in Matematica consistette in un lavoro di ricomposizione teorica e numerica di una congettura di Alberto Bressan, atta al superamento del paradosso dello "Scallop Theorem". Purcell nel 1977 formalizzò questo famoso paradosso secondo cui un nuotatore 1-dim (scallop), che si muove aprendo e chiudendo alternativamente le sue valve, non ha uno spostamento netto in un fluido viscoso (nel modello Stokes), data la reversibilità nel tempo delle equazioni del moto.

Nella tesi di laurea magistrale, condotta in collaborazione anche con il prof. Antonio De Simone della Sissa, si entrò in dettaglio nello studio del sistema nuotatore-fluido, coinvolgendo la teoria geometrica del controllo meccanico di nuotatori modellizzati finito-dimensionalmente.
La tesi è divisa in tre parti, una è stata sviluppata e portata avanti in collaborazione con il prof. Antonio De Simone della Sissa, il prof François Alouges dell'École Polytechnique di Parigi e altri due ricercatori francesi, Laetitia Giraldi e Pierre Martinon. Con loro abbiamo analizzato e definito una struttura cinematica generale per trattare il problema dell'auto-propulsione in un fluido a bassi numeri di Reynolds. Abbiamo formulato il problema in termini di un potenziale di gauge A, che ci fornisce il moto rigido netto risultante da un arbitrario cambiamento di forma. Per studiare a fondo le implicazioni che la controllabilità del nuotatore può avere sulla realizzazione di dispositivi bio-ispirati, abbiamo costruito un modello nuovo per micro nuotatori filiformi, che è più maneggevole.

Abbiamo presentato un modello discreto di un nuotatore filiforme che nuota propagando bending waves lungo il suo corpo e in cui le interazioni idrodinamiche sono trattate usando l'approssimazione locale della Resistive Force Theory (RFT). Il modello è facile da assemblare e risolvere e sorprendentemente accurato. Inoltre abbiamo provato che per il numero di link N maggiore di 3 e per quasi ogni lunghezza dei link, usati per approssimare il corpo del nuotatore, questo è controllabile in tutto il piano. I risultati ot-

tenuti in questa parte sono stati pubblicati durante il dottorato nelle seguenti pubblicazioni:

- P.Martinon, L. Giraldi and M. Zoppello.
  "Controllability and Optimal Strokes for N-link Micro-swimmer"
  Conference on Decision and Control 2013.

- F.Alouges, A. DeSimone, L. Giraldi, and M. Zoppello
  "Self-propulsion of slender micro-swimmers by curvature control: N-link swimmers".
  International Journal of Non-Linear Mechanics, 2013.

Successivamente ci siamo focalizzati sul trovare una strategia di nuoto che facesse muovere l'N-link swimmer tra due configurazioni fissate nel minimo tempo e sul trovare anche il design migliore (rapporto tra le lunghezze dei link) per massimizzare lo spostamento. Le simulazioni numeriche sono consistenti con le nostre predizioni teoriche per piccole deformazioni. Maggiori dettagli si trovano nell'ariticolo:

- P.Martinon, L. Giraldi and M. Zoppello.
  "Optimal design of the three-link Purcell swimmer"
  Physical Review E (2014)

Nella seconda parte della tesi si studia la natura geometrica del problema del nuoto di un corpo continuo deformabile immerso in un fluido bidimensionale ideale incomprimibile e irrotazionale. Si affronta un problema nuovo ed originale: lo studio delle proprietà di controllabilità di un sistema dinamico che parte con impulso iniziale non nullo. Reinterpretando le forze idrodinamiche esercitate dal fluido sul corpo come termini cinetici e descrivendo i cambiamenti di forma con un numero finito di parametri, si ottengono le equazioni del moto. Usando poi tecniche classiche in teoria del controllo si è in grado di ottenere risultati interessanti sulla controllabilità di questo tipo di sistemi.

In più dettaglio: (i) se il nuotatore parte con impulso iniziale nullo, ritroviamo risultati presenti in letteratura, più precisamente siamo sempre in grado di trovare una velocità di deformazione appropriata che fa spostare il nuotatore tra due configurazioni fissate; (ii) se invece il corpo parte con impulso iniziale diverso da zero, il nuotatore può auto-propellersi in quasi ogni direzione se è in grado di deformarsi con velocità sufficientemente elevata. Il fatto che teniamo conto della presenza di un impulso iniziale non nullo e l'analisi della controllabilità del sistema sembra innovativo e rende lo

studio del nuoto in fluidi ideali più accurato e completo. I risultati prodotti in questa parte, sviluppati nel secondo anno di dottorato, sono stati inseriti nel lavoro

- M. Zoppello, F. Cardin.
  "Swim like motion of bodies immersed in a fluid" Submitted (2014).

Infine nella terza parte, affrontata durante l'ultimo anno di dottorato, abbiamo svolto uno studio di fattibilità per la realizzazione ingegneristica di nuotatori microscopici artificiali, formati da una testa, usata come contenitore, e da una sottile coda flessibile costituita da materiale permanentemente magnetico, messi in moto da un campo magnetico esterno oscillante. I nostri risultati, illustrati nell'articolo:

- F. Alouges, A. DeSimone, L. Giraldi, M. Zoppello
  "Can magnetic multilayers propel artificial micro-swimmers mimicking sperm cells?" SoftRobotics (2015).

indicano che, per un sistema caratterizzato da parametri geometrici consistenti con quelli ottenibili dalle moderne tecniche di costruzione e da valori realistici dei parametri magneto-elastici (ad esempio quelli del Permalloy), possono essere ottenute interessanti performance di nuoto usando campi magnetici facilmente producibili in laboratorio. La nostra analisi mostra che i nuotatori magneto elastici da noi descritti si muovono con un meccanismo molto diverso da quelli precedentemente riportati nella letteratura sui filamenti magneto elastici. Infatti la deformazione del nuotatore consiste di una rotazione globale e di una deformazione fluente con curvatura spaziale costante, entrambe oscillanti nel tempo alla stessa frequenza del campo magnetico esterno, ma con una traslazione di fase.

Contents

Ringraziamenti **i**

Riassunto **iii**

Introduction **5**

1 Geometrical setting of deformable bodies immersed in a fluid **13**
1.1 Preliminaries 13
1.1.1 Lie Groups 13
1.1.2 Fiber Bundles and Connections 16
1.2 Geometry 20
1.2.1 Gauge potential 22
1.3 Tools in geometric control theory 25
1.4 Reynolds number 28

2 Ideal fluids **31**
2.1 Structure of equations of motion 31
2.1.1 Geometry of control equations 31
2.2 Model 36
2.2.1 System of coordinates 36
2.2.2 Shape changes 37
2.2.3 Rigid motions 42
2.2.4 Dynamics for ideal fluid 43
2.2.5 The Gauge potential and the equations of motion . . . 49
2.3 Swimmer controllability 57
2.3.1 Case $\mathbf{p}^*(0) = 0$ 57
2.3.2 Case $\mathbf{p}_0^* \neq 0$ 61

3 Viscous fluids **67**
3.1 Planar bodies 68
3.1.1 Determining the gauge potential 68

3.1.2 The two dimensional techniques 70
3.1.3 Infinitesimal deformations 73

4 Flagellar microrganisms 77
4.1 Mathematical setting of the problem 77
4.1.1 Kinematics of the N-link swimmer 78
4.1.2 Equations of motion 79
4.1.3 Geometric aspects 83
4.2 Applications 84
4.2.1 Purcell's 3−link swimmer 84
4.2.2 Displacement for square strokes of small amplitude . . 85
4.2.3 Displacement for square strokes of large amplitude . . 87
4.2.4 $N-$link swimmers 89
4.2.5 N-link approximation of Taylor's swimming sheet . . . 90
4.2.6 N-link approximation of sperm cell swimmer 93
4.3 Controllability 97
4.3.1 Regularity 98
4.3.2 Controllability of the Purcell Swimmer (N=3) 98
4.3.3 Controllability of the N-link swimmer 100
4.4 Minimum time optimal control problem for the N-Link swimmer 101
4.4.1 Optimal Time Control Problem Statement 101
4.4.2 Optimization Strategy 102
4.5 Numerical simulations for the Purcell swimmer ($N = 3$) 103
4.5.1 The classical Purcell stroke 104
4.5.2 Comparison of the optimal stroke with the classical Purcell stroke 105
4.5.3 Optimization of other movements: y-displacement and rotation 109
4.6 Optimal design of the three link Purcell swimmer 110
4.6.1 Optimal strokes 111
4.6.2 Optimal swimmer design 112
4.6.3 Numerical simulations 115

5 Magneto-elastic flagellar microswimmer 121
5.1 Formulation of the problem 123
5.1.1 Elasticity 124
5.1.2 Hydrodynamics 124
5.1.3 Magnetism 125
5.1.4 Governing equations 126
5.2 A case study 127
5.2.1 Straight swimming 127

5.2.2 Swimming in circles 130
5.2.3 Turning abruptly 132
5.2.4 The swimming mechanism: propagation of bending waves along the tail is not necessary for propulsion . . 133

Conclusions and Perspectives **136**

Appendix A **139**

Appendix B **146**

Appendix C **151**

Bibliography **154**

Introduction

What does it mean *swimming*? How does mathematics can treat this problem? These questions have been addressed for the first time in the fiftie's by G.I. Taylor [81], he claims that swimming is the ability to advance in a fluid in the absence of external propulsive forces by performing cyclic shape changes. While large objects which propel themselves in air or water use inertia in the surrounding fluid, the same idea cannot be transferred to problems of propulsion in microscopic bodies for which the stresses due to viscosity may be many thousands of times as great as those due to inertia. Later Purcell in 1977 in [70] formalized the famous *Scallop theorem* according to which a swimmer that moves like a scallop, opening and closing reciprocally its valves, cannot achieve any net motion in a viscous fluid, because of the time reversibility of the equations. Moreover Purcell presented a model of a swimmer composed by three rigid links, that is able to overcome this paradox.

In this thesis we are interested in studying several aspects of the propulsion of a deformable continuous body, finitely controlled, in a fluid. After the first pioneering papers quoted before, [81, 70], this kind of systems is attracting again an increasing interest in recent literature. Many authors focus on two different type of fluids. Some of them consider bodies immersed in an ideal incompressible fluid [18, 43, 52, 55, 56, 62, 65] that propel themselves thanks to vortex shedding (see the literature of S.D. Kelly and the papers quoted therein, e.g. [50, 78]) or to internal forces since in this case the hydrodynamic equations turn out to be linear. Other are interested in swimming at micro scale in a Stokes fluid [7, 8, 48, 67, 77], because in this regime the inertial terms can be neglected and the hydrodynamic equations are again linear.
Here the aim is to build a robust and exhaustive mathematical model, which is essential to realize artificial devices mimicking the behavior of real organisms. The design of artificial devices to be used in different contexts, from medicine to various kind of flight and navigation, asks for a careful mechan-

ical recognition of the model we are studying. This is obviously provided by a long-lasting tradition which goes back to the beginning of the Calculus of Variations and reaches the modern development of Analytical Mechanics, arriving to a suitable Lagrangian/Hamiltonian formalism (see [79]). On the other hand, the aim of producing sophisticated technologies where human intervention can play a crucial role, leads naturally to connect this classical mathematical area with Control Theory, a discipline born in the Fifties' of the previous century and today become essential background of both theoretical mathematicians and engineers dealing with highly technical issues. The geometrical formalization of control theory has brought into the field many mathematical concepts and structures, from differential geometry and related areas. The combined use of these tools has led to new results on several important control-theoretical questions, such as: controllability, osservability, robustness, tracking and optimal control. The control of general mechanical systems can be addressed in at least two ways. The first, standard way, consists in regarding "generalized forces" as controls, within either a Lagrangian or a Hamiltonian formalism. In the second one, started at the end of the previous century [19, 20, 21, 61], the controller acts on the system by directly assigning the values of some of the coordinates, the latter so regarded as control parameters. The evolution of the remaining coordinates (together with their conjugate momenta) can be determined by solving a control system. The use of the coordinates as controls lead us to obtain a fibration of the configuration space and to use the tools of differential geometry. We will use the "hard device" approach in the first chapters of this work, while in the end we give some hints on how it is possible to use the control on external forces in order to plan the motion of the system.

We now describe the physical environment in which we are interested. Let us consider the Navier-Stokes equations

$$\begin{gathered} \rho\big(\frac{\partial v}{\partial t} + (v \cdot \nabla)v\big) = -\nabla p + \eta \Delta v \\ \text{div } v = 0 \end{gathered} \tag{1}$$

a dimensionless number arises naturally writing them in a dimensionless form. This is done by rescaling position and velocity with $x^* = \frac{x}{L}$ and $v^* = \frac{v}{V}$, where L and V are characteristic length scale and velocity associated with the flow. Reynolds number (Re) is defined by

$$Re = \frac{VL\rho}{\eta} = \frac{VL}{\nu} \tag{2}$$

where $\nu = \frac{\eta}{\rho}$ is the kinematic viscosity of the fluid. The Reynolds number quantifies the relative importance of inertial versus viscous effects.

$\boxed{Re \to \infty}$

In the first part of this work, we focus on the special case in which the body is immersed in a fluid whose Reynolds number tends to infinity ($Re \to \infty$). Therefore since the inertial effects dominate on the viscous ones we can consider the body as immersed in an ideal, incompressible and irrotational fluid. This special case has an interesting geometric nature and there is an attractive mathematical framework for it. We exploit this intrinsic geometric structure of the problem inspired by [76, 77] and [64], in which they interpret the system in terms of gauge field on the space of shapes. The choice of taking into account the inertia can apparently lead to a more complex system, but neglecting the viscosity the hydrodynamic equations are still linear, and this fact makes the system more manageable. The same fluid regime and existence of solutions of these hydrodynamic equations has been studied in [43] regarding the motion of rigid bodies.
There are different ways of describing the deformation of the swimmer, some authors, such as V.V. Kozlov and his coworkers, [55, 56] analyze the case in which the motion of the body occurs due to the internal displacement of masses, instead we start from an early idea of Alberto Bressan [18] and some unpublished developments, according to which the shape changes can be described by a finite number of parameters. These kind of systems, where the controls are precisely given by further degrees of freedom of the systems, as we have said before, have been first studied deeply by Aldo Bressan, see e.g. [19, 20, 21]. In this framework we highlight that the composed system "fluid-swimmer" is Lagrangian geodesic. Next, coupling this fact with some techniques developed in [65], we are able to show that the kinetic energy of the system (i.e. the Lagrangian) is *bundle-like*, a concept by Bruce Reinhart [72] and introduced in control theory by Franco Rampazzo in [71]. This leads us to express the equations of motion as linear control equations, where any quadratic term is vanishing, radically simplifying our final analysis on the system. The geometric construction of the control dynamic equations follows substantially the line of thought of [23, 61].
At a first glance, the deformations of the swimmer are naturally given by diffeomorphisms, that are infinite dimensional objects. By considering a planar setting and making use of complex analysis, as suggested in [25, 65] the Riemann Mapping Theorem plays a crucial role in describing the shape changes of the swimmer. It turns out that the diffeomorphisms can be parametrized by appropriate complex converging series. In the literature other authors

exploit the same way of describing the shape changes by conformal maps, for example in [65], in which they take into account only a finite number of terms to represent the diffeomorphisms. We follow substantially an analogous approach to merge this idea with the setting of Alberto Bressan. The choice of using a finite number of parameters means that the kind of deformations that we consider is more restricted but still enough to describe a wide range of swimmers.
In order to have a more manageable system that the one in [65], we establish a connection between the use of complex and real shape parameters. We show that, if we consider small shape changes, a well precise choice of the real and imaginary part of the shape parameters leads to obtain exactly the same deformation proposed in [64], which use a rather different parametrization governed by suitable small deformation. Therefore we gained a description of our system with a finite number of parameters/coordinates, which is essential to control the shape coordinates, to steer the swimmer between two different configurations. In this environment we recover the well known *Scallop Theorem* [6] in the case we have only one real shape parameter. Thanks to the idea of using a finite number of parameters we can reduce our dynamic equations to a control system. The controllability issue has been recently linked to the problem of swimming [3, 51, 48] since it helps in solving effectively motion planning or optimal control problems.

Differently from what was done in other works, we focus our attention on a crucial problem: the presence of an initial impulse. The case of zero initial linear momentum is well studied in literature concerning systems of different nature: both in the multi-particle or many-bodies field, [44, 46, 45], and shape changing bodies, [62, 64, 65, 24], as the equation of motion are a driftless affine control system whose controllability can be studied using classical techniques. Instead, the case of a non vanishing initial impulse leads us to a more complex system since the equations of motion involve also a non zero drift term and their controllability is more tricky to study. Therefore we have two contributions to the motion of the system: the first one that is purely geometrical and determined by the structure of the problem, and the second one, strictly linked to the presence of a non vanishing initial impulse (see formula (2.80) chapter 2).
The controllability of this kind of systems is studied in detail, and among other facts it is worth noting that we need at least three real shape parameters to make the system controllable. We have three state parameters, three conjugate variables and at least three controls. Despite the evident complexity of the computations linked to this number of variables, we managed to obtain interesting results about its controllability.

$\boxed{Re \to 0}$

In the second part (see chapters 3,4) of this work we deal with the problem of swimming in an another type of fluid, also in this case reformulated in terms of a gauge field on the space of shapes. We focus of the case in which $Re \to 0$ and the rate of change of data driving the flow is slow, therefore the Navier-Stokes equations can be approximated by the Stokes ones

$$\begin{aligned} -\eta\Delta v + \nabla p &= 0 \\ \text{div } v &= 0 \end{aligned} \tag{3}$$

which are commonly used to study the hydrodynamics at low Reynolds number that has a rather special and unique character. Contrary to what happens in the ideal case studied before, the effects of the inertia are negligible, which is the case of bacteria or unicellular microorganisms. In the absence of inertia, the motion of a swimmer through a fluid is completely determined by the geometry of the sequence of shapes that the swimmer assumes. It is independent of any variation in the rates at which different parts of the sequence are run through. We show that the problem of self-propulsion at low Reynolds number naturally resolves itself into the computation of a Gauge potential that describes the net translation and rotation resulting from an arbitrary infinitesimal deformation of a shape. We compute explicitly the Gauge potential in the case of strokes involving infinitesimal deformations of a circle.

Since the problem is complex, due to the hydrodynamics equations, we discuss a reduced model to compute the motion of slender swimmers which propel themselves by propagating a bending wave along their body. Our approach is based on the use of Resistive Force Theory for the evaluation of the viscous forces and torques exerted by the surrounding fluid, and on discretizing the kinematics of the swimmer by representing its body through an articulated chain of N rigid links capable of planar deformations, as was done in [47] to describe snake locomotion. The resulting system of ODEs governing the motion of the swimmer is easy to assemble and to solve, making our reduced model a valuable tool in the design and optimization of bio-inspired engineered micro-devices. We test the accuracy and robustness of our approach on three benchmark examples: Purcell's 3-link swimmer [70], Taylor's swimming sheet [81] and some recent quantitative observations of circular motion of a sperm cell [33]. An explicit formula for the displacement of Purcell's 3-link swimmer generated by a stroke of small amplitude is also discussed.

Similarly to what was done before, low Reynolds number swimming can be considered as a control problem which is linear in the control, and without

drift [7]. We prove that the N-link swimmer is controllable in the whole plane for $N \geq 3$ and for almost every set of sticks length. As a direct result, there exists an optimal swimming strategy to reach a desired configuration in minimum time. Numerical experiments for $N = 3$ (Purcell swimmer) suggest that the optimal strategy is periodic, namely a sequence of identical strokes. Our results indicate that this candidate for an optimal stroke indeed gives a better displacement speed than the classical Purcell stroke.

Moreover regarding still the Purcell swimmer, we address the optimal design issue, namely finding the optimal length ratio between the two lateral equal links and the central one, which maximizes displacement of the swimmer [37]. A similar issue has been studied in [80] where a Fourier expansion is used to derive an optimal design. Here, techniques from the control theory are used to approximate the leading order term of the swimmer's displacement. The maximization of this leading term gives a theoretical value for the optimal link ratio.

Engineering applications

After presenting and analyzing in detail the idea of controlling the shape of our swimmer in either the ideal or Stokes regime, we deal with the problem of realizing effectively an artificial device. In the last part of the thesis we would like to provide a feasibility study for the engineering of microscopic artificial swimmers consisting of a cargo head and of a flexible thin film tail made of a permanent magnetic material, and propelled by an external oscillating magnetic field (see Figure 1)

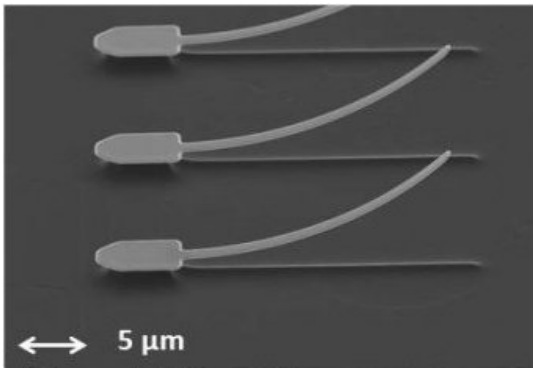

Figure 1: An example of a group of artificial micro swimmer with a cargo head and a flexible tail

We formulate and solve the equations governing the dynamics of swimmer [4]. This is a variant of the model swimmer proposed by Dreyfus et al.

in 2005 [31], whose tail is a filament obtained from the assembly of superparamagnetic beads. The swimmer is actuated by an oscillating magnetic field, and its geometry is inspired by that of sperm cells. Using values for the geometric and material parameters which are realistic for a magnetic multi-layer, we show that the model swimmer can reach swimming speeds exceeding one body-length per second, under reasonable values of the driving magnetic field. This provides a proof of principle for the viability of this kind of microswimmers. In addition, we discuss the possibility to steer the system along curved paths. Finally, we compare the propulsion mechanism (swimming "gait") of our swimmer with that of sperm cells. The main difference between the two is that, contrary to its biological template, our artificial system does not rely on the propagation of bending waves along the tail, at least for the range of material and geometric parameters explored in this work. Finally we put in evidence the fact that a microswimmer which is composed of two links and actuated by an oscillating magnetic field, displays a net motion, showing a way of overcoming the Scallop theorem.

The great part of the results presented in this thesis are new, more precisely the ones presented in Chapters 4 and 5 have been taken from papers published during my PhD by A. DeSimone, F. Alouges, L. Giraldi, P. Martinon and me, [3, 4, 36, 37], and the material in Chapter 2 has been already submitted by F. Cardin and me. The results presented in chapter 3 are taken from a paper of Shapere and Wilczek [77] and are needed to bridge the cases of different Reynolds numbers.

Chapter 1

Geometrical setting of deformable bodies immersed in a fluid

In this chapter we present the geometrical setting that we use to describe the dynamical system of a planar deformable bodies immersed in a fluid. At this stage we do not specify the kind of fluid in which it is immersed that can be either ideal and incompressible or a viscous one with low Reynolds number. Our aim is to show that the motion of this deformable body through the fluid is completely determined by the geometry of the sequence of shapes that the idealized swimmer assumes, and to determine it.
First of all let us provide some preliminaries that are fundamental to describe the geometry of the kind of systems that we analyze.

1.1 Preliminaries

This section covers some auxiliary mathematical topics, in particular from Lie groups, fiber bundles and connections that we shall need later. This summary will be helpful to set the notation, fill in some gaps, and to provide a guide to the literature for needed background.

1.1.1 Lie Groups

Let us start from some geometric and algebraic notions on Lie groups, that arise in discussing conservation laws for mechanical and control systems and in the analysis of systems with some underlying symmetry.

Definition 1.1. *A Lie group is a smooth manifold G that is a group with identity element $e = gg^{-1} = g^{-1}g$, and for which the group operations of multiplication, $(g, h) \mapsto gh$ for $g, h \in G$, and inversion, $g \mapsto g^{-1}$, are smooth.*

Before giving a brief description of some of the theory of Lie groups we mention an important example: the group of linear isomorphisms of $\mathbb{R}^n$ to itself. This is a Lie group of dimension n^2 called the general linear group and denoted by $GL(n, \mathbb{R})$. The conditions for a Lie group are easily checked. This is a manifold, since it is an open subset of the linear space of all linear maps of $\mathbb{R}^n$ to itself; the group operations are smooth, since they are algebraic operations on the matrix entries.

Definition 1.2. *A matrix Lie group is a set of invertible $n \times n$ matrices that is closed under matrix multiplication and that is a submanifold of $\mathbb{R}^{n \times n}$.*

Lie groups are frequently studied in conjunction with Lie algebras, which are associated with the tangent spaces of Lie groups as we now describe.

Definition 1.3. *For any pair of $n \times n$ matrices A, B we define the matrix Lie bracket $[A, B] = AB - BA$.*

Proposition 1.1. *The matrix Lie bracket operation has the following two properties:*

(i) For any $n \times n$ matrices A and B, $[B, A] = -[A, B]$ (this is the property of skew-symmetry).

(ii) For any $n \times n$ matrices A, B, and C,
$[[A, B], C] + [[B, C], A] + [[C, A], B] = 0$. (This is known as the Jacobi identity.)

As is known, properties (i) and (ii) above are often thought as the definition of more general Lie brackets (than $AB - BA$) on vector spaces called Lie algebras.

Definition 1.4. *A (matrix) Lie algebra $\mathfrak{g}$ is a set of $n \times n$ matrices that is a vector space with respect to the usual operations of matrix addition and multiplication by real numbers (scalars) and that is closed under the matrix Lie bracket operation $[\,\cdot\,, \cdot\,]$.*

Proposition 1.2. *For any matrix Lie group G, the tangent space at the identity $T_I G$ is a Lie algebra.*
As usual, for matrix Lie groups one denotes $e = \mathbb{I}$

We now describe an example that plays an important role in mechanics and control.

The planar Euclidean Group

Consider the Lie group of all 3×3 matrices of the form

$$\begin{pmatrix} R & d \\ 0 & 1 \end{pmatrix} \tag{1.1}$$

where $R \in SO(2)$ and $d \in \mathbb{R}^2$. This group is usually denoted by $SE(2)$ and is called the special Euclidean group. The corresponding Lie algebra, $se(2)$, is three-dimensional and is spanned by

$$\mathcal{A}_1 = \begin{pmatrix} 0 & -1 & 0 \\ 1 & 0 & 0 \\ 0 & 0 & 0 \end{pmatrix} \qquad \mathcal{A}_2 = \begin{pmatrix} 0 & 0 & 1 \\ 0 & 0 & 0 \\ 0 & 0 & 0 \end{pmatrix} \qquad \mathcal{A}_3 = \begin{pmatrix} 0 & 0 & 0 \\ 0 & 0 & 1 \\ 0 & 0 & 0 \end{pmatrix} \tag{1.2}$$

The special Euclidean group is of central interest in mechanics since it describes the set of rigid motions and coordinate transformations on the plane. Let G be a matrix Lie group and let $\mathfrak{g} = T_I G$ be the corresponding Lie algebra. The dimensions of the differentiable manifold G and the vector space $\mathfrak{g}$ are of course the same, and there must be a one-to-one local correspondence between a neighborhood of 0 in $\mathfrak{g}$ and a neighborhood of the identity element I in G. An explicit local correspondence is provided by the exponential mapping $exp : \mathfrak{g} \mapsto G$, which we now describe. For any $A \in \mathbb{R}^{n \times n}$ (the space of $n \times n$ matrices). $exp(A)$ is defined by

$$exp(A) := I + A + \frac{1}{2!}A^2 + \frac{1}{3!}A^3 + \dots \tag{1.3}$$

This map for $SE(2)$ can be defined by the exponential of the elements of the Lie algebra $se(2)$. More precisely

$$exp(\theta \mathcal{A}_1) = \begin{pmatrix} \cos\theta & -\sin\theta & 0 \\ \sin\theta & \cos\theta & 0 \\ 0 & 0 & 1 \end{pmatrix} \tag{1.4}$$

$$\exp(x\mathcal{A}_2) = \begin{pmatrix} 1 & 0 & x \\ 0 & 1 & 0 \\ 0 & 0 & 1 \end{pmatrix} \quad \exp(y\mathcal{A}_2) = \begin{pmatrix} 1 & 0 & 0 \\ 0 & 1 & y \\ 0 & 0 & 1 \end{pmatrix} \tag{1.5}$$

Since $[\mathcal{A}_i, \mathcal{A}_j] = 0$ for all $i, j = 1, 2, 3$, we have that $\forall(\theta, x, y) \in \mathbb{R}^3 \equiv \mathfrak{g} = se(2)$:

$$\exp(\theta\mathcal{A}_1 + x\mathcal{A}_2 + y\mathcal{A}_3) = \exp(\theta\mathcal{A}_1)\exp(x\mathcal{A}_2)\exp(y\mathcal{A}_3)$$

that is clearly elements of $SE(2)$.

We now define the action of a Lie group G on a manifold Q. Roughly speaking, a group action is a group of transformations of Q indexed by elements of the group G and whose composition in Q is compatible with group multiplication in G.

Definition 1.5. *Let Q be a manifold and let G be a Lie group. A left action of a Lie group G on Q is a smooth mapping $\Phi : G \mapsto Q$ such that*

(i) $\Phi(e, q) = q$ *for all* $q \in Q$,

(ii) $\Phi(g, \Phi(h, q)) = \Phi(gh, q)$ *for all* $g, h \in G$ *and* $q \in Q$,

(iii) $\Phi(g, \cdot)$ *is a diffeomorphism for each* $g \in G$.

A Lie group acts on its tangent bundle by the tangent map. We can consider the left or the right action of G on $\mathfrak{g}$ by: $T_eL_g\xi$ or $T_eR_g\xi$, where L_g and R_g denote left and right translations, respectively; so if $g = g(t)$ is a curve in G, then there exists a time dependent $\xi(\cdot) \in \mathfrak{g}$ such that

$$\dot{g}(t) = T_eL_{g(t)}\xi(t) = g(t)\xi(t) \tag{1.6}$$

and similarly for the right action.
Given left action of a Lie group G on Q, $\Phi : G \times Q \to Q$, and ξ an element of the Lie algebra $\mathfrak{g}$ then $\Phi^\xi : \mathbb{R} \times Q \to Q : (t, q) \longmapsto \Phi(\exp t\xi, q)$ is a flow on Q, the corresponding vector field on Q is called **infinitesimal generator** of Φ corresponding to ξ, is denoted by $\xi_Q(q)$

$$\xi_Q(q) = \frac{d}{dt}\Phi(\exp t\xi, q)|_{t=0}\,. \tag{1.7}$$

1.1.2 Fiber Bundles and Connections

Fiber bundles provide a basic geometric structure for the understanding of many mechanical and control problems.

A fiber bundle essentially consists of a given space (the base) together with another space (the fiber) attached at each point, plus some compatibility conditions. More formally, we have the following:

Definition 1.6. *Let $\mathcal{S}$ be a differentiable base manifold and G a Lie group. A differentiable manifold Q is called* principal fiber bundle *if the following conditions are satisfied:*

1 G acts on Q to the left, freely and differentiably:

$$\Phi : G \times Q \to Q \tag{1.8}$$

writing $\Phi(g, q) = \Phi_g \cdot q = g \cdot q$.

2 $\mathcal{S} = Q/G$ and the canonical projection $\pi : Q \to \mathcal{S}$ is differentiable

3 Q is locally trivial, namely every point $s \in \mathcal{S}$ has a neighborhood U such that $\pi^{-1}(U) \subset Q$ is isomorphic to $U \times G$, in the sense that $q \in \pi^{-1}(U) \mapsto (\pi(q), \phi(q)) \in U \times G$ is a diffeomorphism such that $\phi : \pi^{-1}(U) \to G$ satisfies $\phi(g \cdot q) = g\phi(q), \forall g \in G$

An important additional structure on a bundle is a **connection**. Suppose we have a bundle and consider (locally) a section of this bundle, i.e., a choice of a point in the fiber over each point in the base. We call such a choice a "field". The idea is to single out fields that are "constant". For vector fields on a linear space, for example, it is clear what we want such fields to be; for vector fields on a manifold or an arbitrary bundle, we have to specify this notion. Such fields are called "horizontal". A connection is used to single out horizontal fields, more precisely fields which live in a subspace of the the tangent space, and is chosen to have other desirable properties, such as linearity.

Definition 1.7. *Let $(Q, \mathcal{S}, \pi, G)$ be a principal fiber bundle. the kernel of $T_q\pi$ denoted by $V_q := \{v \in T_qQ | T_q\pi(v) = 0\}$, is the subspace of T_qQ tangent to the fiber through q and is called vertical subspace. A connection on the principal fiber bundle is a choice of a tangent subspace $H_q \subset T_qQ$ at each point $q \in Q$ called horizontal subspace such that:*

(1) $T_qQ = H_q \oplus V_q$

(2) For all $g \in G$ and $q \in Q$, $T_q\Phi_g \cdot H_q = H_{g \cdot q}$

(3) H_q depends differentiably on q

Hence, for any $q \in Q$, we have that $T_q\pi$ determines an isomorphism $H_q \cong T_{\pi(q)}\mathcal{S}$: for all $T_qQ \ni v = v_{V_q} + v_{H_q}$ and we have that $T_{\pi(q)}(v) = v_{H_q} \in \mathcal{S}$. In other words the choice of an horizontal subspace can be seen also as the choice of a vector valued "connection one form" which vanishes on the horizontal vectors.

It follows the definition

Definition 1.8. *An Ehresmann connection A is a vector valued one form such that*

(i) A is vertical valued: $A_q : T_q \longrightarrow V_q$ is a linear map for each point $q \in Q$

(ii) A is a projection: $A(v) = v$ for all $v \in V_q$.

In the special case in which $(Q, \mathcal{S}, \pi, G)$ is a principal fiber bundle the previous conditions on $A : TQ \longrightarrow \mathfrak{g}$ read:

(i) $A(\xi_Q(q)) = \xi$ for all $\xi \in \mathfrak{g}$ and $q \in Q$, where $\xi_Q(q)$ is the infinitesimal generator of the left action of G on Q (1.7).

(ii) A is equivariant:
$$A(T_q(\Phi_g(v))) = Ad_g(A(v))$$
for all $v \in T_qQ$ and $g \in G$ where Φ_g denotes the given action of G on Q and where Ad denotes the adjoint action of G on $\mathfrak{g}$ defined as
$$Ad_g := T_e(L_g \circ R_{g^{-1}}) : \mathfrak{g} \to \mathfrak{g}\,.$$

Therefore it is evident that the horizontal subspace H_q is the kernel of A_q.
n the case in which there is a metric $h(q)$ in our manifold Q, we have a special way to define the horizontal subspace: it is the orthogonal with respect to the metric to the vertical subspace.

$$H_q = \{w \in T_qQ : \langle w, h(q)v\rangle = 0, \forall v \in V_q\} \tag{1.9}$$

In this special case our connection A is called *mechanical connection* (see [63] and therein references). We now would like to express the connection in coordinates, in order to do this we first introduce the following definition

Definition 1.9. *Let us consider the following diagram*

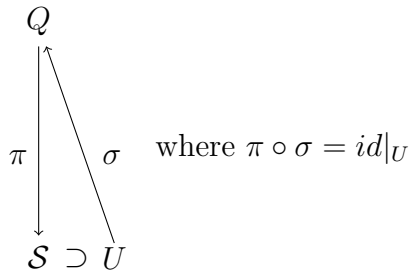

The functions like σ are ***sections*** *and we call $\Gamma(U, Q)$ the set of all sections from U in Q.*

Alternatively often a connection is introduced as a derivation ∇ as follows. Let ∇ be a map

$$\begin{aligned}&\nabla : \Gamma(Q) \to \Gamma(Q \otimes T^*\mathcal{S}) \quad \text{such that}\\ &\nabla(\sigma_1 + \sigma_2) = \nabla(\sigma_1) + \nabla(\sigma_2)\\ &\nabla(f\sigma) = f\nabla(\sigma) + \sigma \otimes df \quad \text{if } f \text{ is a } C^\infty \text{ function.}\end{aligned}$$

Let now $\mathbf{e}$ be a local basis of sections of the principal fiber bundle, in this basis the connection one-form A can be expressed as

$$e_a A^a_b = \nabla e_b \qquad a, b = 1 \cdots dim(Q).$$

If we change basis in $\Gamma(Q)$, say $\mathbf{e} = \tilde{\mathbf{e}}\Omega$, the connection A changes, i.e.

$$\begin{aligned}\tilde{\mathbf{e}}\tilde{A} =& \nabla\tilde{\mathbf{e}} = \nabla(\mathbf{e}\Omega^{-1}) = (\nabla\mathbf{e})\Omega^{-1} + \mathbf{e}d\Omega^{-1} = \mathbf{e}A\Omega^{-1} + \mathbf{e}d\Omega^{-1}\\ &= \tilde{\mathbf{e}}\Omega A\Omega^{-1} + \tilde{\mathbf{e}}\Omega d\Omega^{-1}\end{aligned}$$

therefore A and $\tilde{A}$ satisfy the following relation

$$\tilde{A} = \Omega A\Omega^{-1} + \Omega d\Omega^{-1} \tag{1.10}$$

Let $u(t)$ be a smooth curve in $\mathcal{S}$ passing through the point $P = u(0)$. Let $q \in Q_P = \pi^{-1}(P)$ be any point in the fiber of Q over P. We would like to find a smooth curve $\gamma(t)$ in Q such that $\pi(\gamma(t)) = u(t)$, $\gamma(0) = q$, and $\gamma'(t) \in H_{\gamma(t)}$ (i.e., the tangent vectors to the curve $\gamma(t)$ are horizontal).

From the usual theory of differential equations it follows that such a curve $\gamma(t)$ exists and is unique, at least locally at any point $q \in Q$ (i.e., for small values of t). The curve γ is called a **horizontal lift** of u. Regarding the tangent vectors, for any $q \in Q$ and any vector $\dot{u} \in T_{\pi(q)}\mathcal{S}$ there exists a unique vector $v \in H_q \subset T_qQ$ such that $T_q\pi : v \mapsto \dot{u}$. The vector v is called the **horizontal lift** of $\dot{u}$.

Given an Ehresmann connection we can define the horizontal lift of curves in $\mathcal{S}$, hence we can also define a notion of parallel transport that allows us to identify different fibers of Q.

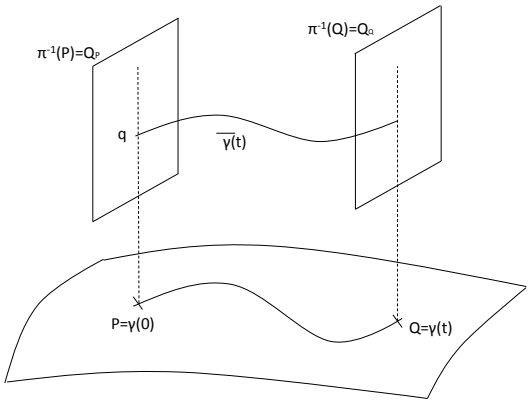

Figure 1.1: Horizontal lift of the curve $u(t)$

Note that, in general, the parallel transport will be path-dependent. If we start with two different curves $u_1(t)$ and $u_2(t)$, such that $u_1(0) = u_2(0) = P$ and $u_1(\bar{t}) = u_2(\bar{t}) = S$, then the horizontal lifts γ_1 and γ_2 at a point $q \in Q_P$ will not meet, in general, at a point in the fiber Q_S, i.e., we will have $\gamma_1(\bar{t}) \neq \gamma_2(\bar{t})$. This gap on the fiber is called **holonomy** and depends on the choice of the connection and on the topology of the base manifold. In particular if it is connected the holonomy depends on the base point only up to conjugation [54].

1.2 Geometry

As we have seen, in the general theory, connections are associated with bundle mappings, which project larger spaces onto smaller ones. The larger space is the bundle, and the smaller space is the base. Directions in the larger space that project to a point are vertical directions. The connection is a specification of a set of directions, the horizontal directions, at each point, which complements the space of vertical directions. In general, we can expect that for a horizontal motion in the bundle corresponding to a cyclic motion in the base, the vertical motion will undergo a shift, called a phase shift, between the beginning and the end of its path. The magnitude of the shift will depend on the curvature of the connection and the area that is enclosed by the path in the base space: it is exactly the holonomy. This shift in the vertical element is often given by an element of a group, such as a rotation

or translation group, and is called also the **geometric phase**. Referring to what said in the previous subsection, the motion is determined only by the geometrical properties of the system if it starts with zero initial impulse. In many examples, the base space is the control space in the sense that the path in the base space can be chosen by suitable control inputs to the system, i.e. changes in internal shape. In the locomotion setting, the base space describes the internal shape of the object, and cyclic paths in the shape space correspond to the movements that lead to translational and rotational motion of the body.
Nevertheless the shape changes are not the only ones to determine a net motion of the body. More generally, this motion can always be decomposed into two components: the geometric phase, determined by the shape of the path and the area enclosed by it, and the **dynamic phase**, driven by the internal kinetic energy of the system characterized by the impulse. It is important to stress the difference between the two phases. The geometric phase is due entirely to the geometric structure of the system. Instead the dynamic phase is present if and only if the system has non zero initial impulse or if the impulse is not a conserved quantity. More precisely if the curvature of the connection is null, not necessarily the system does not move after a cyclic motion in the base: a net motion can result if the system starts with non zero initial impulse, and this motion is entirely due to the dynamic phase.

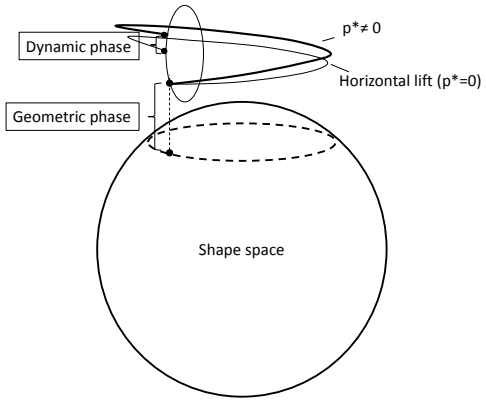

Figure 1.2: Geometric phase and dynamic phase.

Figure (1.2) shows a schematic representation of this decomposition for general rigid body motion. In this figure the sphere represents the base space, with a loop in the shape space shown as a circular path on the sphere. The

closed circle above the sphere represents the fiber of this bundle attached to the indicated point. Given any path in the base (shape) space, there is an associated path, called the horizontal lift, that is independent of the time parametrization of the path and of the initial vertical position of the system see. Following the lifted path along a loop in the shape space leads to a net change in vertical position along the fiber. This net change is just the geometric phase. On top of that, but decoupled from it, there is the motion of the system driven by the impulse, (if it is not zero) which leads to the dynamic phase. Combining these two provides the actual trajectory of the system.

1.2.1 Gauge potential

Let us consider a planar body immersed in a 2 dimensional fluid, which moves changing its shape. For the moment we do not specify the kind of fluid in which it is immersed that can be either ideal and incompressible or a viscous one with low Reynolds number. Our aim is to show that the motion of this deformable body through the fluid is completely determined by the geometry of the sequence of shapes that the idealized swimmer assumes, and to determine it. This idea was introduced by Shapere and Wilczek in [77] [76] and developed in [25], where they apply geometrical tools to describe the motion of a deformable body in a fluid, focusing their attention on the Stokes regime.
The configuration space of a deformable body is the space of all possible shapes. We should distinguish between the space of shapes located somewhere in the plane and the more abstract space of unlocated shapes. The latter space can be obtained from the space *cum* locations by making the quotient with the group of rigid motions in the plane, i.e declaring two shapes with different centers of mass and orientation to be equivalent. The first problem we wish to solve can be stated as follows: what is the net rotation and translation which results when a deformable body undergoes a given sequence of unoriented shapes? The problem is intuitively well posed: when a body changes its shape in some way a net rotation and translation is induced. For example, if the system is composed simply by the body, its net rigid motion can be computed by making use of the law of conservation of momentum, if instead the body is immersed in an ideal incompressible fluid this motion can be found by solving the Euler equations for the fluid flow with boundary condition on the surface of the body with the shape corresponding to the given deformation.
These remarks may seem straightforward, but we encounter a crucial ambiguity trying to formulate the problem more specifically. Namely how can we

specify the net motion of an object which is continuously changing shape? To quantify this motion it is necessary to attach a reference frame to each unlocated shape. This is equivalent to choosing a standard location for each shape; more precisely to each unlocated shape there now corresponds a unique located shape. Once a choice of standard locations for shapes has been made, then we shall say that the rigid motion required to move between two different configurations is the displacement and rotation necessary to align their centers and axes. In what follows we shall develop a formalism, already used in [77] [76], which ensures us that the choice of axes for the unlocated shapes is completely arbitrary and that the rigid motion on the physical space is independent from this choice. This will be clear soon below.
Now let s parametrize the boundary of a shape $S(s)$, ad let $S_0(s)$ be the associated unlocated shape. Then

$$S(s) = \mathcal{R}S_0(s)$$

where $\mathcal{R}$ is a rigid motion. We emphasize that S and S_0 are parametrized shapes.
In considering the problem of self propulsion, we assume that our swimmer has control on its form. A swimming stroke is therefore specified by a time dependent sequence of unlocated shapes $S_0(t)$ (the s-dependence is implicit. The corresponding sequence of located shapes $S(t)$ are related by

$$S(t) = \mathcal{R}(t)S_0(t) \tag{1.11}$$

where $\mathcal{R}$ is a time dependent rigid motion. This relation expresses how to recover the located shapes $S(t)$ given the unlocated ones, i.e. $S_0(t)$. It is clear that we are dealing with a fiber bundle: the located shapes $S(t)$ live on the big manifold $Q = SE(2) \times \mathcal{S}$ and the unlocated ones, $S_0(t)$, live on the base manifold obtained by the quotient of the manifold Q by the plane euclidean group $SE(2)$, i.e $\mathcal{S} = Q/SE(2)$.

To make (1.11) more explicit we introduce a matrix representation for the group of Euclidean motions, of which $\mathcal{R}$ is a member. A two dimensional rigid motion consisting of a rotation R followed by a translation d may be represented as a 3×3 matrix

$$[R, d] = \begin{pmatrix} R & d \\ 0 & 1 \end{pmatrix} \tag{1.12}$$

where R is an ordinary 2×2 rotation matrix, d is a 2 component column vector. This is the matrix representation of the plane euclidean group action $SE(2)$ on the manifold Q where the located shapes $S(t)$ live on.

Now in considering the problem of self propulsion we shall assume that our swimmer has control over its form but cannot exert net forces and torques on itself. A swimming stroke is therefore specified by a time-dependent sequence of forms, or equivalently unlocated shapes $S_0(t)$. The located shape will then be expressed exactly by formula (1.11).

Our problem of determining the net rigid motion of the swimmer thus resolves itself into the computation of $\mathcal{R}(t)$ given $S_0(t)$. In computing this displacement it is most convenient to begin with infinitesimal motions and to build up finite motions by integrating. So let us define the infinitesimal motion $A(t)$ by

$$\frac{d\mathcal{R}}{dt} = \mathcal{R}\big(\mathcal{R}^{-1}\frac{d\mathcal{R}}{dt}\big) \equiv \mathcal{R}A \tag{1.13}$$

In this formula we can recognize the differential equation corresponding to formula (1.6), from which we understand that A take values in the Lie algebra of the plane euclidean group: $\mathfrak{g} = se(2)$. For any given infinitesimal change of shape A, formula (1.13), describes the net overall translation and rotation which results. We can integrate it to obtain

$$\mathcal{R}(t_2) = \mathcal{R}(t_1)\bar{P}\exp\Big[\int_{t_1}^{t_2} A(t)\,dt\Big] \tag{1.14}$$

where $\bar{P}$ denotes a reverse path ordering, known in literature as chronological series [1]:

$$\bar{P}\exp\Big[\int_{t_1}^{t_2} A(t)\,dt\Big] = 1 + \int_{t_1<t<t_2} A(t)\,dt + \iint_{t_1<t'<t<t_2} A(t)A(t')\,dt\,dt' + \cdots \tag{1.15}$$

The assignment of center and axes can be arbitrary, so we should expect that physical results are independent of this assignment. How does this show up in our formalism? A change in the choice of centers and axes can equally well be thought of as a change (rigid motion) of the standard shapes, let us write

$$\tilde{S}_0 = \Omega(S_0)S_0 \tag{1.16}$$

The located shapes $S(t)$ being unchanged, (1.11) requires us to define [77] [76]

$$\tilde{\mathcal{R}}(t) = \mathcal{R}(t)\Omega^{-1}(S_0(t))$$

From this, the transformation law of A follow

$$\tilde{A} = \Omega A\Omega^{-1} + \Omega\frac{d\Omega^{-1}}{dt} \tag{1.17}$$

from which we can recognize the transformation laws (1.10) of an Ehresmann connection called also **Gauge potential**, as explained in [77] . Our freedom in choosing the assignment of axes shows up as a freedom of gauge choice on the space of standard shapes. Accordingly the final relationship between physical shapes is manifestly independent of such choices.
Our aim will be to compute this gauge potential $A \in se(2)$ in function of the unlocated shapes S_0 that our swimmer is able to control.
The important fact to note is that the geometry which underline this kind of system does not depend on the kind of fluid chosen; the difference will emerge later when we will focus of two kind of fluids: the ideal incompressible and irrotational one and, on the other hand, a Stokes viscous fluid. The way to compute the equations of motion, will be different since the hydrodynamics of each kind of fluid is very particular.

1.3 Tools in geometric control theory

Let us consider the following control system

$$\dot{q} = \mathcal{F}(q, u) \tag{1.18}$$

where q are local coordinates for smooth manifold Q with $\dim Q = n$ and $u : [0, T] \to U \subset \mathbb{R}^m$ is the set of admissible controls. The unique solution of (1.18) at time $t \geq t_0$ with initial condition $q(t_0) = q_0$ and input function $u(\,\cdot\,)$ is denoted $q(t, t_0, q_0, u)$.

Definition 1.10.

- *The **reachable set** $R^V(q_0, T)$ is the set of points in Q which are reachable from q_0 at exactly time $T > 0$, following trajectories which, for $t \leq T$ remain in a neighborhood V of q_0*

- *The system (1.18) is **locally accessible** from x_0 if, for any neighborhood V of q_0 and all $T > 0$ the set $R^V_T(q_0) = \bigcup_{t \leq T} R^V(q_0, t)$ contains a non empty open set.*

- *The system (1.18) is **locally strong accessible** from q_0 if for any neighborhood V of q_0 and all $T > 0$ sufficiently small, the set $R^V(q_0, T)$ contains a non empty open set.*

- *The system (1.18) is **controllable**, if for every q_1 , $q_2 \in Q$ exists a finite time $T > 0$ and an admissible control $u : [0, T] \to U$ such that $q(T, 0, q_1, u) = q_2$*

- *The system (1.18) is **small time locally controllable (STLC)** from $q_0 \in M$ if, for any neighborhood V of q_0 and all $T > 0$, q_0 is an interior*

point of the set $R_T^V(q_0)$, that is a whole neighborhood of q_0 is reachable from q_0 at arbitrary small time.

Let now suppose the system (1.18) to be an affine non linear control system, namely

$$\dot{q} = \mathcal{F}(q,u) = f(q) + \sum_{j=1}^{m} g_j(q)u_j \tag{1.19}$$

We now present some general results for this type of control systems

Definition 1.11. *The **strong accessibility algebra** $\mathcal{C}_0$ is the smallest subalgebra of the Lie algebra of smooth vector fields on M containing the control vector fields $g_1 \dots g_m$, which is invariant under the drift vector field f, that is $[f,X] \in \mathcal{C}_0$, $\forall X \in \mathcal{C}_0$, every element of the algebra $\mathcal{C}_0$ is a linear combination of repeated Lie brackets of the form $[X_k,[X_{k-1},[\dots,[X_1,g_j]\dots]]]$ for $j = 1 \dots m$ and where $X_i \in \{f,g_1,\dots,g_m\}$.*

*The **strong accessibility distribution** C_0 is the corresponding involutive distribution $C_0(q) = \{X(q) | X \in \mathcal{C}_0\}$.*

Proposition 1.3. *Let q_e be an equilibrium point of the system (1.19). The linearization of the system (1.19) at q_e is controllable if*

$$rank\Big[g|\frac{\partial f}{\partial q}g|\big(\frac{\partial f}{\partial q}\big)^2 g|\dots|\big(\frac{\partial f}{\partial q}\big)^{n-1}g\Big]|_{q_e} = n \tag{1.20}$$

We say that the Strong Accessibility Rank Condition at $q_0 \in Q$ is satisfied if

$$\dim C_0(q_0) = n \tag{1.21}$$

Proposition 1.4. *We say that the system (1.19) is locally strong accessible from q_0 if the strong accessibility rank condition is satisfied.*

Proposition 1.5. *If the system (1.19) is driftless, namely*

$$\dot{q} = \sum_{i=1}^{m} u_i g_i(q) \tag{1.22}$$

its controllability is equivalent to its strong accessibility.

Theorem 1.1. *(Chow (see [29])) Let m,$n \in \mathbb{N}$ and let $(f_i)_{i=1,n}$ be $\mathcal{C}^\infty$ vector fields on $\mathbb{R}^n$. Consider the control system, of state trajectory $\mathbf{q}$,*

$$\dot{q} = \sum_{i=1}^{m} u_i f_i(\mathbf{q}), \tag{1.23}$$

with input function $\mathbf{u} = (u_i)_{i=1,m} \in L^\infty([0,+\infty[, \mathbf{B}_{\mathbb{R}^n}(0,r))$ *for some* $r > 0$. *Let* $\mathcal{O}$ *an open and connected set of* $\mathbb{R}^n$ *and assume that*

$$\mathbf{L}ie_{\mathbf{q}}(f_1, ...f_m) = \mathbb{R}^n \quad \mathbf{q} \in \mathcal{O}$$

Then the system (1.23) is controllable, i.e., for every $\mathbf{q}_0$, $\mathbf{q}_1$ *in* $\mathcal{O}$ *and for every* $T > 0$ *exists* $\mathbf{u} \in L^\infty((0,T), \mathbf{B}_{\mathbb{R}^n}(0,r))$ *such that* $\mathbf{q}(0) = \mathbf{q}_0$ *and* $\mathbf{q}(T) = \mathbf{q}_1$ *and* $\mathbf{q}(t) \in \mathcal{O}$ *for every* $t \in [0,T]$.

Theorem 1.2 ((Orbit (see [49]))**.** *Let* Q *be an analytic manifold, and* $\mathcal{F}$ *a family of analytic vector fields on* Q. *Then*

a) each orbit of $\mathcal{F}$ *is an analytic submanifold of* Q, *and*

b) if N *is an orbit of* $\mathcal{F}$, *then the tangent space of* N *at* x *is given by* $Lie_x(\mathcal{F})$. *In particular the dimension of* $Lie_x(\mathcal{F})$ *is constant as* x *varies on* N.

Let us recall the definition of iterated Lie brackets [29]

Definition 1.12. *Let* $f \in C^\infty$ *and* $g \in C^\infty$ *we define by induction on* $k \in \mathbb{N}$ $ad_f^k g \in C^\infty$

$$ad_f^0 g := g$$
$$ad_f^{k+1} g := [f, ad_f^k g],\ \forall k \in \mathbb{N}.$$

We are now ready to give a sufficient condition for small time local controllability

Theorem 1.3. *Assume that the controlled vector fields* $g_1 \cdots g_m$ *generate a Lie algebra* $\mathcal{L}ie\{g_1 \cdots g_m\}$ *that satisfies* $\mathcal{L}ie\{g_1 \cdots g_m\} = T_qQ$ *for all* q *in* Q *then the corresponding affine system*

$$\dot{q} = f(q) + \sum_{i=1}^{m} g_i(q) u_i$$

is strongly controllable whenever there are no restrictions on the size of the controls.

Theorem 1.4. *(see [38]) Assume that the drift term is bounded but non zero and the vectors* $ad_f^k g_i(q)$ $\forall i \in \{1 \cdots m\}$ $\quad k \in \{0, 1, \cdots\}$ *together with the vectors* $[g_i, g_j](q)$ *for all pairs* $i, j \in \{1, \cdots, m\}$ *span* $\mathbb{R}^n$. *Then the affine control system is* ***small time locally controllable*** *from* q, *if the controls are sufficiently large, i.e with controls* $\lambda \dot{u}$ *and* $\dot{u} \in \{|\dot{u}_i| < 1, i = 1, \cdots, m\}$ *for some large scalar* $\lambda > 0$.

1.4 Reynolds number

In this section we describe how it is possible to characterize the kind of fluid involved in the following chapters. It is well known that there is a system of partial differential equations describing the motion of a simple 2-dimensional viscous incompressible fluid (a Newtonian fluid): the Navier Stokes equations.

$$\rho\big(\frac{\partial v}{\partial t} + (v \cdot \nabla)v\big) = -\nabla p + \eta \Delta v$$
$$\text{div } v = 0$$

where v and p are the velocity and the pressure in the fluid, ρ is the fluid density, and η its viscosity. For simplicity external forces, such as gravity, have been dropped from the right hand side of the first equation, which expresses the balance between forces and rate of change of linear momentum. The second equation constrains the flow to be volume preserving, in view of incompressibility.
These equations can be put in a dimensionless form using the following definitions

$$x^{'} = \frac{x}{L} \qquad y^{'} = \frac{y}{L}$$
$$v^{'} = \frac{v}{V} \qquad p^{'} = \frac{pL}{\eta V}$$
$$\nabla^{'} = \mathbf{e}_x \frac{\partial}{\partial x^{'}} + \mathbf{e}_y \frac{\partial}{\partial y^{'}} = L\nabla \qquad t^{'} = t\frac{V}{L}$$

Here, U and L are a characteristic velocity and a characteristic length. Then

$$\rho \frac{\partial (V v^{'})}{\partial (\frac{L}{V} t^{'})} + \rho V v^{'} \cdot \frac{1}{L} \nabla^{'} V v^{'} = -\frac{1}{L^2} \nabla^{'} (\eta V p^{'}) + \eta \frac{1}{L^2} \nabla^{'2} (V v^{'})$$

Assuming ρ constant and multiplying both sides by $\frac{L^2}{\eta V}$ gives

$$Re(\frac{\partial v^{'}}{\partial t^{'}} + v^{'} \cdot \nabla^{'} v^{'}) = -\nabla^{'} p^{'} + \Delta^{'} v^{'}$$
$$\text{div } v^{'} = 0 \tag{1.24}$$

where Re is a dimensionless parameter known as the **Reynolds number**. Pressure is a parameter fixed by the observer, so it follows that the only other force is inertia force. Furthermore, the relative magnitudes of the pressure and inertial forces are describe by the Reynolds number, defined as

$$Re = \frac{F_{inertial}}{F_{viscous}} = \frac{VL\rho}{\eta}.$$

For high Reynolds number flow ($Re \to \infty$), the viscous force is small compared to the inertia force, so it can be neglected, leaving Euler's equation of inviscid motion

$$\begin{aligned} \rho\big(\frac{\partial v}{\partial t} + (v \cdot \nabla)v\big) &= -\nabla p \\ \text{div } v &= 0 \end{aligned} \tag{1.25}$$

For low Reynolds number ($Re \to 0$), the inertia term is smaller than the viscous term and can therefore be ignored, leaving the Stokes equations

$$\begin{aligned} \Delta v &= \nabla p \\ \text{div } v &= 0 \end{aligned} \tag{1.26}$$

These two different regimes are those in analysis in our work. Since the Reynolds number depends linearly on the characteristic length and velocity of the system and decreases as the viscosity increases we can make different assumptions on these quantities and obtain different regimes. In the first case of study, supposing to have a fluid with vanishing viscosity, we will consider a body immersed in a fluid with high Reynolds number, and as we have seen, the equations are the Euler's one. Next in the second case, we consider swimming at micro-scales, therefore we focus on the case of a low Reynolds number fluid, where the hydrodynamics is described by the Stokes equations.

Chapter 2

Ideal fluids

We now focus on a planar swimmer immersed in a fluid at high Reynolds number, i. e. with viscosity low enough to be negligible. This is the case of a body immersed in an ideal and incompressible fluid. The dynamical problem of its self propulsion has been reduced to the calculation of the gauge potential A. In our model we assume that the allowed motions, involving the same sequence of forms will include additional time-dependent rigid displacements. In other words the actual motion will be the composition of the given motion sequence $S_0(t)$ and rigid displacements.

2.1 Structure of equations of motion

In this section we present the geometrical framework underlying dynamical control systems. We derive the equations of motion and discuss how to use the geometrical tools introduced before to gain informations on our system.

2.1.1 Geometry of control equations

In this subsection we derive the local dynamic equations for the control system $(Q, h, \mathcal{F})$ where $\mathcal{F}$ is a smooth k-dimensional foliation on Q, and h is the Riemaniann metric on the manifold Q, as done in [61]. As is well known, on a set $U \subset Q$ adapted for the foliation, $\mathcal{F}$ coincides with the model foliation of $\mathbb{R}^n$ by k-dimensional hyperplanes. Let $\phi : U \longrightarrow \mathbb{R}^n$, $\phi(P) = (x, y)$ be a local chart of Q in U, distinguished for $\mathcal{F}$, so that ϕ maps $\mathcal{F}|_U$ into the trivial fibration $\pi(x, y) = y$. Set $q = (x, y) \in Q$; given a path $u(t) \in \pi(\phi(U))$, we suppose that for every t, the reaction forces that implement the (ideal) constraint $y \equiv u(t)$ are workless with respect to the set $V_{q(t)}U = \ker T_{q(t)}\pi$ of the virtual displacements compatible with the constraint $y \equiv u(t)$.

Let $(Q, h, \mathcal{F})$ be a foliated Riemanian manifold, let $U \subset Q$ be an open set adapted for $\mathcal{F}$ an let $q = (x, y)$. If $T(q, \dot{q}) = \frac{1}{2}\dot{q}^t h(q)\dot{q}$ is the kinetic energy of the unconstrained system $(Q, h, \mathcal{F})$, then the kinetic energy of the system subject to the time dependent constraint $y \equiv u(t)$ is $T(x, u(t), \dot{x}, \dot{u}(t))$. The related dynamic equations are, in Lagrangian formalism

$$\frac{d}{dt}\frac{\partial T}{\partial \dot{x}} - \frac{\partial T}{\partial x} = 0 \tag{2.1}$$

These can be put in Hamiltonian form by performing a partial legendre transformation on the $\dot{x}$- variables. When we identify y with $u(t)$ and $\dot{y}$ with $\frac{d}{dt}u(t)$, the above Lagrange equations are equivalent to

$$\dot{x} = \frac{\partial H}{\partial p}(x, p, u, \dot{u}) \qquad\qquad \dot{p} = -\frac{\partial H}{\partial x}(x, p, u, \dot{u})\,. \tag{2.2}$$

We call these equations *control equations*. Let

$$\dot{q}^t h(q)\dot{q} = \dot{x}^t \mathcal{C}\dot{x} + \dot{x}^t \mathcal{M}\dot{y} + \dot{y}^t \mathcal{M}^t \dot{x} + \dot{y}^t \mathcal{B}\dot{y} \tag{2.3}$$

be the local block representation of the metric h in $\phi(U)$, where $\mathcal{C}, \mathcal{B}$ are symmetric and invertible respectively $k \times k$ and $(n-k) \times (n-k)$ matrices.

To every $q \in U$ denote with $H_q U$ the subspace orthogonal to $V_q U = \ker T_q\pi$ with respect to h. Referring to the local expression of h in U, it is easy to see that $H_q U$ is the space orthogonal to the vectors $(e_i, 0)_{i=1\cdots n}$ with respect to the metric h .

$$H_q U = \{(\dot{x}, \dot{y}) \in T_q U \text{ such that } \mathcal{C}(q)\dot{x} + \mathcal{M}(q)\dot{y} = 0\}\,.$$

Therefore $H_q U$ can be equivalently assigned through the $V_q U$-valued connection one form defined in Definition 1.8

$$A(q) = (dx + C(q)dy) \otimes \frac{\partial}{\partial x} \qquad \text{where (see 2.6) } C = \mathcal{C}^{-1}\mathcal{M} \tag{2.4}$$

whose kernel and range are respectively $H_q U$ and $V_q U$. Now we consider the orthogonal splitting of a vector into its horizontal ad vertical components

$$v = v^v + v^h = A(q)v + hor(T_q\pi v) = (\dot{x} + C\dot{y}, 0) + (-C\dot{y}, \dot{y})$$

Using the above decomposition, we get the induced splitting of the kinetic energy metric tensor into its vertical and horizontal part:

$$h(q)dq \otimes dq = \mathcal{C}(q)A(q) \otimes A(q) + K(q)dy \otimes dy \tag{2.5}$$

where $K(q) = \mathcal{B} - \mathcal{M}^t\mathcal{C}^{-1}\mathcal{M}$.

Definition 2.1. *The Riemannian metric h is **bundle-like** for the foliation $\mathcal{F}$ iff on a neighborhood U with adapted coordinates (x, y) the above orthogonal splitting of g holds with $K = K(y)$.*

The importance of this notion will be clear in the following subsection. Using this notation we want to rewrite the control equations.

From

$$p = \frac{\partial T}{\partial \dot{x}} = \mathcal{C}\dot{x} + \mathcal{M}\dot{y}$$

we obtain

$$\dot{x} = \mathcal{C}^{-1}p - \mathcal{C}^{-1}\mathcal{M}\dot{u} = \mathcal{C}^{-1}p - C\dot{u} \tag{2.6}$$

Substituting (2.6) in (2.3) and recalling that $-\frac{\partial H}{\partial x} = \frac{\partial T}{\partial x}$ we have

$$\dot{p} = -\frac{\partial H}{\partial x} = \frac{\partial T}{\partial x} = -\frac{1}{2}p^t\frac{\partial \mathcal{C}^{-1}1}{\partial x}p + p^t\frac{\partial C}{\partial x}\dot{u} + \frac{1}{2}\dot{u}^t\frac{\partial(\mathcal{B} - \mathcal{M}^t\mathcal{C}^{-1}\mathcal{M})}{\partial x}\dot{u} \tag{2.7}$$

Therefore the control equations are

$$\begin{cases} \dot{x} = \mathcal{C}^{-1}p - \mathcal{C}^{-1}\mathcal{M}\dot{u} \\ \dot{p} = -\frac{1}{2}p^t\frac{\partial \mathcal{C}^{-1}}{\partial x}p + p^t\frac{\partial C}{\partial x}\dot{u} + \frac{1}{2}\dot{u}^t\frac{\partial(\mathcal{B}-\mathcal{M}^t\mathcal{C}^{-1}\mathcal{M})}{\partial x}\dot{u} \end{cases} \tag{2.8}$$

We now introduce, following [61], the global version of the above dynamic equations when Q is the total space of a surjective submersion $\pi : Q \longrightarrow \mathcal{S}$. Let VQ be the vertical subbundle and V^*Q the dual of VQ. Denote with $p_Q : T^*Q \longrightarrow Q$ the cotangent projection and set $\tilde{\pi} := \pi \circ p_Q$, $\tilde{\pi} : V^*Q \longrightarrow \mathcal{S}$. If (x, y) are local fibered coordinates on Q, (x, y, p) are local fibered coordinates on V^*Q. Moreover, denote with $z = (x, p)$ the local coordinates on the $\tilde{\pi}$-fiber over y. Now, to every $y \in \mathcal{S}$, $\tilde{\pi}^{-1}(y)$ is a fiber canonically simplettomophic to $T^*(\pi^{-1}(y))$, representing the phase space of the constrained system restricted to the π-fiber over y.

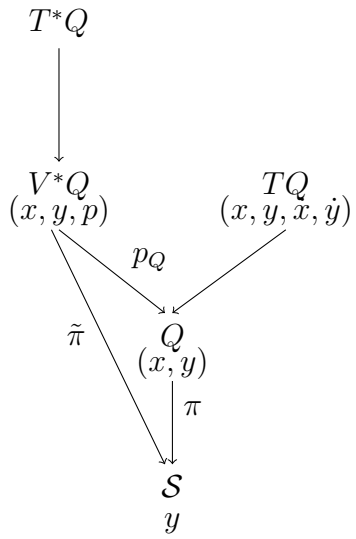

Suppose that a control vector field $\dot{u}$ is given on $\mathcal{S}$ and that the path $u(t)$ is an integral curve of $\dot{u}$. Then the dynamic equations (2.6) and (2.7) are the local expression of a vector field $D_{\dot{u}}$ over V^*Q that projects on $\dot{u}$ by $\tilde{\pi}$. Moreover the field $D_{\dot{u}}$ is tangent to the fiber of $\tilde{\pi}$ only if the control is trivial: $\dot{u}$ vanishing. Let us suppose that the control is given by a curve $u : [t_1, t_2] \to \mathcal{S}$ in $\mathcal{S}$ that is the integral curve of the vector field $\dot{u}$. Thus the movement of the system is described by a differentiable curve $\gamma : [t_1, t_2] \to Q$ such that $\pi(\gamma(t)) = u(t)$. Note that $\frac{d\gamma}{dt} : [t_1, t_2] \to TQ$ is the natural increase of the curve γ in the fiber tangent to Q. Composing $\frac{d\gamma}{dt}$ with the Legendre transform $\mathcal{L}_T Q \to T^*Q$ and with the projection $\tau : T^*Q \to V^*Q$ we obtain the parametric curve $\hat{\gamma} = \tau \circ \mathcal{L} \circ \frac{d\gamma}{dt} : [t_1, t_2] \to V^*Q$ which represent the evolution of the system taking into account the control.

Let $hor_Q : T\mathcal{S} \longrightarrow TQ$ denote the horizontal lift of the Ehresmann connection, introduced in the previous section, and p_Q the cotangent projection, using the above definitions we introduce the function

$$K_{\dot{u}} : V^*Q \longrightarrow \mathbb{R} \qquad K_{\dot{u}} \circ p_Q^{-1}(q) = (hor_Q(q)(\dot{u}))^t h(q) hor_Q(q)(\dot{u})$$

Theorem 2.1. *To every control vector field $\dot{u}$ on $\mathcal{S}$, the corresponding dynamic vector field $D_{\dot{u}}$ can be expressed as the sum of three terms:*

$$D_{\dot{u}} = X_{H_0} - X_{K_{\dot{u}}} + hor(\dot{u}) \tag{2.9}$$

with

$$X_{H_0} = \mathcal{C}^{-1} p \frac{\partial}{\partial x} - \frac{1}{2} p^t \frac{\partial \mathcal{C}^{-1}}{\partial x} p \frac{\partial}{\partial p} \tag{2.10}$$

$$- X_{K_{\dot{u}}} = \frac{1}{2} \dot{u}^t \frac{\partial K}{\partial x} \dot{u} \frac{\partial}{\partial p} \tag{2.11}$$

$$hor(\dot{u}) = \big(\frac{\partial}{\partial y} - C \frac{\partial}{\partial x} + p^t \frac{\partial C}{\partial x} \frac{\partial}{\partial p} \big) \dot{u} \tag{2.12}$$

where X_{H_0} is the Hamiltonian vector field corresponding to the case of locked control, $X_{K_{\dot{u}}}$ is the Hamiltonian vector field on V^*Q associated to $K_{\dot{u}}$ and hor is the horizontal lift of an Ehresmann connection on $\tilde{\pi} : V^*Q \longrightarrow \mathcal{S}$ entirely determined by π and the metric. These equations are exactly the control equations (2.8).

Proof: [23] □

The importance of initial impulse

In what follows let us suppose that the metric h is **bundle like**.

Proposition 2.1. *The control system* (2.8) *is of two different types depending on the value of the initial value of the x conjugate variables p.*

1. *Case* $\boxed{p(0) = 0}$
   The system (2.8) *is an affine non linear driftless control system;*
2. *Case* $\boxed{p(0) \neq 0}$
   The system (2.8) *is an affine non linear control system with drift.*

Proof: Since we have supposed to have a bundle like metric we have that

$$\frac{\partial K(y)}{\partial x} = \frac{\partial (\mathcal{B} - \mathcal{M}^t \mathcal{C}^{-1} \mathcal{M})(y)}{\partial x} = 0 \,.$$

Therefore the control equation (2.8) becomes

$$\begin{cases} \dot{x} = \mathcal{C}^{-1} p - \mathcal{C}^{-1} \mathcal{M} \dot{u} \\ \dot{p} = -\frac{1}{2} p^t \frac{\partial \mathcal{C}^{-1}}{\partial x} p + p^t \frac{\partial C}{\partial x} \dot{u} \end{cases} \tag{2.13}$$

Case $p(0) = 0$.
The function $p(t) = 0$ is the unique solution of $(2.13)_2$ according to the Cauchy theorem. Thus $(2.13)_1$ becomes a driftless control system.

$$\dot{x} = -\mathcal{C}^{-1} \mathcal{M} \dot{u}$$

It is clear that this last equation is entirely determined by the connection (see (2.4)). Therefore in the case of null initial impulse case only the geometry of the system determines its motion.
Case $p(0) \neq 0$.
In this case the equation $(2.13)_2$ has no trivial solution that is $p(t) \neq 0$. Thus $(2.13)_1$ is a non linear control system with drift determined exactly by the presence of a non zero p

$$\dot{x} = \mathcal{C}^{-1}p - \mathcal{C}^{-1}\mathcal{M}\dot{u}$$

The presence of the drift is crucial because in this case the motion of the system is determined both by the connection (given by the geometry) and by the impulse, that is non zero. This proves the importance of the initial value of p. □

In this work we analyze both the cases. The one with zero initial impulse is well studied in literature for many systems [65, 64, 44, 46, 45]. The one with $p(0) \neq 0$ is becoming of increasing interest since the presence of the impulse influences deeply the motion, as we have seen. We deal with this problem that is more complex and tricky to study because of the presence of the drift.

2.2 Model

In this section we describe in detail the way in which we modelize a 2-dim deformable body immersed in an ideal irrotational fluid.

2.2.1 System of coordinates

Let $(O, \mathbf{e}_x, \mathbf{e}_y)$ be a reference Galilean frame by which we identify the physical space to $\mathbb{R}^2$. At any time the swimmer occupies an open smooth connected domain $\mathcal{B}$ and we denote by $\mathcal{F} = \mathbb{R}^2 \setminus \bar{\mathcal{B}}$ the open connected domain of the surrounding fluid. The coordinates in $(O, \mathbf{e}_x, \mathbf{e}_y)$ are denoted with $x = (x_1, x_2)^T$ and are usually called spatial coordinates. Let us call $(-x_2, x_1)^T = x^\perp$.
Attached to the swimmer, we define also a moving frame $(O^*, \mathbf{e}_x^*, \mathbf{e}_y^*)$. Its choice is made such that its origin coincides at any time with the center of mass of the body. This frame represents the choice of the axes in the space of unlocated shapes. As we have shown before, the computation of the net rigid motion of the swimmer due to shape changes is independent from this choice that accordingly is arbitrary. The fact that this frame has always its

origin in the center of mass is a matter of convenience: indeed this choice, and others (see Remark 2.2), tell us that the body frame is the one in which the kinetic energy of the body is minimal [58].
We denote by $x^* = (x_1^*, x_2^*)^T$ the related so called body coordinates. In this frame and at any time the swimmer occupies a region $\mathcal{B}^*$ and the fluid the domain $\mathcal{F}^* := \mathbb{R}^2 \setminus \bar{\mathcal{B}}^*$.
We define also the *computational space*, that is the Argand-Gauss plane which we will need only to perform explicit calculations, endowed with the frame $(\mathbf{O}, \mathbf{E}_x, \mathbf{E}_y)$ and in which the coordinates are denoted $z = (z_1, z_2)^T$. In this space D is the unit disk and $\mathcal{O} := \mathbb{R}^2 \setminus \bar{D}$.

2.2.2 Shape changes

Banach spaces of sequences. Inspired by [65], we denote any complex sequence by $\mathbf{c} := (c_k)_{k\geq 1}$ where for any $k \geq 1$, $c_k := a_k + ib_k \in \mathbb{C}$, a_k, $b_k \in \mathbb{R}$. Most of the complex sequences we will consider live in the Banach space

$$\mathcal{S} := \big\{(c_k)_{k\geq 1} \ : \ \sum_{k\geq 1} k(|a_k| + |b_k|) < +\infty\big\}$$

endowed with its natural norm $\|\mathbf{c}\|_{\mathcal{S}} := \sum_{k\geq 1} k(|a_k| + |b_k|)$. This space is continuously embedded in

$$\mathcal{T} := \big\{(c_k)_{k\geq 1} \ : \ \sup_{z\in\partial D} \big|\sum_{k\geq 1} k c_k z^k\big| < +\infty\big\}$$

whose norm is $\|\mathbf{c}\|_{\mathcal{T}} := \sup_{z\in\partial D} |\sum_{k\geq 1} k c_k z^k|$, where D is the unit disk of the computational space.

Definition 2.2. *x We call $\mathcal{D}$ the intersection of the unit ball of $\mathcal{T}$ with the space $\mathcal{S}$.*

This space will play an important role in the description of the shape changes that will follow.
Finally we introduce also the Hilbert space

$$\mathcal{U} := \big\{(c_k)_{k\geq 1} \ : \ \sum_{k\geq 1} k(|a_k|^2 + |b_k|^2) < +\infty\big\}$$

whose norm is $\|\mathbf{c}\|_{\mathcal{U}} := \sqrt{\sum_{k\geq 1} k(|a_k|^2 + |b_k|^2)}$. According to Parseval's identity we have

$$\sum_{k\geq 1} k|c_k|^2 \leq \sum_{k\geq 1} k^2|c_k|^2 = \frac{1}{2\pi}\int_0^{2\pi} \big(\sum_{k\geq 1} kc_k e^{-ik\theta}\big)^2\, d\theta \leq \sup_{z\in\partial D} \big|\sum_{k\geq 1} kc_k z^k\big|^2$$

Therefore we have the following space inclusions

$$\mathcal{S} \subset \mathcal{T} \subset \mathcal{U}$$

We have introduced these spaces because they will be crucial in the description of the shape changes of the idealized swimmer.

Description of the shape changes

Following the line of thoughts of [65] and [25] the shape changes of the swimmer are described with respect to the moving frame $(O^*, \mathbf{e}_x^*, \mathbf{e}_y^*)$ by a $\mathcal{C}^1$ diffeomorphism $\chi(\mathbf{c})$, depending on a *shape variable* $\mathbf{c} \in \mathcal{D}$ which maps the closed unit disk $\bar{D}$ of the computational space onto the domain $\mathcal{B}^*$ in the body frame. The diffeomorphisms $\chi(\mathbf{c})$ allows us to associate to each sequence $\mathbf{c}$ a shape of the swimmer in the body frame. We can write, according to our notation, that for any $\mathbf{c} \in \mathcal{D}$ (see definition 2.2),

$$\chi(\mathbf{c}) : \mathbb{C} \supset \bar{D} \to \mathbb{R}^2 \equiv (O^*, \mathbf{e}_x^*, \mathbf{e}_y^*) \tag{2.14}$$

and $\bar{\mathcal{B}}^* = \chi(\mathbf{c})(\bar{D})$.
We now explain how to build the map $\chi(\mathbf{c})$ for any given sequence $\mathbf{c}$, see Fig 2.1.

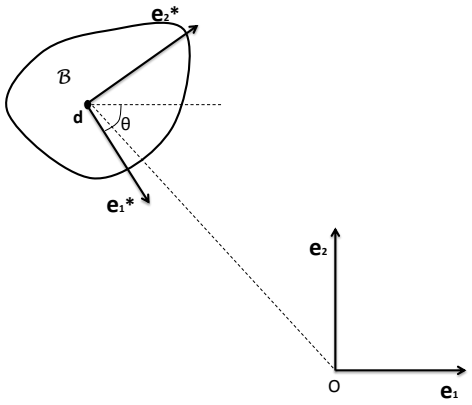

Figure 2.1: The physical space and the body frame.

Theorem 2.2 (Riemann Mapping Theorem)**.** *Let $\mathcal{K}$ be a simply connected open bounded subset of $\mathbb{C}$ with $0 \in \mathcal{K}$. Then there exists an holomorphic isomorphism $f : D \to \mathcal{K}$ with $f(0) = 0$. Any other isomorphisms with $f(0) = 0$ are of the form $z \mapsto f(rz)$ with $r \in \partial D$ a rotation. All functions f can be extended to an homeomorphism of $\bar{D}$ onto $\bar{\mathcal{K}}$ if and only if $\partial\mathcal{K}$ is a Jordan curve.*

Defining $\mathbb{C}_\infty = \{\mathbb{C} \cup \infty\}$, if $\mathcal{O} = \mathbb{C}_\infty \setminus \bar{D}$, from the isomorphism f we have also an isomorphism from D to the exterior $\mathcal{F}^*$; we apply to $\mathcal{F}^*$ the inversion $\rho(z) := \frac{1}{z}$ obtaining the open simply connected G, we find another Riemann- isomorphism $g : D \to G$ with $g(0) = 0$. Then we consider $h = \rho \circ g = \frac{1}{g} : D \to \mathcal{F}^*$. The function g is injective around zero, therefore $g^{'}(0) \neq 0$, it follows that h has a pole of the first order in zero and therefore has a Laurent expansion

$$h(z) = \frac{1}{z} + \frac{g^{''}(0)}{2} + \sum_{k=1}^{\infty} c_k z^k \tag{2.15}$$

We now have the area theorem [68]: if a function like h is injective on the punctured disk then we have

$$\sum_{k=1}^{\infty} k|c_k|^2 \leq 1 \tag{2.16}$$

If we want an isomorphism of $\mathcal{O}$ on $\mathcal{F}^*$ we take $\phi(\mathbf{c})(z) = h(\frac{1}{z})$

$$\phi(\mathbf{c})(z) = z + \sum_{k=1}^{\infty} \frac{c_k}{z^k} \tag{2.17}$$

We now suppose that the boundary of $\mathcal{B}^*$ is a Jordan curve, i.e. simple closed curve in the plane, therefore the function $\phi(\mathbf{c})$ can be extended to homeomorphism on the boundary. Now $\phi(\mathbf{c}) : \bar{\mathcal{O}} \to \mathcal{F}^*$ can be extended continuously to all $\mathbb{C}_\infty$ setting in the interior of D

$$\chi(\mathbf{c})(z) := z + \sum_{k\geq 1} c_k \bar{z}^k \,, \qquad (z \in \bar{D}) \tag{2.18}$$

Since $\bar{z} = \frac{1}{z}$ on ∂D we deduce that the following map is continuous in $\mathbb{C}$ for all $\mathbf{c} \in \mathcal{D}$:

$$\Phi(\mathbf{c})(z) := \begin{cases} \chi(\mathbf{c})(z) & \text{if } z \in D \\ \phi(\mathbf{c})(z) & \text{if } z \in \bar{\mathcal{O}} = \mathbb{C}_\infty \setminus D \end{cases} \tag{2.19}$$

Proposition 2.2. *For all $\mathbf{c} \in \mathcal{D}$, $\chi(\mathbf{c}) : \bar{D} \to \bar{\mathcal{B}}^*$ and $\phi(\mathbf{c}) : \bar{\mathcal{O}} \to \bar{\mathcal{F}}^*$ are both well defined and invertible. Further, $\chi(\mathbf{c})|_D$ is a $\mathcal{C}^1$ diffeomorphism, $\phi(\mathbf{c})|_{\mathcal{O}}$ is a conformal mapping and $\Phi(\mathbf{c})$ is an homeomorphism form $\mathbb{C}$ onto $\mathbb{C}$.*

Proof: [65] □

Remark 2.1. *Despite the generality of the Riemann Mapping Theorem, the way in which we decided to represent our diffeomorphism, lead us to some restrictions. Indeed in order to be sure that also $\chi(\mathbf{c})$ is well defined -from proposition 2.2- we need to impose the restrictive condition $\mathbf{c} \in \mathcal{D}$, see* (2.16)*, meaning that the shape variables have to be finitely bounded for both the norms of $\mathcal{S}$ and $\mathcal{T}$. To summarize we can say that to use the shape variable $\mathbf{c} \in \mathcal{D}$ allows us to describe all of the bounded non-empty connected shapes of the body that are not too far from the unit ball, accordingly to some criteria that we specify below.*

From the relation

$$x^* = \chi(\mathbf{c})(z) \,, \tag{2.20}$$

$(z \in D)$ we deduce that the area elements dx^* and dz of respectively $\mathcal{B}^*$ and D can be deduced one from the other by the identity.

$$dx^* := J(\mathbf{c})(z)dz, \quad (z \in D,\, x^* := \chi(\mathbf{c})(z))$$

where $J(\mathbf{c})(z) := |\det D\chi(\mathbf{c})(z)|$, $(z \in D)$.
The density $\rho^*_{\mathbf{c}}$ of the deformed idealized swimmer can be deduced from a given constant density $\rho_0 > 0$ by the conservation mass principle:

$$\rho^*_{\mathbf{c}}(x^*) = \frac{\rho_0}{J(\mathbf{c})(\chi(\mathbf{c})^{-1}(x^*))}, \qquad (x^* \in \mathcal{B}^*)$$

We define the element of mass in D by $dm_0 := \rho_0 dz$ and likewise $dm^* := \rho^*_{\mathbf{c}} dx^*$, is the element of mass in $\mathcal{B}^*$. Then the area of the body is given by (see 2.18)

$$Vol(\mathcal{B}) = \int_D J(\mathbf{c})(z)\, dz = \int_D 1 - \Big|\sum_{k\geq 0}(k+1)c_{k+1}\bar{z}^k\Big|^2 dz = \pi(1-\|\mathbf{c}\|^2_{\mathcal{U}}) \quad (2.21)$$

According to the incompressibility of the fluid both viewed in the physical frame $(O, \mathbf{e}_x, \mathbf{e}_y)$ and in the body frame $(O^*, \mathbf{e}^*_x, \mathbf{e}^*_y)$, its area has to be constant. We draw the same conclusion for the area of our idealized swimmer because its area is nothing but the complementary of the area of the fluid. Therefore we deduce that the function $t \mapsto \|\mathbf{c}(t)\|_{\mathcal{U}} = (\|c(0)\|_{\mathcal{U}})$ has to be constant. Thus we define the space

$$\mathcal{E}(\mu) = \big\{\mathbf{c} \in \mathcal{D} \,:\, \|\mathbf{c}\|_{\mathcal{U}} = \mu\big\} \quad (2.22)$$

moreover this set is not empty if and only if $\mu < 1$ and differentiating by time (2.21) we get an equivalent formulation for the conservation of the body area

$$\sum_{k\geq 1} k(\dot{a}_k a_k + \dot{b}_k b_k) = 0 \quad (2.23)$$

This gives us the first condition to impose on the shape changes in order to be physically allowable. Another condition is given by the fact that the motion we are considering is self-propelled, therefore the Newton's laws ensure that the linear and angular momenta of the swimmer with respect to its attached frame $(O^*, \mathbf{e}^*_x, \mathbf{e}^*_y)$ have to be and remain zero when it undergoes shape changes. Hence we get the condition

$$\frac{d}{dt}\Big(\int_{\mathcal{B}^*} x^*\, dm^*\Big) = 0 \quad (2.24)$$

which leads to

$$\int_D \dot{\chi}(\mathbf{c})\, dm_0 = 0$$

which is intrinsically satisfied since the body frame has its origin in the center of mass.

Regarding the angular momentum we find

$$\int_D \dot{\chi}(\mathbf{c}) \cdot \chi(\mathbf{c})^{\perp} \, dm_0 = 0 \tag{2.25}$$

This condition after some algebra gives the identity

$$\sum_{k \geq 1} \frac{1}{k+1} (\dot{b}_k a_k - \dot{a}_k b_k) = 0 \tag{2.26}$$

Remark 2.2 (Minimal Kinetic Energy)**.** *It is worth noting that these conditions tell us that the body frame that we have chosen is exactly the one of the minimal kinetic energy. Indeed there are two conditions to verify. The first one is that the velocity of the center of mass is null in this frame* (2.24)*. This condition is clearly satisfied by the fact that the origin of the frame coincides with the center of mass at any time. The second condition is that the angular momentum with respect to the body frame has to be null, that is exactly condition (2.25).*

Remark 2.3. *The orientation of the frame remains arbitrary and does not effect the fact that it is the frame of minimal kinetic energy. One of the most used conventions to define a possible orientation of such a system is to choose as axes the eigenvectors of the moment of inertia of our body. Obviously as we have said before this choice does not effect the located shape, since it is independent on the choice of the frame.*

These conditions lead us to give the following definition

Definition 2.3 (Physically allowable control)**.** *A smooth function $t \mapsto \mathbf{c}(t)$ is said to be physically allowable when:*

i There exist $\mu > 0$ such that $\mathbf{c}(t) \in \mathcal{E}(\mu)$ for all $t \geq 0$.

ii Constraint (2.23) and (2.26) are satisfied.

The condition i specifies in a more rigorous way what we meant by shapes near the circle in the remark (2.1).

2.2.3 Rigid motions

The overall motion of our body in the fluid is, as said before, the composition of its shape changes with a rigid motion. The shape changes have been described in the previous subsection and, as we will see, the Gauge potential A described at the beginning depends only on the shape variable $\mathbf{c}$ that is

$$A = A(\mathbf{c}) \tag{2.27}$$

this will be evident in the next sections.
The net rigid motion is described by an element of the planar euclidean group as explained in subsection 1.2.1. More precisely it is given by a translation $\mathbf{d}$, which is the position of the center of mass, and a rotation R of an angle θ, that gives the orientation of the moving frame $(O^*, \mathbf{e}_x^*, \mathbf{e}_y^*)$ with respect to the physical one.
Let the shape changes be frozen for a while and consider a physical point x attached to the body. Then there exists a smooth function $t \mapsto (\mathbf{d}(t), \theta(t))$ such that the point's coordinates in $(O, \mathbf{e}_x, \mathbf{e}_y)$ are given by $x = R(\theta)x_0 + \mathbf{d}$. Next compute the time derivative expression $(\dot{\mathbf{d}}, \dot{\theta})$. We deduce that the Eulerian velocity of the point is $\mathbf{v}_d(x) = \dot{\theta}(x - \mathbf{d})^\perp + \dot{\mathbf{d}}$. It can be also expressed in the moving frame $(O^*, \mathbf{e}_x^*, \mathbf{e}_y^*)$ and reads $\mathbf{v}_d^* = \dot{\theta}(x^*)^\perp + \dot{\mathbf{d}}^*$ where

$$\begin{pmatrix} \dot{\mathbf{d}}^* \\ \dot{\theta} \end{pmatrix} = \mathcal{R}(\theta)^T \begin{pmatrix} \dot{\mathbf{d}} \\ \dot{\theta} \end{pmatrix} \tag{2.28}$$

where $\mathcal{R}$ is an element of the euclidean group $SE(2)$ of pure rotation.

Remark 2.4. *Notice that $\dot{\mathbf{d}}^*$ is not the time derivative of some $\mathbf{d}^*$ but only a symbol to expresse the velocity $\dot{\mathbf{d}}$ in the body frame.*

Let us return to the general case where the shape changes are taken into account. We deduce that the Eulerian velocity at a point x of $\mathcal{B}$ is

$$v(x) = \dot{\theta}(x - \mathbf{d})^\perp + \dot{\mathbf{d}} + \mathcal{R}(\theta)\dot{\chi}(\mathbf{c})[\chi(\mathbf{c})^{-1}(R(\theta)^T(x - \mathbf{d}))]$$

where the last term represent the velocity of deformation and is computed deriving the relation 2.20 and taking into account that $x = R^T(\theta)x^* = R^T(\theta)\chi(\mathbf{c})(z)$. When we express this velocity in the moving frame we get

$$v^*(x^*) = (\dot{\theta}x^{*^\perp} + \dot{\mathbf{d}}^*) + \dot{\chi}(\mathbf{c})(\chi(\mathbf{c})^{-1}(x^*))\,, \tag{2.29}$$

which is more compact and will be useful in what follows.

2.2.4 Dynamics for ideal fluid

In this section we use some well known ideas developed for example in some works of A. Bressan [18], which further simplify the system of our idealized swimmer.
We assume that the shape changes of our swimmer can be described by a finite number of shape parameters, i.e. $\mathbf{c} = (c_1, \cdots, c_m)$, thus we can call $\mathbf{q} = (q_1, \cdots, q_{m+3}) = (\mathbf{d}, \theta, c_1, \cdots, c_m)$. This choice is widely spread in recent literature as in [18, 64], and implies that we focus only on a class of

deformations which consist of particular shape changes that are sufficient to describe a wide range of swimmer behaviors. Let us call $\tilde{\chi}$ the diffeomorphism which describes the superimposition of the shape changes with a rigid motion, more precisely $\tilde{\chi}(\mathbf{q})(z) := [R(\theta), \mathbf{d}] \circ \chi(\mathbf{c})(z)$ Assuming that there are no external forces, we wish to derive a system of equations describing the net motion of the body due to the shape changes and of the surrounding fluid expressed in the moving frame. Let $N = m + 3$ and

$$T(\mathbf{q}, \dot{\mathbf{q}}) = \frac{1}{2} \sum_{i,j=1}^{N} A_{i\,j}(\mathbf{q}) \dot{q}^i \dot{q}^j \tag{2.30}$$

describe the kinetic energy of the body. For simplicity, we assume that the surrounding fluid has unit density. Calling $v = v(x,t)$ its velocity at the point x, the kinetic energy of the surrounding fluid is given by

$$K = \int_{\mathcal{F}} \frac{|v(x)|^2}{2}\, dx \tag{2.31}$$

If the only active force is due to the scalar pressure p, the motion of the fluid is governed by the Euler equation for non-viscous, incompressible fluids:

$$v_t + v \cdot \nabla v = -\nabla p \tag{2.32}$$

supplemented by the incompressibility condition

$$\text{div } v = 0.$$

In addition, we need a boundary condition

$$\left\langle v - \sum_{k=1}^{N} \frac{\partial \tilde{\chi}(\mathbf{q})(z)}{\partial q_k} \dot{q}_k,\ -z \frac{\tilde{\chi}'(\mathbf{q})(z)}{|\tilde{\chi}'(\mathbf{q})(z)|} \right\rangle = 0 \tag{2.33}$$

$-z\frac{\tilde{\chi}'(\mathbf{q})(z)}{|\tilde{\chi}'(\mathbf{q})(z)|} = n(x)$, $(x = \tilde{\chi}(\mathbf{q})(z),\ z \in \partial D)$ denotes the unit outer normal to the set $\tilde{\chi}(\mathbf{c})(D) = \mathcal{B}$ at the point x, and is computed making the complex derivative of the function $\tilde{\chi}(\mathbf{q})(z)$ expressed in polar coordinates that is

$$n = i\frac{\partial_\sigma(\tilde{\chi}(\mathbf{q})(e^{i\sigma}))}{|\partial_\sigma(\tilde{\chi}(\mathbf{q})(e^{i\sigma}))|} = -e^{i\sigma}\frac{\tilde{\chi}'(\mathbf{q})(e^{i\sigma})}{|\tilde{\chi}'(\mathbf{q})(e^{i\sigma})|} = -z\frac{\tilde{\chi}'(\mathbf{q})(z)}{|\tilde{\chi}'(\mathbf{q})(z)|} \tag{2.34}$$

which states that the velocity of the fluid has to be tangent to the surface of the body. To find the evolution of the coordinate $\mathbf{q}$, we observe that

$$\frac{d}{dt}\frac{\partial T}{\partial \dot{q}_k} = \frac{\partial T}{\partial q_k} + F_k \qquad k = 1 \cdots N \tag{2.35}$$

where T is the kinetic energy of the body and F_i are the components of the external pressure forces acting on the boundary of $\mathcal{B}$. To determine these forces, we observe that, in connection with a small displacement of the q^i coordinate, the work done by the pressure forces is

$$\delta W = -\delta q^k \cdot \int_{\partial D} \left\langle -z\frac{\tilde{\chi}'(\mathbf{q})(z)}{|\tilde{\chi}'(\mathbf{q})(z)|}, \frac{\partial \tilde{\chi}(\mathbf{q})}{\partial q_k}(z) \right\rangle p(\tilde{\chi}(\mathbf{q})(z))J(\mathbf{q})(z)\, d\sigma \quad (2.36)$$

The equations of motion for are

$$\frac{d}{dt}\frac{\partial T}{\partial \dot{q^k}} = \frac{\partial T}{\partial q^k} - \int_{\partial D} \left\langle -z\frac{\tilde{\chi}'(\mathbf{q})(z)}{|\tilde{\chi}'(\mathbf{q})(z)|}, \frac{\partial \tilde{\chi}(\mathbf{q})}{\partial q_k}(z) \right\rangle p(\tilde{\chi}(\mathbf{q})(z))J(\mathbf{q})(z)\, d\sigma \quad (2.37)$$

We now show that, in the case of irrotational flow, the coupled system can be reduced to a finite dimensional impulsive Lagrangian system. It is well known (see [43, 60]) that the velocity field of the fluid can be determined by setting $v = \nabla\psi$ and solving the Neumann problem in the exterior domain

$$\begin{cases} \Delta\psi = 0 & x \in \mathcal{F} \\ n \cdot \nabla\psi = n \cdot v(x)|_{x=\tilde{\chi}(\mathbf{q})(z)} & x \in \partial\mathcal{B} \\ |\psi| \to 0 & |x| \to \infty \end{cases} \quad (2.38)$$

where the boundary condition reads

$$n \cdot v(x) = -z\frac{\tilde{\chi}'(\mathbf{q})(z)}{|\tilde{\chi}'(\mathbf{q})(z)|} \cdot \sum_k \frac{\partial \tilde{\chi}(\mathbf{q})}{\partial q_k}(z)\dot{q_k} \quad (2.39)$$

Let us now consider the function $\tilde{\phi}(\mathbf{q}) : \mathbb{R}^2 \setminus D \to \mathbb{R}^2$ defined by the composition of $\phi(\mathbf{q})(z)$ with the rigid motion $[R, \mathbf{d}]$, that clearly on the boundary of D coincides with the function $\tilde{\chi}(\mathbf{q})$. From the linearity of (2.38) the solution will be linear in $\dot{\mathbf{q}}$.

$$\psi(z, \mathbf{q}, \dot{\mathbf{q}}) = \sum_{k=1}^{N} \gamma_k(z, \mathbf{q})\dot{q_k} \quad (2.40)$$

The motion of the fluid can be obtained by solving the ordinary differential equation

$$\frac{d}{dt}\tilde{\phi}(\mathbf{q})(z) = \frac{\partial \psi}{\partial x^L}(x, \mathbf{q}, \dot{\mathbf{q}})|_{x=\tilde{\phi}(\mathbf{q})(z)} \quad (2.41)$$

precisely

$$v_L(x, \mathbf{q}, \dot{\mathbf{q}}) = \sum_k \frac{\partial \tilde{\phi}(\mathbf{q})}{\partial q_k}(z)\dot{q_k} = \sum_k \frac{\partial \gamma_k}{\partial x^L}(x, \mathbf{q})\dot{q_k}|_{x=\tilde{\phi}(\mathbf{q})(z)} \quad (2.42)$$

This has to be true for all curve $\mathbb{R} \ni t \longmapsto \mathbf{q}(t)$, with $\mathbf{c}$ as in definition (2.3) thus we have

$$\frac{\partial \tilde{\phi}(\mathbf{q})}{\partial q_k}(z) = \frac{\partial \gamma_k}{\partial x^L}(x, \mathbf{q})|_{x=\tilde{\phi}(\mathbf{q})(z)} \tag{2.43}$$

We now prove that the term of the equations of motion relative to the pressure forces is a kinetic term

$$\begin{aligned} F_k = &- \int_{\partial D} -z \frac{\tilde{\phi}'(\mathbf{q})(z)}{|\tilde{\phi}'(\mathbf{q})(z)|} \frac{\partial \tilde{\phi}(\mathbf{q})}{\partial q_k}(z) p(\tilde{\phi}(\mathbf{q})(z)) J(\mathbf{q})(z)\, d\sigma = \\ &- \int_{\partial D} -z \frac{\tilde{\phi}'(\mathbf{q})(z)}{|\tilde{\phi}'(\mathbf{q})(z)|} \frac{\partial \gamma_k}{\partial x^L}(\tilde{\phi}(\mathbf{q})(z)) p(\tilde{\phi}(\mathbf{q})(z)) J(\mathbf{q})(z)\, d\sigma = \\ &= - \int_{\partial \mathcal{B}} n^L(x) \frac{\partial \gamma_k}{\partial x^L} p\, dx \end{aligned} \tag{2.44}$$

applying the divergence theorem to (2.44)

$$\begin{aligned} &= \int_{x \in \mathcal{F}} \frac{\partial}{\partial x^L} \left(\frac{\partial \gamma_k}{\partial x^L} p \right) dx = \int_{x \in \mathcal{F}} \big(p \underbrace{\Delta \gamma_k}_{=0} + \nabla \gamma_k \cdot \nabla p \big)\, dx = \\ &= \int_{x \in \mathcal{F}} \nabla \gamma_k \cdot \nabla p\, dx = \int_{z \in \mathbb{R}^2 \setminus D} \frac{\partial \tilde{\phi}(\mathbf{q})}{\partial q_k} \cdot \big(-v_{,t} - v \cdot \nabla v \big) \hat{J}(\mathbf{q})(z)\, dz = \\ &= - \int_{z \in \mathbb{R}^2 \setminus D} \frac{\partial \tilde{\phi}(\mathbf{q})}{\partial q_k} \cdot \frac{d}{dt} v \hat{J}(\mathbf{q})(z)\, dz = \\ &= - \int_{z \in \mathbb{R}^2 \setminus D} \left[\frac{d}{dt} \left(\frac{\partial \tilde{\phi}(\mathbf{q})_L}{\partial q_k} v_L \right) - v_L \frac{\partial^2 \tilde{\phi}(\mathbf{q})}{\partial q_j \partial q^k} \dot{q}_k \right] \hat{J}(\mathbf{q})(z)\, dz \end{aligned}$$

where $\hat{J}(\mathbf{q})(z)$ is the determinant of the jacobian matrix of the function $\tilde{\phi}(\mathbf{c})(z)$. Let us define

$$T^f = \frac{1}{2} \int_{x \in \mathcal{F}} |v|^2\, dx = \frac{1}{2} \sum_{i,j}^{N} \tilde{A}_{i\,j} \dot{q^i} \dot{q^j}$$

then

$$F_k = -\Big(\frac{d}{dt} \int_{x \in \mathcal{F}} \frac{\partial |v|^2}{\partial \dot{q^k}}\, dx - \int_{x \in \mathcal{F}} \frac{\partial |v|^2}{\partial q^k}\, dx \Big) = -\frac{d}{dt} \frac{\partial T^f}{\partial \dot{q^k}} + \frac{\partial T^f}{\partial q^k}$$

In conclusion the system body+fluid is geodesic of Lagrangian

$$T = T^{body} + T^f \tag{2.45}$$

In what follows for simplicity we will express all the quantities in the moving frame $(O^*, \mathbf{e}_x^*, \mathbf{e}_y^*)$, denoting the total kinetic energy in this frame as $\overset{*}{T}$. We will now compute explicitly the Lagrangian. Let us start with the kinetic energy of the swimmer. Since we have chosen the body frame as the one of minimal kinetic energy, according to Konig theorem, there is a decoupling between the kinetic energy of the body due to its rigid motion and that due to its shape changes, recalling (2.30):

$$\overset{*}{T}^{body} := \frac{1}{2}m|\dot{\mathbf{d}}^*|^2 + \frac{1}{2}I(\mathbf{c})\dot{\theta}^2 + \frac{1}{2}\int_{\mathcal{B}^*}\left|\dot{\chi}(\mathbf{c})(\chi(\mathbf{c})^{-1}(x^*))\right|^2 dm^* \tag{2.46}$$

where $I(\mathbf{c})$ is the moment of inertia of the body thought as rigid with frozen shape, and the last term being the kinetic energy of deformation. It can be computed as follows:

$$\int_{\mathcal{B}^*}\left|\dot{\chi}(\mathbf{c})(\chi(\mathbf{c})^{-1}(x^*))\right|^2 dm^* = \int_D \left|\dot{\chi}(\mathbf{c})(z)\right|^2 dm_0 = \pi\rho_0 \sum_{k=1}^{m} \frac{|\dot{c}_k|^2}{k+1}$$

where we used the formula (2.18) to compute the integral. Note that accordingly to remark (2.3) the kinetic energy of the body in the frame $(O^*, \mathbf{e}_x*, \mathbf{e}_y^*)$ does not depend on the orientation of the frame but only on its angular velocity.

Kinetic energy of the fluid

Since we are interested on the effect of the shape changes of the swimmer on the fluid, in this subsection we will compute all the quantities in the body frame. As we have seen in subsection 1.2.1 we can recover the rigid motion of the swimmer due to its deformation, exploiting the Gauge potential.
The kinetic energy of the fluid reads

$$\overset{*}{T}^{f} := \frac{1}{2}\int_{\mathcal{F}^*} |u^*|^2 \, dm_f^* = \frac{1}{2}\int_{\mathcal{F}^*} |\nabla\psi^*|^2 \, dm_f^* \tag{2.47}$$

There $u^* = \nabla\psi^*$ and ψ^* is the solution of the Neumann problem

$$\begin{cases} \Delta\psi^* = 0 & x \in \mathcal{F}^* \\ n(x^*)\cdot\nabla\psi^* = n(x^*)\cdot v(x^*)|_{x^*=\chi(\mathbf{q})(z)} & x^* \in \partial\mathcal{B}^* \\ |\psi^*| \to 0 & |x^*| \to \infty \end{cases} \tag{2.48}$$

which is the same Neumann problem (2.38) expressed in the body frame. Indeed since the Laplacian operator is invariant under rototranslations, the function $\psi^*(x^*) = \psi([R(\theta), \mathbf{d}](x))$ is harmonic.

We will use complex analysis to compute the potential function ψ^*. We define the function $\xi(z) := \psi^*(\phi(\mathbf{c})(z))$, $(z \in \mathcal{O})$, where ψ^* is the potential function defined in (2.48) expressed in the moving frame and recalling (2.17) $\phi(\mathbf{c})(z)$ is the conformal map from $\bar{\mathcal{O}} = \mathbb{C} \setminus D$ to the external domain $\mathcal{F}^*$. According to classical properties of conformal mappings, the function ξ is harmonic in $\mathcal{O}$ and the following equality holds:

$$\frac{1}{2}\int_{\mathcal{F}^*} |\nabla\psi^*|^2 \, dm_f^* = \frac{1}{2}\int_{\mathcal{O}} |\nabla\xi|^2 \, dm_f^0 \tag{2.49}$$

The main advantage of this substitution is that ξ is defined in the fixed domain $\mathcal{O}$, whereas ψ^* was defined in $\mathcal{F}^*$ depending on $\mathbf{c}$.
In the moving frame is now easier to compute explicitly the boundary condition of the Neumann problem. The outer normal to $\partial\mathcal{B}^*$ is, recalling (2.34)

$$n(x^*) := n_1(x^*) + in_2(x^*) = -z\frac{\phi^{'}(\mathbf{c})(z)}{|\phi^{'}(\mathbf{c})(z)|} \tag{2.50}$$

where $\phi^{'}(\mathbf{c})(z)$ is the complex derivative of $\phi(\mathbf{c})$. Recalling the following identity

$$\frac{\partial_n \xi_j^r(z)}{|\phi^{'}(\mathbf{c})(z)|} = \partial_n \psi_j^{*^r}(x^*) \qquad (x^* = \phi(\mathbf{c})(z)) \tag{2.51}$$

and taking into account the expression (2.29) of v^*, we deduce that the Neumann boundary condition (2.39) reads

$$\begin{aligned}\partial_n\xi(z) = \nabla\xi \cdot n = &-\dot{d}_1^*\Re(z\phi^{'}(\mathbf{c})(z)) - \dot{d}_2^*\Im(z\phi^{'}(\mathbf{c})(z)) - \dot{\theta}\Im(\overline{\phi(\mathbf{c})(z)}z\phi^{'}(\mathbf{c})(z)) \\ &- \Re(\overline{\dot{\chi}(\mathbf{c})}z\phi^{'}(\mathbf{c})(z)) \, .\end{aligned} \tag{2.52}$$

This equality leads us to introduce the functions $\xi_j^r(\mathbf{c})\,(j = 1, 2, 3)$ and $\xi^d(\mathbf{c})$ as being harmonic in $\mathcal{O}$ and satisfying the following Neumann boundary conditions:

$$\partial_n\xi_1^r(\mathbf{c})(z) = -\Re(z\phi^{'}(\mathbf{c})(z)), \tag{2.53}$$

$$\partial_n\xi_2^r(\mathbf{c})(z) = -\Im(z\phi^{'}(\mathbf{c})(z)), \tag{2.54}$$

$$\partial_n\xi_3^r(\mathbf{c})(z) = -\Im(\overline{\phi(\mathbf{c})(z)}z\phi^{'}(\mathbf{c})(z)), \tag{2.55}$$

$$\partial_n\xi^d(\mathbf{c})(z) = -\Re(\overline{\dot{\chi}(\mathbf{c})}z\phi^{'}(\mathbf{c})(z)), \qquad (z \in \partial D). \tag{2.56}$$

In this way we spilt the harmonicity and the Neumann boundary conditions of the function ξ into the same properties for the functions $\xi_j^r(\mathbf{c})\,(j = 1, 2, 3)$

and $\xi^d(\mathbf{c})$.
Next we have for all $\mathbf{c} \in \mathcal{D}$

$$\Re(\overline{\dot{\chi}(\mathbf{c})} z\phi^{'}(\mathbf{c})(z)) = \sum_{k=1}^{m} \dot{a}_k \Re(z^{k+1}\phi^{'}(\mathbf{c})(z)) + \dot{b}_k \Im(z^{k+1}\phi^{'}(\mathbf{c})(z))$$

We introduce therefore the functions $\xi_k^a(\mathbf{c})$ and $\xi_k^b(\mathbf{c})$, harmonic in $\mathcal{O}$ and satisfying the boundary conditions:

$$\partial_n \xi_k^a(\mathbf{c})(z) = -\Re(z^{k+1}\phi^{'}(\mathbf{c})(z)) - ka_k \tag{2.57}$$
$$\partial_n \xi_k^b(\mathbf{c})(z) = -\Im(z^{k+1}\phi^{'}(\mathbf{c})(z)) - kb_k \tag{2.58}$$

The extra terms ka_k, kb_k have to be added for the boundary data to satisfy the so called *compatibility condition* - $\int_{\partial\mathcal{B}^*} n(x^*) \cdot v^*(x^*)\, dx^* = 0$ - necessary to ensure the well-posedness of the Neumann problems. Observe that under condition (2.26) we recover

$$\sum_{k=1}^{m} \dot{a}_k \partial_n \xi_k^a(\mathbf{c}) + \dot{b}_k \partial_n \xi_k^b(\mathbf{c}) = \partial_n \xi^d(\mathbf{c}) \tag{2.59}$$

Starting from the relations (2.53) - (2.55) on the normal derivatives $\partial_n \xi_i^r$ $i = 1, 2, 3$ and from the relation above for $\partial_n \xi^d$, we would like to gain the same property of linearity for the function ξ.

Proposition 2.3 (Potential decomposition)**.** *According to the* ***Kirchhoff law*** *the formulas* (2.53) - (2.55) *and* (2.59) *imply that for any allowable control (in the sense of (2.3)) the following identities hold in the sobolev space* $H^1(\mathcal{O})$*:*

$$\xi(\mathbf{c}) = \dot{d}_1^* \xi_1^r(\mathbf{c}) + \dot{d}_2^* \xi_2^r(\mathbf{c}) + \dot{\theta}\xi_3^r(\mathbf{c}) + \langle \xi^d(\mathbf{c}), \dot{\mathbf{c}} \rangle, \tag{2.60}$$
$$\langle \xi^d(\mathbf{c}), \dot{\mathbf{c}} \rangle = \sum_{k=1}^{m} \dot{a}_k \xi_k^a(\mathbf{c}) + \dot{b}_k \xi_k^b(\mathbf{c}). \tag{2.61}$$

From the linearity of this expression with respect to $\dot{\mathbf{d}}^*$, $\dot{\theta}$, $\dot{\mathbf{c}}$ and since the gradient function preserves the linearity, we deduce that the kinetic energy of the fluid is a quadratic function of $\dot{\mathbf{d}}^*$, $\dot{\theta}$, $\dot{\mathbf{c}}$.

2.2.5 The Gauge potential and the equations of motion

According to what proved in the preceding section the Lagrangian of our system is a quadratic form in $(\dot{\mathbf{d}}^*, \dot{\theta}, \dot{\mathbf{c}})$, therefore it can be written in blocks

as follows

$$\overset{*}{T}(\dot{\mathbf{d}}^*, \dot{\theta}, \dot{\mathbf{c}}) = \frac{1}{2}\Big((\dot{\mathbf{d}}^{*^T}, \dot{\theta})\mathbb{M}_r(\mathbf{c})\begin{pmatrix}\dot{\mathbf{d}}^* \\ \dot{\theta}\end{pmatrix} + 2(\dot{\mathbf{d}}^{*^T}, \dot{\theta})\mathbb{N}(\mathbf{c})\dot{\mathbf{c}} + \dot{\mathbf{c}}^T\mathbb{M}_d(\mathbf{c})\dot{\mathbf{c}}\Big) \quad (2.62)$$

where $\mathbb{M}_r$, $\mathbb{N}$ and $\mathbb{M}_d$ play the role of the matrices $\mathcal{C}$ $\mathcal{M}$ and $\mathcal{B}$, introduced in the section 2.1.1, respectively

Remark 2.5. *It is worth noting that in the physical space the kinetic energy is*

$$T(\mathbf{d}, \theta, \mathbf{c}, \dot{\mathbf{d}}, \dot{\theta}, \dot{\mathbf{c}})$$

When it is expressed in the body frame instead it becomes

$$\overset{*}{T}(\mathbf{c}, \dot{\mathbf{d}}^*, \dot{\theta}, \dot{\mathbf{c}})$$

This expression does not depend on $\mathbf{d}$ *and* θ *due to the symmetry of our model with respect to the position and orientation of the body in the fluid.*

As we have seen in the first section we are interested in determining the Gauge potential A associated to our system which is

$$A = \mathcal{R}^{-1}\frac{d\mathcal{R}}{dt} = \dot{\theta}\begin{pmatrix}\begin{pmatrix}0 & 1\\ -1 & 0\end{pmatrix} & R(\theta)^T\begin{pmatrix}\dot{d}_1\\ \dot{d}_2\end{pmatrix}\\ 0\quad 0 & 0\end{pmatrix} = \dot{\theta}\begin{pmatrix}\begin{pmatrix}0 & 1\\ -1 & 0\end{pmatrix} & \begin{pmatrix}\dot{d}_1^*\\ \dot{d}_2^*\end{pmatrix}\\ 0\quad 0 & 0\end{pmatrix} \quad (2.63)$$

Since all the matrices $\mathbb{M}_r$, $\mathbb{N}$ and $\mathbb{M}_d$ depend only on $\mathbf{c}$, the kinetic energy is independent from $\mathbf{d}$ and θ and the metric that it defines is **bundle like** (see Definition 2.1). In the principal fiber bundle $SE(2) \times \mathcal{S} \to \mathcal{S}$, the Gauge potential A depends on the kinetic energy, through the equations of motion, therefore also A does not depend on the state variables.
We now need to determine $(\dot{d}_1^*, \dot{d}_2^*, \dot{\theta})$. In order to do this we compute the Hamiltonian associated to the Lagrangian function performing a partial legendre transformation on the $\dot{\mathbf{q}}^*$ variables.
Before passing to formal calculations we recall how to interpret the connection introduced before in the cotangent bundle setting following the steps presented in subsection 2.1.1. This construction was presented also in [23, 61]. Let VQ be the vertical subbundle and V^*Q the dual of VQ. Denote with $p_Q : T^*Q \longrightarrow Q$ the cotangent projection and set $\tilde{\pi} := \pi \circ p_Q$, $\tilde{\pi} : V^*Q \longrightarrow \mathcal{S}$. If $(\mathbf{d}, \theta, \mathbf{c})$ are local fibered coordinates on Q, $(\mathbf{d}, \theta, \mathbf{c}, \mathbf{p}^*)$ are local fibered coordinates on V^*Q. Suppose that a control vector field $\dot{\mathbf{c}}$ is given on $\mathcal{S}$ and that the path $\mathbf{c}(t)$ is an integral curve of $\dot{\mathbf{c}}$. Then the equations of motion

are the local expression of a vector field $D_{\dot{\mathbf{c}}}$ over V^*Q that projects on $\dot{\mathbf{c}}$ by $\tilde{\pi}$. Moreover the field $D_{\dot{\mathbf{c}}}$ is tangent to the fiber of $\tilde{\pi}$ only if the control is vanishing.
Recalling that $\mathbf{q} = (q_1, \cdots, q_{m+3}) = (\mathbf{d}, \theta, \mathbf{c})$

$$\mathbf{p}^* = \left(\frac{\partial \overset{*}{T}}{\partial \dot{q}_i^*}\right)_{i=1,2,3} = \mathbb{M}_r(\mathbf{c}) \begin{pmatrix} \dot{\mathbf{d}}^* \\ \dot{\theta} \end{pmatrix} + \mathbb{N}(\mathbf{c})\dot{\mathbf{c}}$$

which defines the translational and angular impulses of the system body plus fluid. From this we obtain

$$\begin{pmatrix} \dot{\mathbf{d}}^* \\ \dot{\theta} \end{pmatrix} = \mathbb{M}_r^{-1}(\mathbf{c})\mathbf{p}^* - \mathbb{M}_r^{-1}(\mathbf{c})\mathbb{N}(\mathbf{c})\dot{\mathbf{c}} \tag{2.64}$$

This expression is very convenient to study the motion of the shape-changing body since it gives the velocity with respect to the shape variable.

It is easy to recognize the terms of the sum in which the control equations are split according to Theorem 2.1 :

$$X_{H_0} = \begin{pmatrix} \mathbb{M}_r^{-1}(\mathbf{c})\mathbf{p}^* \\ \underline{0} \end{pmatrix} \qquad X_{K_{\dot{\mathbf{c}}}} = 0$$

and

$$hor(\dot{\mathbf{c}}) = \begin{pmatrix} -\mathbb{M}_r^{-1}(\mathbf{c})\mathbb{N}(\mathbf{c})\dot{\mathbf{c}} \\ \dot{\mathbf{c}} \end{pmatrix}$$

Note thus that we are exactly in the case of a **bundle-like metric** Therefore the equations of motion regarding the state variables are exactly the ones given by formula (2.64).

To obtain the equations of motion regarding the conjugate variables, we follow the method explained in Lamb [57] and Munnier [65]: we introduce $\mathbf{P}$ and Π, the translational and angular impulses, as well as $\mathbf{L}$ and Λ, the impulses relating to the deformations:

$$\begin{gathered} \begin{pmatrix} \mathbf{P} \\ \Pi \end{pmatrix} = \mathbb{M}_r(\mathbf{c}) \begin{pmatrix} \dot{\mathbf{d}}^* \\ \dot{\theta} \end{pmatrix} \qquad \begin{pmatrix} \mathbf{L} \\ \Lambda \end{pmatrix} = \mathbb{N}(\mathbf{c})\dot{\mathbf{c}} \\ \mathbf{p}^* = \begin{pmatrix} \mathbf{P} + \mathbf{L} \\ \Pi + \Lambda \end{pmatrix} \end{gathered} \tag{2.65}$$

We start from the Lagrange equations

$$\frac{d}{dt}\frac{\partial T}{\partial \dot{q}_i} - \frac{\partial T}{\partial q_i} = 0, \qquad i = 1, 2, 3$$

and recall that $\overset{*}{T}(\mathbf{c}, \dot{\mathbf{d}}^*, \dot{\theta}, \dot{\mathbf{c}}) = T(\mathbf{c}, R(\theta)\dot{\mathbf{d}}^*, \dot{\theta}, \dot{\mathbf{c}})$.
Therefore recalling that $\partial_\theta R(\theta) = -R(\frac{\pi}{2})R(\theta)$

$$\begin{aligned}
\frac{d}{dt}\frac{\partial T}{\partial \dot{\mathbf{d}}} - \frac{\partial T}{\partial \mathbf{d}} &= \frac{d}{dt}\Big(\frac{\partial \overset{*}{T}}{\partial \dot{\mathbf{d}}^*}R(\theta)\Big) = \frac{d}{dt}(\mathbf{P}+\mathbf{L}) - \dot{\theta}(\mathbf{P}+\mathbf{L})^\perp \\
\frac{d}{dt}\frac{\partial T}{\partial \dot{\theta}} - \frac{\partial T}{\partial \mathbf{d}} &= \frac{d}{dt}(\frac{\partial \overset{*}{T}}{\partial \dot{\theta}}) - R(\theta)^T\dot{\mathbf{d}}\cdot(\mathbf{P}+\mathbf{L})^\perp = \\
&= \frac{d}{dt}(\Pi+\Lambda) - \dot{\mathbf{d}}^*\cdot(\mathbf{P}+\mathbf{L})^\perp
\end{aligned} \tag{2.66}$$

from these equations we get

$$\begin{aligned}
\frac{d}{dt}\begin{pmatrix} p_1^* \\ p_2^* \end{pmatrix} + \dot{\theta}\begin{pmatrix} -p_2^* \\ p_1^* \end{pmatrix} = 0 \\
\frac{d}{dt}p_3^* - \dot{d}_2^* p_1^* + d_1^* p_2^* = 0
\end{aligned} \tag{2.67}$$

Therefore the equations of motion in the body coordinates are

$$\begin{cases}
\begin{pmatrix} \dot{\mathbf{d}}^* \\ \dot{\theta} \end{pmatrix} = \mathbb{M}_r^{-1}(\mathbf{c})\mathbf{p}^* - \mathbb{M}_r^{-1}(\mathbf{c})\mathbb{N}(\mathbf{c})\dot{\mathbf{c}} \\
\dot{p}_1^* = \dot{\theta}p_2^* \\
\dot{p}_2^* = -\dot{\theta}p_1^* \\
\dot{p}_3^* = \dot{d}_2^* p_1^* - \dot{d}_1^* p_2^*
\end{cases} \tag{2.68}$$

Notice that these equations are exactly the ones presented in [64] which describe the evolution of the state and the conservation of the impulse.

Equivalence in using real shape variables or complex ones

Since we are interested in studying small deformation around a circular shape, see remark 2.1, in order to describe it we can also try to express the distance of each point on the boundary of the circle in function of the shape parameters $\mathbf{c} = \mathbf{a} + i\mathbf{b}$. Let us consider deformation described by m shape parameters. According to formula (2.18) the deformation can be written as:

$$\chi(\mathbf{c})(z) = z + \sum_{k=1}^{m} c_k \bar{z}^k \quad \text{for } z \in D$$

therefore the modulus of a point on the boundary described in polar coordinates by $z = e^{i\sigma}$ is given by

$$\begin{aligned}|\chi(\mathbf{c})(z)|^2 =&(z + \sum_{k=1}^{m} c_k \bar{z}^k)(\bar{z} + \sum_{k=1}^{m} \bar{c}_k z^k) = \\ &\Big(1 + \sum_{k=1}^{m} (a_k \cos((k+1)\sigma) + b_k \sin((k+1)\sigma)) \\ &+ \sum_{h,k=1}^{m} (a_k + ib_k)(a_h - ib_h)\Big)\end{aligned} \tag{2.69}$$

taking the square root and using the Taylor expansion around $\mathbf{c} = \underline{0}$ which corresponds to the circular shape we obtain

$$|\chi(\mathbf{c})(z)| = \big(1 + \sum_{k=1}^{m} (\frac{a_k}{2} \cos((k+1)\sigma) + \frac{b_k}{2} \sin((k+1)\sigma))\big) + \sum_{k=1}^{m} o(c_k^2) \tag{2.70}$$

where we can neglect all the terms of order grater or equal than 2 supposing a_k, b_k small for all k, for example of order ϵ.

Remark 2.6. *Following this construction we have that to each complex shape parameter correspond two real ones, i.e its real and immaginary part. Therefore in practice to describe the deformation of the swimmer we need to prescribe both the real and immagineary part of each complex number c_k.*

For example in the case $m = 2$ taking

$$a_1 = 2\epsilon s_1 \qquad b_1 = 0 \qquad a_2 = 2\epsilon s_2 \qquad b_2 = 2\epsilon s_3 \tag{2.71}$$

we find exactly the formula for the swimmer deformation proposed by Mason and Burdick in ([64]).

$$F(\sigma, s) = \big[1 + \epsilon(s_1 \cos(2\sigma) + s_2 \cos(3\sigma) + s_3 \sin(3\sigma))\big] \tag{2.72}$$

Note that in this specific case we do not need to impose the conservation of area and of linear momentum because the two conditions (2.23) and (2.26) are not necessary if we neglect any contribution of order ϵ^2.

This proves the equivalence of using the complex shape variables $\mathbf{c}$ or the real ones $\mathbf{s}$ for deformations near the identity i.e., a_k and b_k of order ϵ. Therefore we can use both the constructions depending on what we need.

We can express the equations of motion (2.68) using the real parameters s_k as shape parameters instead of c_k obtaining:

$$\begin{cases} \begin{pmatrix} \dot{\mathbf{d}}^* \\ \dot{\theta} \end{pmatrix} = \bar{\mathbb{M}}_r^{-1}(\mathbf{s})\mathbf{p}^* - \bar{\mathbb{M}}_r^{-1}(\mathbf{s})\bar{\mathbb{N}}(\mathbf{s})\dot{\mathbf{s}} \\ \dot{p}_1^* = \dot{\theta} p_2^* \\ \dot{p}_2^* = -\dot{\theta} p_1^* \\ \dot{p}_3^* = \dot{d}_2^* p_1^* - \dot{d}_1^* p_2^* \end{cases} \tag{2.73}$$

where the matrices $\bar{\mathbb{M}}_r$ and $\bar{\mathbb{N}}$ have the same physical meaning of the matrices $\mathbb{M}_r$ and $\mathbb{N}$ but are expressed using the real shape parameters $\mathbf{s}$.
From now on we focus only on shape transformations near the identity, like (2.72) so that we can use real shape parameters to describe the deformation of the system.

Curvature of the connection: geometric and dynamic phase

In this subsection we deal with the problem of having a net motion performing cyclical shape changes. Looking at equations $(2.73)_1$ is evident that there are two contributions: the one of $\overline{\mathbb{M}}_r^{-1}(\mathbf{s})\mathbf{p}^*$ which involves the impulse and $-\overline{\mathbb{M}}_r^{-1}(\mathbf{s})\overline{\mathbb{N}}(\mathbf{s})\dot{\mathbf{s}}$ which is entirely geometrical.

- $\boxed{\mathbf{p}^* = 0}$

  First, let us suppose that the system starts with zero initial impulse, i.e. $\mathbf{p}^*(0) = 0$. With this assumption the last three equations of the system (2.73) have as unique solution the null one therefore, the first term of equation $(2.73)_1$ vanishes and the infinitesimal relationship between shape changes and body velocity is described by the local form of the connection computed above. Moreover we take into account the reconstruction relation (2.28), which links the state velocity expressed in the body frame with the one expressed in the physical frame,

  $$\dot{g} = \begin{pmatrix} \dot{\mathbf{d}} \\ \dot{\theta} \end{pmatrix} = - \begin{pmatrix} R(\theta) & 0 \\ 0 & 1 \end{pmatrix} \overline{\mathbb{M}}_r^{-1}(\mathbf{s})\overline{\mathbb{N}}(\mathbf{s})\dot{\mathbf{s}} = -gA_i(\mathbf{s})\dot{s}^i \tag{2.74}$$

  where g is an element of the planar euclidean group $SE(2)$. From these we recognize the expression of the Gauge potential (1.13).
  We would like to find a solution for this equations that will aid in designing or evaluating motions that arise from shape variations. Because

$SE(2)$ is a Lie group this solution will generally have the form

$$g(t) = g(0)e^{z(t)}$$

where $z \in se(2)$, the Lie algebra relative to $SE(2)$. An expansion for the Lie algebra valued function $z(t)$ is given by the Campbell-Hausdorff formula

$$z = \bar{A} + \frac{1}{2}\overline{[\overline{A}, A]} + \frac{1}{3}\overline{[[\overline{A}, A], A]} + \frac{1}{12}[\overline{A}, \overline{[\overline{A}, A]}] + \cdots \tag{2.75}$$

$$\overline{A}(t) \equiv \int_0^t A(\tau)\dot{\mathbf{s}}(\tau)\, d\tau$$

To obtain useful results in the spatial coordinates, examine the group displacement resulting from a periodic path $\alpha : [0, T] \to \mathbb{R}^m$, such that $\alpha(0) = \alpha(T)$. Taylor expand A_i about $\alpha(0)$ and then regroup, simplify, apply integration by parts and use that the path is cyclic

$$z(\alpha) = -\frac{1}{2}F_{ij}(\alpha(0)) \int_\alpha ds^i\, ds^j + \frac{1}{3}(F_{ij,k} - [A_i, F_{jk}])(\alpha(0)) \int_\alpha ds^i\, ds^j\, ds^k + \cdots \tag{2.76}$$

where

$$F_{ij} \equiv A_{j,i} - A_{i,j} - [A_i, A_j] \tag{2.77}$$

is called **curvature of the connection**.
For proportionally small deformations, the displacement experienced during one deformation cycle is:

$$g_{disp} = e^{z(\alpha)} \approx \exp\Big(-\frac{1}{2}F_{ij}(\alpha(0)) \int_\alpha ds^i\, ds^j\Big) \tag{2.78}$$

If the curvature F is not null this displacement gives us the so called **geometric phase** that is the statement of the well-known Ambrose-Singer theorem [22].

- $\boxed{\mathbf{p}^* \neq 0}$

Let now suppose that the system starts with an initial impulse which is non zero. Thus the last three equations of (2.73) are not trivial. First of all we need to integrate this equations, which in function of the deformation $\mathbf{s}$ and $\dot{\mathbf{s}}$ take the form

$$\begin{cases} \dot{p}_1^* = \big(\overline{\mathbb{M}}_r^{-1}(\mathbf{s})\mathbf{p}^*\big)_3 p_2^* - \big(A(\mathbf{s})\dot{\mathbf{s}}\big)_3 p_2^* \\ \dot{p}_2^* = -\big(\overline{\mathbb{M}}_r^{-1}(\mathbf{s})\mathbf{p}^*\big)_3 p_1^* + \big(A(\mathbf{s})\dot{\mathbf{s}}\big)_3 p_1^* \\ \dot{p}_3^* = \big(\overline{\mathbb{M}}_r^{-1}(\mathbf{s})\mathbf{p}^*\big)_2 p_1^* - \big(A(\mathbf{s})\dot{\mathbf{s}}\big)_2 p_1^* - \big(\overline{\mathbb{M}}_r^{-1}(\mathbf{s})\mathbf{p}^*\big)_1 p_2^* + \big(A(\mathbf{s})\dot{\mathbf{s}}\big)_1 p_2^* \end{cases} \tag{2.79}$$

these can be solved once the shape $\mathbf{s}$ is prescribed as a function of time, and as before we choose a periodic shape path $\alpha : [0, T] \to \mathbb{R}^m$,with $\alpha(0) = \alpha(T)$.
Let us now consider the equations of motion regarding the state variables. We have both the contributions: the geometrical one, already studied in the case with zero impulse, and also the one depending on the impulse $\mathbf{p}^*$.

$$\dot{g} = g\Big(\overline{\mathbb{M}}_r^{-1}(s)\mathbf{p}^* - A_i(s)\dot{s}^i\Big) \tag{2.80}$$

As before the integration of this term along $\alpha(t)$ gives

$$g_{disp} = g(0)e^{z(t)}$$

where

$$z = \overline{Z} + \frac{1}{2}\overline{[\overline{Z}, Z]} + \frac{1}{3}\overline{[[\overline{Z}, Z], Z]} + \frac{1}{12}[\overline{Z}, \overline{[\overline{Z}, Z]}] + \cdots \tag{2.81}$$

$$\overline{Z} := \int_0^t \overline{\mathbb{M}}_r^{-1}(\tau)\mathbf{p}^*(\tau) - A(\tau)\dot{\mathbf{s}}(\tau)\, d\tau$$

In order to see that g_{disp} is effectively the sum of two contribution let us focus on the third equation of (2.80). It is

$$\dot{\theta} = \big(\overline{\mathbb{M}}_r^{-1}(\mathbf{s})\mathbf{p}^*\big)_3 - \big(A(\mathbf{s})\dot{\mathbf{s}}\big)_3$$

from this we can easly recognize two terms. The first one integrated along α is

$$\int_0^T \big(\overline{\mathbb{M}}_r^{-1}(\alpha(\tau))\mathbf{p}^*(\tau)\big)_3\, d\tau\,, \tag{2.82}$$

which value depends strictly on the evolution of the impulse $\mathbf{p}^*$ given by equations $(2.73)_{2-4}$. The second term is the geometric contribution analyzed in the previous section which depends on the curvature of the connection.
Once we have integrated this system and obtained the time evolution of θ we can solve also the ODEs regarding $\dot{\mathbf{d}}$ which are

$$\dot{\mathbf{d}} = R(\theta)\big(\overline{\mathbb{M}}_r^{-1}(\mathbf{s})\mathbf{p}^*\big)_{1,2} - R(\theta)\big(A(\mathbf{s})\dot{\mathbf{s}}\big)_{1,2} \tag{2.83}$$

Also for these two equations it is clear that there are two terms. One is always the geometric one, depending only on the shape $\mathbf{s}$ and $\dot{\mathbf{s}}$. The other one integrated over α gives

$$\int_0^T R(\theta(\tau))\big(\overline{\mathbb{M}}_r^{-1}(\alpha(\tau))\mathbf{p}^*(\tau)\big)_{1,2}\, d\tau \tag{2.84}$$

which is due to the presence of the impulse.
The two additional terms (2.82) and (2.84) are exactly the so called **dynamic phase** presented in section 1.2 and represent the gap on the fiber (d_1, d_2, θ) performed by the swimmer after a periodical change of shape.

2.3 Swimmer controllability

In this section we will focus on the controllability of our system, i.e. its ability to move everywhere in the plane changing its shape.

Let us consider the control system (2.68), since they involve the impulse $\mathbf{p}^*$ we have two different type of control system depending on the initial value of this impulse. If it is zero, we have a non linear drifltess affine control system, whose controllability can be proved with classical techniques, instead if it is not zero we have a non linear affine system with drift, which is more tricky to study.

Remark 2.7 (Scallop Theorem)**.** *Note that in the case of zero initial impulse, if we have only one real shape parameter we are exactly in the case of the famous* ***Scallop Theorem*** *according to which if the swimmer performs a cyclical shape change α the net motion of the swimmer after a period is null.*

$$\begin{pmatrix} \Delta\mathbf{d} \\ \Delta\theta \end{pmatrix} = \int_0^T A(s(t))\dot{s}(t)\,dt = \int_{\alpha(0)}^{\alpha(T)} A(\alpha)\,d\alpha = 0 \quad \textit{since } \alpha(0) = \alpha(T) \tag{2.85}$$

Remark 2.8. *According to the definition of allowable controls (2.3) we need to have almost two complex shape parameters different from zero. Indeed if we describe the system's deformation only by one complex parameter, since it has to satisfy the conditions (2.23) and (2.26) in order to be allowable it turns out that it has to be zero. Now we are interested in using real shape parameters, and as we have seen in remark 2.6, to each complex parameter correspond at least two real parameters, the real and the imaginary part. Therefore the last observation implies that we need almost three real parameters s_1, s_2, s_3.*

Now let us study the controllability of this system in both cases of interest: $\mathbf{p}_0^* = 0$ and $\mathbf{p}_0^* \neq 0$.

2.3.1 Case $\mathbf{p}^*(0) = 0$

In this subsection we want to study the controllability of the system which starts with zero impulse. According to what said before this means that we

deal with a non linear driftless affine control system.

Case of 3 real shape parameters

We have already noticed that we need at least two complex parameters in order to be able to have some physically allowable controls. This means that the minimum number of real parameters have to be at least three. To begin we study exactly the case of three real controls, then we will generalized the results obtained to a larger number of parameters. More precisely, suppose that the deformation of our swimmer is governed by s_1, s_2, s_3 and according to [64] its shape is described in polar coordinates in the body frame by

$$F(\sigma, s) = 1 + \epsilon(s_1 \cos(2\sigma) + s_2 \cos(3\sigma) + s_3 \sin(3\sigma)) \tag{2.86}$$

The perfect irrotational fluid has density ρ and the potential ψ^* can be determined solving the Laplace problem with Neumann boundary conditions following the steps described the preceding sections.
After that it is possible to compute the expression of the connection and the equations of motion

$$\begin{pmatrix} \dot{\mathbf{d}}^* \\ \dot{\theta} \\ \dot{p}_1^* \\ \dot{p}_2^* \\ \dot{p}_3^* \\ \dot{s}_1 \\ \dot{s}_2 \\ \dot{s}_3 \end{pmatrix} = \begin{pmatrix} -(1-\mu)s_2 \\ -(1-\mu)s_3 \\ 0 \\ 0 \\ 0 \\ -(1-\mu)(s_3 p_1^* + s_2 p_2^*) \\ 1 \\ 0 \\ 0 \end{pmatrix} \epsilon^2 u_1 + \begin{pmatrix} -s_1 \\ 0 \\ -\frac{2\pi\rho s_3}{M} \\ \frac{2\pi\rho s_3 p_2^*}{M} \\ -\frac{2\pi\rho s_3 p_1^*}{M} \\ s_1 p_2^* \\ 0 \\ 1 \\ 0 \end{pmatrix} \epsilon^2 u_2 + \begin{pmatrix} 0 \\ -s_1 \\ -\frac{2\pi\rho s_2}{M} \\ -\frac{2\pi\rho s_2 p_2^*}{M} \\ \frac{2\pi\rho s_2 p_1^*}{M} \\ -s_1 p_2^* \\ 0 \\ 0 \\ 1 \end{pmatrix} \epsilon^2 u_3 \tag{2.87}$$

with $\mu = \frac{2\pi\rho}{M+\pi\rho}$ and M the mass of our body.

Due to the change of variables (2.28), the equations of motion have to be supplemented with a so-called reconstruction equation allowing to recover $\mathbf{d}$ knowing θ:

$$\begin{pmatrix} \dot{\mathbf{d}} \\ \dot{\theta} \\ \dot{p}_1^* \\ \dot{p}_2^* \\ \dot{p}_3^* \\ \dot{s}_1 \\ \dot{s}_2 \\ \dot{s}_3 \end{pmatrix} = \begin{pmatrix} \mathcal{R}(\theta) \begin{pmatrix} -(1-\mu)s_2 \\ -(1-\mu)s_3 \\ 0 \end{pmatrix} \\ 0 \\ 0 \\ -(1-\mu)(s_3 p_1^* + s_2 p_2^*) \\ 1 \\ 0 \\ 0 \end{pmatrix} \epsilon^2 u_1 + \begin{pmatrix} \mathcal{R}(\theta) \begin{pmatrix} -s_1 \\ 0 \\ -\frac{2\pi\rho s_3}{M} \end{pmatrix} \\ \frac{2\pi\rho s_3 p_2^*}{M} \\ -\frac{2\pi\rho s_3 p_1^*}{M} \\ s_1 p_2^* \\ 0 \\ 1 \\ 0 \end{pmatrix} \epsilon^2 u_2 + \begin{pmatrix} \mathcal{R}(\theta) \begin{pmatrix} 0 \\ -s_1 \\ -\frac{2\pi\rho s_2}{M} \end{pmatrix} \\ -\frac{2\pi\rho s_2 p_2^*}{M} \\ \frac{2\pi\rho s_2 p_1^*}{M} \\ -s_1 p_2^* \\ 0 \\ 0 \\ 1 \end{pmatrix} \epsilon^2 u_3 \tag{2.88}$$

Theorem 2.3. *The control system (2.88) is controllable almost everywhere.*

Proof: First of all note that system (2.88) is clearly of the type

$$\dot{q} = \sum_{i=1}^{3} g_i(\theta, \mathbf{p}^*, \mathbf{s}) u_i$$

Since the initial impulses are zero it is reduced to only six non trivial equations, indeed we easily have that

$$\mathbf{p}^*(t) = 0 \quad \forall t$$

is a solution of the equations regarding $\mathbf{p}^*$ (2.79).
Accordingly to theorem (1.5) to prove the controllability it suffices to verify the Lie algebra rank condition, i.e $dim\big(\mathcal{L}ie\{g_i\}_{i=1,2,3}\big) = 6$. We compute all the vector fields g_i and the Lie brackets of the first order $[g_i, g_j]$ with $i \neq j$ (details in the Appendix) and compute their determinant

$$\det\Big\{g_1, g_2, g_3, [g_1, g_2], [g_2, g_3], [g_1, g_3]\Big\} = \frac{4\pi\mu\rho\epsilon^{18}\left(\mu M - 2\pi(\mu-1)\rho\left(s_2^2 + s_3^2\right)\right)}{M^2} \tag{2.89}$$

which is not null almost everywhere.
Thus $g_1, g_2, g_3, [g_1, g_2], [g_2, g_3], [g_1, g_3]$ are linearly independent for almost any values of the parameters and $dim(Lie\{g_i, i = 1, 2, 3\}) = 6$, which proves the controllability result. □

General Case: $m > 3$

In this subsection we deal with a generalization of the previous controllability result. Suppose that the shape of the swimmer is described by m real parameters s_i, $i = 1 \cdots m$, which define a transformation near to the identity, whose expression is a generalization of formula (2.86). Moreover recall that we are still in the assumption that the swimmer starts with zero initial impulse in body coordinates. In this case the equations of motion turn out to be

$$\begin{pmatrix} \dot{x} \\ \dot{y} \\ \dot{\theta} \\ \dot{s}_1 \\ \vdots \\ \dot{s}_m \end{pmatrix} = \sum_{i=1}^{m} \tilde{g}_i u_i \tag{2.90}$$

Note that also in this case, since the initial value of $\mathbf{p}^*$ is null, $\mathbf{p}^*(t) = 0$ is still a solution and therefore $\mathbf{p}^*$ does not appear in the system. We now investigate the controllability of the system (2.90).

Theorem 2.4. *The control system (2.90) is controllable almost everywhere.*

Proof: First of all observe that if we keep constant and equal to zero the last $m - 3$ controls, i.e. $u_i = 0$, $i = 4 \cdots m$ the last $m - 3$ equations gives us easily $s_i(t) \equiv 0 \quad \forall t, \quad \forall m \geq 4$. This means that the shape of the swimmer is actually described by only 3 parameters. Therefore the remaining control equations have to be the same of the ones obtained in the previous section with $m = 3$. This implies that the first six components of the vectors $\tilde{g}_j|_{s_i \equiv 0 i=4 \cdots m}$, $j = 1, 2, 3$ have to be equal to the vectors g_i defined before. As a consequence we have that

$$Lie\{\begin{pmatrix} g_i \\ \underline{0} \end{pmatrix}, i = 1, 2, 3\} \subset Lie\{\tilde{g}_i,\, i = 1 \cdots m\} \tag{2.91}$$

Moreover we have also that the vector space generated by the last $m - 3$ vector fields $\tilde{g}_i$ evaluated at $s_i \equiv 0$, $i = 1, 2, 3$ have to be contained in the Lie algebra generated by all the $\tilde{g}_i$, since they are some of the generators.

$$span\{\tilde{g}_j|_{s_i \equiv 0,\, i=1,2,3},\, j \geq 4\} \subset Lie\{\tilde{g}_i,\, i = 1 \cdots m\} \tag{2.92}$$

Furthermore we have also obviously that

$$Lie\{\begin{pmatrix} g_i \\ \underline{0} \end{pmatrix},\ i=1,2,3\} \cap span\{\tilde{g}_j|_{s_i\equiv 0,\, i=1,2,3},\ j\geq 4\} = \{\underline{0}\} \tag{2.93}$$

This implies

$$\begin{aligned} dim\Big(Lie\{\tilde{g}_i,\ i=1\cdots m\}\Big) \geq & \underbrace{dim\Big(Lie\{\begin{pmatrix} g_i \\ \underline{0} \end{pmatrix},\ i=1,2,3\}\Big)}_{=6} + \\ & + \underbrace{dim\Big(span\{\tilde{g}_j|_{s_i\equiv 0,\, i=1,2,3},\ j\geq 4\}\Big)}_{\geq m-3} \end{aligned} \tag{2.94}$$

where the first equality derives from the proof done before in the case $m = 3$. Thus finally we obtain that

$$dim\Big(Lie\{\tilde{g}_i,\ i=1\cdots m\}\Big) \geq m+3 \tag{2.95}$$

which proves the controllability of the system. □

2.3.2 Case $\mathbf{p}_0^* \neq 0$

Let us suppose that our deformable body has an initial constant impulse $\mathbf{p}_0^*$ that is not null. As a consequence our control system is a system with drift of dimension $m + 6$.

Case of 3 shape parameters

We start we the simplest case of three control shape parameters; the deformation is the same as before and it is given by formula (2.86). Since we start with an initial impulse that is not null we have the following control

system with drift

$$\begin{pmatrix} \dot{\mathbf{d}}^* \\ \dot{\theta} \\ \dot{p}_1^* \\ \dot{p}_2^* \\ \dot{p}_3^* \\ \dot{s}_1 \\ \dot{s}_2 \\ \dot{s}_3 \end{pmatrix} = \begin{pmatrix} \overline{\mathbb{M}}_r^{-1}(\mathbf{s})\mathbf{p}^* \\ (\overline{\mathbb{M}}_r^{-1}(\mathbf{s})\mathbf{p}^*)_3 p_2^* \\ (\overline{\mathbb{M}}_r^{-1}(\mathbf{s})\mathbf{p}^*)_3 p_1^* \\ (\overline{\mathbb{M}}_r^{-1}(\mathbf{s})\mathbf{p}^*)_2 p_1^* - (\overline{\mathbb{M}}_r^{-1}(\mathbf{s})\mathbf{p}^*)_1 p_2^* \\ 0 \\ 0 \\ 0 \end{pmatrix} +$$

$$+ \begin{pmatrix} -(1-\mu)s_2 \\ -(1-\mu)s_3 \\ 0 \\ 0 \\ 0 \\ -(1-\mu)(s_3 p_1^* + s_2 p_2^*) \\ 1 \\ 0 \\ 0 \end{pmatrix} \epsilon^2 u_1 + \begin{pmatrix} -s_1 \\ 0 \\ -\frac{2\pi\rho s_3}{M} \\ \frac{2\pi\rho s_3 p_2^*}{M} \\ -\frac{2\pi\rho s_3 p_1^*}{M} \\ s_1 p_2^* \\ 0 \\ 1 \\ 0 \end{pmatrix} \epsilon^2 u_2 + \begin{pmatrix} 0 \\ -s_1 \\ -\frac{2\pi\rho s_2}{M} \\ -\frac{2\pi\rho s_2 p_2^*}{M} \\ \frac{2\pi\rho s_2 p_1^*}{M} \\ -s_1 p_2^* \\ 0 \\ 0 \\ 1 \end{pmatrix} \epsilon^2 u_3 \,. \tag{2.96}$$

Which taking into account the reconstruction equations becomes

$$
\begin{pmatrix} \dot{\mathbf{d}} \\ \dot{\theta} \\ \dot{p}_1^* \\ \dot{p}_2^* \\ \dot{p}_3^* \\ \dot{s}_1 \\ \dot{s}_2 \\ \dot{s}_3 \end{pmatrix} = \begin{pmatrix} \mathcal{R}(\theta)\overline{\mathbb{M}}_r^{-1}(\mathbf{s})\mathbf{p}^* \\ (\overline{\mathbb{M}}_r^{-1}(\mathbf{s})\mathbf{p}^*)_3 p_2^* \\ (\overline{\mathbb{M}}_r^{-1}(\mathbf{s})\mathbf{p}^*)_3 p_1^* \\ (\overline{\mathbb{M}}_r^{-1}(\mathbf{s})\mathbf{p}^*)_2 p_1^* - (\overline{\mathbb{M}}_r^{-1}(\mathbf{s})\mathbf{p}^*)_1 p_2^* \\ 0 \\ 0 \\ 0 \end{pmatrix} +
$$

$$
+ \begin{pmatrix} \mathcal{R}(\theta)\begin{pmatrix} -(1-\mu)s_2 \\ -(1-\mu)s_3 \\ 0 \end{pmatrix} \\ 0 \\ 0 \\ -(1-\mu)(s_3 p_1^* + s_2 p_2^*) \\ 1 \\ 0 \\ 0 \end{pmatrix} \epsilon^2 u_1 + \begin{pmatrix} \mathcal{R}(\theta)\begin{pmatrix} -s_1 \\ 0 \\ -\frac{2\pi\rho s_3}{M} \end{pmatrix} \\ \frac{2\pi\rho s_3 p_2^*}{M} \\ -\frac{2\pi\rho s_3 p_1^*}{M} \\ s_1 p_2^* \\ 0 \\ 1 \\ 0 \end{pmatrix} \epsilon^2 u_2 \qquad (2.97)
$$

$$
+ \begin{pmatrix} \mathcal{R}(\theta)\begin{pmatrix} 0 \\ -s_1 \\ -\frac{2\pi\rho s_2}{M} \end{pmatrix} \\ -\frac{2\pi\rho s_2 p_2^*}{M} \\ \frac{2\pi\rho s_2 p_1^*}{M} \\ -s_1 p_2^* \\ 0 \\ 0 \\ 1 \end{pmatrix} \epsilon^2 u_3
$$

Theorem 2.5. *The system (2.97) is strongly controllable almost everywhere if there are no restrictions on the size of the controls, moreover it is also STLC for almost any initial state and impulse, if the controls are sufficently large, i.e. with controls $\lambda\dot{u}$ and $\dot{u} \in \{|\dot{u}_i| < 1, i = 1, \cdots, m\}$ for some large scalar $\lambda > 0$.*

Proof: The system (2.97) is clearly of the type

$$
\dot{q} = \mathbf{f}(q) + \sum_{i=1}^{3} \mathbf{g}_i(q) u_i \qquad (2.98)
$$

Applying theorem (1.3) to prove the strong controllability the condition to verify is that the Lie algebra generated by the vector fields $\mathbf{g}_i$ has the same

dimension of the tangent space, i.e $dim(Lie\{\mathbf{g}_i, i = 1, 2, 3\}) = 9$. Thus we compute the Lie brackets of zero, first and second order of the vectors $\mathbf{g}_i$ (the detailed expressions are in the Appendix).

The determinant of these vetcor fields is

$$\begin{aligned}
&\det\Big\{\mathbf{g}_1, \mathbf{g}_2, \mathbf{g}_3, [\mathbf{g}_1, \mathbf{g}_2], [\mathbf{g}_1, \mathbf{g}_3], [\mathbf{g}_2, \mathbf{g}_3], [\mathbf{g}_1[\mathbf{g}_2, \mathbf{g}_3]], [\mathbf{g}_2[\mathbf{g}_2, \mathbf{g}_3]], [\mathbf{g}_3[\mathbf{g}_2, \mathbf{g}_3]]\Big\} = \\
&\frac{8192}{M^{10}}\pi^7\mu p_2^*\rho^7 s_2^2 s_3^2\epsilon^{36}(Mp_2^* - 2\pi p_1^*\rho s_2 s_3) \\
&\Big(M^2(p_1^*((2(\mu-3)\mu+3)s_2 - \mu s_3) + + p_2^*((2\mu-3)s_2 + ((9-4\mu)\mu - 6)s_3)) - \\
&- 2\pi(\mu-1)M\rho\big(2\mu p_1^* s_2\left(s_2^2 - 2s_3^2\right) - p_1^*(s_2+s_3)\left(4s_2^2 - 3s_2 s_3 + s_3^2\right) - \\
&- p_2^* s_3\left(-2\mu s_2^2 + s_2^2 + s_3^2\right)\big) + 8\pi^2(\mu-1)^2\rho^2 s_2 s_3\left(s_2^2 + s_3^2\right)(p_2^* s_2 - p_1^* s_3)\Big).
\end{aligned} \tag{2.99}$$

Since this determinant is not null except at most a finite number of d_1, d_2, θ, p_1^*, p_2^*, p_3^*, s_1, s_2, s_3, the system (2.88) is strongly controllable almost everywhere if there are no restriction on the size of the controls.
Let us focus now on the proof of the STLC. First we recall the definition of small time locally controllability (STLC).

Definition 2.4. *(see [15] p.*181*) The system* (2.98) *is said to be* small time locally controllable (STLC) *from q_0 if, for any neighborhood V of q_0 and all $T > 0$, q_0 is an interior point of the reachable set from q_0 at time T. In other words, it means that a whole neighborhood of q_0 is reachable from q_0 at arbitrary small time.*

In this case we have to use the theorem 1.4. We note that from the previous section, the matrix $\mathbb{M}_r$ and its inverse are analytic functions of $\{\theta, \mathbf{p}^*, \mathbf{s}\}$ and therefore the drift term $\mathbf{f}$ is bounded. Then, to apply Lemma 1.4 we have to compute the vectors fields involved at a point in which the vector field $\mathbf{f}$ does not vanish. Since we have supposed that the initial value of the impulse $\mathbf{p}^*$ is not null, the drift does not vanish $\forall \mathbf{s}$ because the matrix $\mathbb{M}_r(\mathbf{s})$ is invertible.
In what follows, we denote by q the 9-tuple $(\mathbf{d}, \theta, \mathbf{p}^*, s_1, s_2, s_3)$ and we choose the point $q_0 := (\mathbf{d}, 0, p_1^*, 0, 0, 1, 0, 1)$ $p_1^* \neq 0$, to verify the condition of Lemma 1.4.
By using formal calculation performed by a symbolic computation software (for instance here we used **Mathematica**, to compute the vector fields that are explicited in the Appendix), we are able to express $\mathbf{g}_1(q_0)$, $\mathbf{g}_2(q_0)$, $\mathbf{g}_3(q_0)$, $[\mathbf{g}_1, \mathbf{g}_2](q_0)$, $[\mathbf{g}_1, \mathbf{g}_3](q_0)$, $[\mathbf{g}_2, \mathbf{g}_3](q_0)$, $[\mathbf{f}, \mathbf{g}_1](q_0)$, $[\mathbf{f}, \mathbf{g}_2](q_0)$ and $[\mathbf{f}, \mathbf{g}_3](q_0)$.

The determinant of these 9 vector fields is not null, for any $p_1^* \neq 0$ and almost any values of the parameters ρ and M, and can be computed by

formal calculations

$$\det(\mathbf{g}_1, \mathbf{g}_2, \mathbf{g}_3, [\mathbf{g}_1, \mathbf{g}_2], [\mathbf{g}_1, \mathbf{g}_3], [\mathbf{g}_2, \mathbf{g}_3], [\mathbf{f}, \mathbf{g}_1], [\mathbf{f}, \mathbf{g}_2], [\mathbf{f}, \mathbf{g}_3])(q_0) = \frac{n(p_1^*)}{d} \quad (2.100)$$

where

$$\begin{aligned} n(p_1^*) &= 8192\pi^2 (p_1^*)^6 \epsilon^8 \mu \rho^2 (M\mu - 2\pi(\mu-1)\rho)(8M(\epsilon - \mu + 1) + \\ &\quad + \pi\rho\left(\epsilon^2(34 - 23\mu) + 8\epsilon(\mu - 1) - 4\mu + 4\right)) \\ d &= M^3(8M + 11\pi\epsilon\rho)^4 \end{aligned}$$

Finally, by using the classical analyticity argument (see for instance [7, 8, 36]), since this determinant is an analytic function with respect to position ($\mathbf{d}$), orientation (θ), impulse ($\mathbf{p}^*$) and shape $\mathbf{s}$ it does not vanish for almost all initial position, orientation,impulse and shape. This is conclude the proof of the Theorem.

□

General case $m > 3$

In the case of initial impulse not zero, as we have said before we have a control affine system with drift of dimension $m + 6$.

$$\begin{pmatrix} \dot{d}_1^* \\ \dot{d}_2^* \\ \dot{\theta} \\ \dot{p}_1^* \\ \dot{p}_2^* \\ \dot{p}_3^* \\ \dot{s}_1 \\ \vdots \\ \dot{s}_m \end{pmatrix} = \tilde{\mathbf{f}} + \sum_{i=1}^{m} \tilde{\mathbf{g}}_i u_i \quad (2.101)$$

Theorem 2.6. *The control system (2.101) is strongly controllable if there are no restriction on the size of the controls, moreover it is also STLC for almost any initial state and impulse, if the controls are sufficently large, i.e. with controls* $\lambda\dot{u}$ *and* $\dot{u} \in \{|\dot{u}_i| < 1, i = 1, \cdots, m\}$ *for some large scalar* $\lambda > 0$.

Proof: To prove the strong controllability of the system (2.101) we exploit the theorem (1.4). Thus the condition to prove is that the dimension of the Lie algebra genereted by the control vector fields $\tilde{\mathbf{g}}_i$ has dimension $m + 6$. The proof is similar to the proof of the previous theorem. Using the follofing facts:

- $Lie\{\begin{pmatrix}\mathbf{g}_i\\ \underline{0}\end{pmatrix}, i=1,2,3\} \subset Lie\{\tilde{\mathbf{g}}_i, i=1,\cdots,m\}$
- $span\{\tilde{\mathbf{g}}_j|_{s_i\equiv 0, i=1,2,3}, j\geq 4\} \subset Lie\{\tilde{\mathbf{g}}_i, i=1,\cdots,m\}$
- $Lie\{\begin{pmatrix}\mathbf{g}_i\\ \underline{0}\end{pmatrix}, i=1,2,3\} \cap span\{\tilde{\mathbf{g}}_j|_{s_i\equiv 0, i=1,2,3}, j\geq 4\} = \{\underline{0}\}$

we deduce that

$$dim\Big(Lie\{\tilde{\mathbf{g}}_i,\, i=1\cdots m\}\Big) \geq \underbrace{dim\Big(Lie\{\begin{pmatrix}\mathbf{g}_i\\ \underline{0}\end{pmatrix},\, i=1,2,3\}\Big)}_{=9} + \\ + \underbrace{dim\Big(span\{\tilde{\mathbf{g}}_j|_{s_i\equiv 0,\, i=1,2,3},\, j\geq 4\}\Big)}_{\geq m-3} \tag{2.102}$$

Which proves that $dim\Big(Lie\{\tilde{\mathbf{g}}_i,\, i=1\cdots m\}\Big) = m+6$.
Let us focus now on the STLC part. To deduce this result in the general case we use an argument very similar to the previous one. First of all consider a point $\tilde{q}_0 = (\mathbf{d}, 0, p_1^*, 0, 0, 1, 0, 1, 0, \cdots, 0) = (q_0, 0, \cdots, 0)$ where q_0 is the point chosen in the case of only 3 parameters. Recalling that $\mathbf{g}_i$ and $\mathbf{f}$ are the vector fields of the system with 3 parameters the following relations hold

$$\tilde{\mathbf{g}}_i(\tilde{q}_0) = \begin{pmatrix}\mathbf{g}_i(q_0)\\ \underline{0}\end{pmatrix} \quad i=1,2,3 \quad \tilde{\mathbf{f}}(\tilde{q}_0) = \begin{pmatrix}\mathbf{f}(q_0)\\ \underline{0}\end{pmatrix}. \tag{2.103}$$

Therefore from what we have proved in the case $m=3$

$$dim\Big(span\{[\tilde{\mathbf{g}}_i, \tilde{\mathbf{g}}_j], [\tilde{\mathbf{f}}, \tilde{\mathbf{g}}_i]\ i,j=1,2,3\}(\tilde{q}_0)\Big) = 6\,. \tag{2.104}$$

Moreover note that the last m components of the vector fields $[\tilde{\mathbf{g}}_i, \tilde{\mathbf{g}}_j](\tilde{q}_0)$ and $[\tilde{\mathbf{f}}, \tilde{\mathbf{g}}_i](\tilde{q}_0)$ for $i=1,2,3$ are null. Thus

$$span\{\tilde{\mathbf{g}}_i,\ i=1,\cdots,m\} \cap span\{[\tilde{\mathbf{g}}_i, \tilde{\mathbf{g}}_j], [\tilde{\mathbf{f}}, \tilde{\mathbf{g}}_i]\ i,j=1,2,3\}(\tilde{q}_0) = \{\underline{0}\} \tag{2.105}$$

These last two relations imply that

$$dim\Big(span\{\tilde{\mathbf{g}}_i, [\tilde{\mathbf{g}}_i, \tilde{\mathbf{g}}_j], ad_{\tilde{\mathbf{f}}}^k \tilde{\mathbf{g}}_i\ i,j=1\cdots m,\, i\neq j,\, k\geq 0\}(\tilde{q}_0)\Big) \geq \\ dim\left(span\{\tilde{\mathbf{g}}_i\}(\tilde{q}_0)\right) + dim\Big(span\{[\tilde{\mathbf{g}}_i, \tilde{\mathbf{g}}_j], [\tilde{\mathbf{f}}, \tilde{\mathbf{g}}_i]\ i,j=1,2,3\ i\neq j\}(\tilde{q}_0)\Big) \geq m+6\,. \tag{2.106}$$

This argument proves the STLC around the point $\tilde{q}_0$. In order to obtain the STLC almost everywhere we exploit the same analyticity argument used for the case $m=3$.

□

Chapter 3

Viscous fluids

While in the previous chapter we faced the problem of the self-propulsion of a planar deformable body immersed in an ideal fluid, here we focus on planar swimmers immersed in a viscous fluid. One of the pioneering works in the field is the one by Taylor [81], who established the mathematical setting for the problem of biological self-propulsion powered by thin undulating filaments. He called attention on the paradoxical nature of swimmers of microscopic size: they move by exploiting (viscous) resistance to motion, since at small scales viscous forces dominate over inertial ones. This is apparent by recalling the definition of Reynolds number $Re = \frac{LV}{\nu}$ (see Chapter 1), a dimensionless measure of the relative importance of inertial versus viscous forces, where L is the body size, V is the swimming speed, and ν is the kinematic viscosity to the surrounding fluid ($10^{-6}(\mathrm{m}^2\mathrm{s}^{-1})^{-1}$ for water at room temperature). Since for biological swimmers V is typically of the order of one body length per second, $Re \sim 1$ for organisms of 1-mm size, and $Re \sim 10^{-6} << 1$ when the size drops to 1 μm. It follows that for micron-sized swimmers inertial effects are negligible: Taylor's analysis focussed on a model swimmer consisting of an infinite sheet propelling itself by propagating a sinusoidal traveling wave of deformation, while surrounded by a fluid governed by Stokes equations (the zero-Re-limit of Navier-Stokes equations). In the absence of inertia, the motion of a swimmer through a fluid is completely determined by the geometry of the sequence of shape that the swimmer assumes. We shall show that the problem of self-propulsion at low Reynolds number, naturally resolves itself into the computation of a gauge potential field A on the space of shapes, as said in Chapter 1.

3.1 Planar bodies

In dimension two, there are powerful and quite practical techniques which make explicit calculation of A, for a wide range of shapes. The similarity between the equations of low Reynolds number hydrodynamics and of linear elasticity theory is well known. In two dimensions, complex variable methods developed in the context of elasticity theory [66] can be carried over almost without modifications.

3.1.1 Determining the gauge potential

Since we have already shown in Chapter 1 that the dynamical problem of self-propulsion at low Reynolds number is reduced to the calculation of the gauge potential A, in this section we outline an effective method for determining it.
First let a sequence of forms $S_0(t)$ be given (introduced in subsection 1.2.1 in Chapter 1). In general, this sequence of shapes does not in itself specify a possible motion according to our hypothesis, because it will involve net forces and torques on the swimmer. The allowed motion, involving the same sequence of deformations, will include additional time-dependent rigid displacements. In other words, the actual motion will be the superimposition of the given motion sequence $S_0(t)$ and counterflows corresponding to additional rigid displacements which cancel the forces and torques.
To calculate the counterflows, we solve for the response of the fluid to the trial motion $S_0(t)$. This is given by the solution to the following boundary-value problem for the velocity v of the fluid. The first two equations are the standard equations for incompressible flow at low Reynolds numbers, and the last one is the no-slip boundary condition:

$$\begin{cases} \operatorname{div} v = 0 \\ \Delta(\nabla \times v) = 0 \\ v|_{S_0} = \frac{dS_0}{dt} \end{cases} \tag{3.1}$$

In interpreting the boundary condition it is important to remember that the $S_0(t)$ are really parametrized shapes, $S_0(s,t)$, and that the variation is meant to be taken with s fixed. The force and torques associated with the trial motion can be inferred from the asymptotic behavior of v at spatial infinity. The force on the shape is related to the external force on the fluid at spatial infinity and hence to the asymptotic flow by the conservation of

momentum. Indeed, if σ_{ij} is the stress tensor, then the force on the shape is

$$F_i = \int_{S_0} \sigma_{ij}\, dS_j \tag{3.2}$$

but the stress tensor is conserved, $\partial_i \sigma_{ij} = 0$ (see (3.4) below), so this is

$$F_i = -\int_{\infty} \sigma_{ij}\, dS_j\,. \tag{3.3}$$

Now the stress tensor is given in terms of the velocity, and only the terms that fall off slowly and have the right symmetry survive. Indeed the force is linearly related to the leading term in the asymptotic flow. A similar argument leads to an analogous conclusion for the torque. To cancel these forces and torques, we must correct the motion by subtracting a Stokes flow corresponding to a rigid displacement of the shape with the same leading behavior at infinity as our solution.

Remark 3.1 (Scallop Theorem)**.** *We discuss a notable property of self propulsion at low Reynolds number: the* ***generalized scallop theorem*** *emphasized by Purcell in [70], that we have already recalled in the case of an ideal fluid (see Remark 2.7). According to it a simple hinged object such as the one shown in figure 3.1 cannot swim at low Reynolds number. Any periodic stroke gives no net motion. In our framework this is evident because the space of shapes available to this object is simply a bounded one dimensional angle* $0 \leq \theta \leq 2\pi$*. Thus the displacement induced by moving along the segment are cancelled by those accumulated in the return motion.*

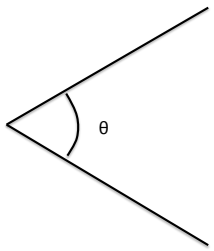

Figure 3.1: A simple hinged microorganism with one degree of freedom cannot swim.

3.1.2 The two dimensional techniques

We now apply complex analysis techniques to study the swimming motion of extended bodies at very low Reynolds number. In the case of planar swimmers the boundary value problem (3.1) can be solved by exploiting complex analysis. The first two equations of (3.1) implies that the two component vector v is the curl of a scalar potential U that is

$$\begin{aligned} v = \nabla \times U \equiv (\frac{\partial U}{\partial y}, -\frac{\partial U}{\partial x}) \\ \nabla \times v = \nabla \times (\nabla \times U) = -\Delta U \end{aligned} \tag{3.4}$$

Thus U satisfies the biharmonic equation

$$\Delta^2 U = 0 \tag{3.5}$$

This equation has been extensively been studied in the theory of elasticity in two dimensions. In elastic boundary value problems, the second partial derivatives of U represent the stresses on the elastic medium. Therefore we can apply the methods of complex analysis to our problem, indeed biharmonic functions have a simple representation in terms of analytic functions. Namely any U satisfying (3.4) can be written in the form

$$\frac{1}{2}U(z,\overline{z}) = \overline{z}\phi(z) + z\overline{\phi(z)} + \psi(z) + \overline{\psi(z)} \tag{3.6}$$

where ϕ and ψ are analytic in $z = x + iy$. As a corollary we obtain an important representation for the velocity field, written as $v = v_x + iv_y$

$$\begin{aligned} v(z) =& \nabla \times U = -\frac{i}{2}\frac{\partial U}{\partial \overline{z}} = -i[\phi(z) + z\overline{\phi'(z)} + \overline{\psi'(z)}] \\ & \phi_1(z) - z\overline{\phi_1'(z)} + \overline{\phi_2(z)} \end{aligned} \tag{3.7}$$

To discuss the swimming of shapes, we will consider an external boundary value problem for U, with $v = \nabla \times U$ specified on the exterior boundary of a compact region Ω in the plane. Let s represent the complex coordinate z restricted to the boundary. Then given $v(s)$ we want to find functions ϕ_1, ϕ_2, analytic in the exterior such that

$$v(s) = \phi_1(s) - s\overline{\phi_1'(s)} + \overline{\phi_2(s)} \tag{3.8}$$

The problem is easily solved if Ω is a **circle**, i.e. we simply equate the Fourier coefficients on both sides of (3.8). Suppose we have the Fourier expansions

$$\begin{cases} v(s) = \sum_{k=-\infty}^{\infty} v_k s^{k+1} \\ \phi_1(s) = \sum_{k<0} a_k s^{k+1} \\ \phi_2(s) = \sum_{k<-1} b_k s^{k+1} \end{cases} \tag{3.9}$$

where $s = e^{i\theta}$. Then (3.8) is equivalent to

$$\sum_{k=-\infty}^{\infty} v_k s^{k+1} = \sum_{k<0} a_k s^{k+1} - \sum_{k<0}(k+1)\overline{a}_k s^{-k+1} + \sum_{k<-1} \overline{b}_k s^{-k-1} \tag{3.10}$$

since $s^{-1} = \overline{s}$. The complete solution is

$$\begin{cases} a_k = v_k \qquad k < 0 \\ b_{-2} = \overline{v}_0 \\ b_k = \overline{v}_{-k-2} + (k+3)v_{k+2} \qquad k < -2 \end{cases} \tag{3.11}$$

Thus solutions with $v(s) = \lambda s^{l+1}$ on the circle correspond to

$$\phi_1(s) = 0 \qquad \phi_2(s) = \overline{\lambda}s \pm -l - 1 \qquad l > -1 \tag{3.12}$$

$$\phi_1(s) = \lambda \qquad \phi_2(s) = 0 \qquad l = -1 \tag{3.13}$$

$$\phi_1(s) = \lambda s^{l+1} \qquad \phi_2(s) = \lambda(l+1)s^{l+1} \qquad l < -1 \tag{3.14}$$

These may be extended to the entire region of the flow, i.e. the exterior of the circle by substituting $s \to z$ and using the representation (3.7). The

results are

$$v = \lambda \overline{z}^{-l-1} \qquad l > -1 \tag{3.15}$$

$$v = \lambda \qquad l = -1 \tag{3.16}$$

$$v = \lambda \overline{z}^{l+1} - \overline{\lambda}(l+1)\overline{z}^{l-1}(z\overline{z}-1) \qquad l < -1 \tag{3.17}$$

This is the complete solution to the boundary value problem when Ω is a circle.
To write it in the two-component vector notation we can take λ real or imaginary in (3.15)-(3.17) to obtain a basis of equivalent solutions

$$\text{for } l \geq -1 \begin{cases} v_l^1(r,\theta) = r^{-l-1}(\cos(l+1)\theta, \sin(l+1)\theta)\,, \\ v_l^2(r,\theta) = r^{-l-1}(-\sin(l+1)\theta, \cos(l+1)\theta) \end{cases} \tag{3.18}$$

and

$$\text{for } l < -1 \begin{cases} v_l^1 = & r^{l+1}(\cos(l+1)\theta - (l+1)(1-r^{-2})\cos(l-1)\theta, \\ & \sin(l+1)\theta + (l+1)(1-r^{-2})\sin(l-1)\theta) \\ v_l^2 = & r^{l+1}(-\sin(l+1)\theta + (l+1)(1-r^{-2})\sin(l-1)\theta, \\ & \cos(l+1)\theta - (l+1)(1-r^{-2})\cos(l-1)\theta) \end{cases} \tag{3.19}$$

It is also useful to have combinations with definite helicity, i.e. that satisfy simple properties under rotation

$$\begin{aligned} w_l^{\pm}(r,\theta) &\equiv \frac{i}{\sqrt{2}}(v_l^1 \mp i v_l^2) \\ &= r^{-l-1} e^{\pm i(l+1)\theta} \frac{1}{\sqrt{2}}(1, \mp i) \qquad (l \geq -1) \\ &= r^{-l-1}\big[e^{\pm i(l+1)\theta}\frac{1}{\sqrt{2}}(1,\mp i) \\ &\quad - (l+1)(1-r^{-2})e^{\pm i(l-1)\theta}\frac{1}{\sqrt{2}}(1,\pm i)\big] \ (l < -1) \end{aligned} \tag{3.20}$$

Rotation of an angle α changes these flows by

$$w_l^{\pm} \to e^{\pm il\alpha} w_l^{\pm} \tag{3.21}$$

REMARK Note that the solution corresponding to translations of the circle involve a rigid motion of the fluid as a whole. This unphysical behavior is known as Stokes' paradox, and is a well known peculiarity of two dimensional low Reynolds number hydrodynamics. Because of our requirement that the

external forces and torques vanish, we never encounter these rigid motions of the circle, in fact we determine the Gauge potentials precisely by subtracting them of. The fact that mathematically, rigid motions of the circle give rise to such long-range motions of the fluid is actually a convenience, since it allows us to identify the necessary counterflows.

3.1.3 Infinitesimal deformations

As we have done for ideal fluids we consider the case of infinitesimal deformation of a shape. Let the standard shape be parametrized by

$$S_0(t) = S_0 + s(t) \tag{3.22}$$

where the $s(t)$ are infinitesimal. We expand it in terms of a fixed basis of vector fields on S_0

$$s(t) = \sum_i \alpha_i(t) w_i \tag{3.23}$$

Then we have the velocity on $S_0(t)$:

$$v(t) = \frac{dS_0(t)}{dt} = \sum_i \dot{\alpha}_i w_i \tag{3.24}$$

Now let us expand the Gauge potentials to second order:

$$\begin{aligned} A_{v(t)}[S_0(t] \approx & A_{v(t)}[S_0] + \sum_i \frac{\partial A_v}{\partial w_i}\dot{\alpha}_i \\ & \approx \sum_j \big(A_{w_j}\dot{\alpha}_j + \sum_i \frac{\partial A_{w_j}}{\partial w_i}\alpha_i\dot{\alpha}_j \big) \end{aligned}$$

As explained in the first chapter che basic object giving the net displacement is the path-ordered exponential integral (1.15)

$$\bar{P}\exp\Big[\int_{t_1}^{t_2} A(t)\,dt\Big] = 1 + \int_{t_1<t<t_2} A(t)\,dt + \iint_{t_1<t'<t<t_2} A(t)A(t')\,dt\,dt' + \cdots$$

around a circle. The first order term gives no contribution, since it is a total derivative. The second-order contributions are terms quadratic in A and linear in its derivatives. Because the chronological integral is gauge covariant for a cyclic path, its Taylor expansion in powers of $s(t)$ must be gauge covariant, order by order. In fact there is a unique second-order gauge covariant term we can have, which is antisymmetric in the indices i and j:

$$F_{w_i w_j} \equiv \frac{\partial A_{w_i}}{\partial w_j} - \frac{\partial A_{w_j}}{\partial w_i} + [A_{w_i}, A_{w_j}] \tag{3.25}$$

which is the **curvature of the connection** already introduced in equation (2.77).
The physical meaning of $F_{w_iw_j}$ is the following. Suppose we make a sequence of successive deformations of S_0 by ϵw_i, ηw_j and $-\epsilon w_i$, $-\eta w_j$; finally we close the sequence of shapes with the bracket $-\epsilon\eta[w_i, w_j]$. Then the net displacement will be $\epsilon\eta F_{w_iw_j}$. It is easily verified that the expansion of (1.15) to second order gives

$$\overline{P}\exp\Big[\oint A dt\Big] = 1 + \frac{1}{2}\oint \sum_{i,j} F_{w_iw_j}\alpha_i\dot{\alpha}_j dt \tag{3.26}$$

We now focus on the nearly circular shapes deformations. To compute the strength tensor F we mudt consider closed paths into the two-dimensional space of shapes. Let v_1, v_2 be two velocity fields on the circle and let $\mathcal{R}(\epsilon v_1, \eta v_2)$ be the rototranslation of the circle induced by the following sequence of motions:

$$S \to S + \epsilon v_1 \to S + \epsilon v_1 + \eta v_2 \to S + \eta v_2 \to S$$

We work to second order in ϵ, η, then by (3.26)

$$\mathcal{R}(\epsilon v_1, \eta v_2) = [1, 0] + \epsilon\eta F_{w_iw_j}$$

F is easily computed by matching the boundary condition $\eta v_2(\theta)$ on the surface of the circle deformed by $\epsilon v_1(\theta)$. If we call the resulting velocity field v_{12}, then $F_{v_1v_2}$ is related to the asymptotics of v_{12} at infinity. Following our prescriptions we find

$$\begin{cases} F^{tr}_{v_1v_2} = \lim_{r\to\infty}\int \frac{d\theta}{2\pi}(v_{12} - v_{21}) \\ F^{rot}_{v_1v_2} = \lim_{r\to\infty}\int \frac{d\theta}{2\pi} r \times (v_{12} - v_{21}) \end{cases} \tag{3.27}$$

where the translational and rotational parts are defined by

$$F_{v_1\,v_2} \equiv \begin{pmatrix} 0 & F^{rot} & F^{tr}_x \\ -F^{rot} & 0 & F^{tr}_y \\ 0 & 0 & 0 \end{pmatrix} \tag{3.28}$$

and the integral is around a large circle. It remains to compute v_{12}. The boundary conditions for v_{12} is

$$\begin{aligned} v_2(\theta) &= v_{12}(x)|_{surf} \\ &\approx v_{12}(r,\theta) + \epsilon(v_1\cdot\nabla)v_{12}(r,\theta)|_{r=1} \\ v_2(\theta) \approx v_{12}(1,\theta) &+ \epsilon(v_1\cdot\nabla)v_{12}(r,\theta)|_{r=1} \end{aligned} \tag{3.29}$$

Thus we can find v_{12}, v_{21} and F from v_1, v_2 obtaining

$$\begin{cases} F^{tr}_{v_1v_2} = \int \frac{d\theta}{2\pi}((v_2\cdot\nabla)v_1 - (v_1\cdot\nabla)v_2)\,, \\ F^{rot}_{v_1v_2} = \Im\int \frac{d\theta}{2\pi} r\times((v_2\cdot\nabla)v_1 - (v_1\cdot\nabla)v_2) \end{cases} \tag{3.30}$$

This formula for the gauge field strength can be generalized to describe tangential deformations of an arbitrary shape, indeed

$$\frac{\partial A_{v_1}}{\partial v_2} - \frac{\partial A_{v_2}}{\partial v_1} = A_{[v_1,v_2]}$$

where

$$[v_1, v_2] = (v_1\cdot\nabla)v_2 - (v_2\cdot\nabla)v_1$$

is the Lie bracket. Thus the complete field strength, like already showed in (3.25), is

$$F_{v_1v_2} = A_{[v_1,v_2]} + [A_{v_1}, A_{v_2}]$$

For the circle the second term vanishes, but it does not in general. When both v_1 and v_2 are tangential fields, the Lie bracket may be completely evaluated in terms of their values on the shape, with no hydrodynamics. Thus for purely tangential motions the form of A determines F directly.
We now insert the vector fields (3.20) into (3.30), the result for the translational part are as follows

$$\begin{aligned} F^{tr}_{m^+n^+} &= \frac{1}{\sqrt{2}}\big[-(m+1)\theta_{-m}\delta_{m+n+1}e_- + (n+1)\theta_n\delta_{m+n+1}e_- \\ &\quad + (m+1)\theta_{-m}\delta_{m+n-1}e_+ - (n+1)\theta_{-n}\delta_{n+n-1}e_+\big] \qquad (3.31) \\ F^{tr}_{m^+-n^-} &= \frac{1}{\sqrt{2}}\big[-(m+1)\theta_{m}\delta_{m-n+1}e_- - (n+1)\theta_n\delta_{-m+n+1}e_+ \\ &\quad + (m+1)\theta_{-m}\delta_{m+n-1}e_- - (n+1)\theta_{-n}\delta_{m+n-1}e_+\big] \qquad (3.32) \\ F^{tr}_{m^+-n^-} &= \frac{1}{\sqrt{2}}\big[(m+1)\theta_{m}\delta_{m-n+1}e_- - (n+1)\theta_n\delta_{-m+n+1}e_+ \\ &\quad + (m+1)\theta_{-m}\delta_{m-n-1}e_+ - (n+1)\theta_{-n}\delta_{-m+n-1}e_-\big] \qquad (3.33) \\ F^{tr}_{m^-n^+} &= -F^{tr}_{n^+m^-} \qquad (3.34) \end{aligned}$$

where $e_\pm = \frac{1}{\sqrt{2}}(1, \pm i)$ and θ_n is zero for negative n and 1 for non negative n. It is understood here that the $+$ and $-$ labels refer to the solution $w^\pm$ in (3.20). The matrix F is antisymmetric, moreover not surprisingly the vast majority of the components of F vanish in the helicity basis. Since under rotation of α $w^\pm$ is multiplied by the phase $e^{\pm il\alpha}$, $e_\pm \to e^{i\alpha}e_\pm$ and F is linear

in its argument and everything about our problem it is symmetric under rotation, we can easily deduce which components of F may be not null. For the rotational part of F we find

$$F^{rot}_{m^+n^+} = -[(m+1)\theta_m - (n+1)\theta_n]\delta_{m+n} \tag{3.35}$$
$$F^{rot}_{m^-n^-} = [(m+1)\theta_m - (n+1)\theta_n]\delta_{m+n} \tag{3.36}$$
$$F^{rot}_{m^+n^-} = -|m+1|\delta_{m-n} \tag{3.37}$$
$$F^{rot}_{m^-n^+} = -F^{rot}_{n^+m^-} \tag{3.38}$$

Once the net rotation and translation of a body due to any sequence of deformations is known, it is natural to study the controllability of the system and to optimize. Thus we wander if fixing any initial and final configuration it is possible to find a suitable rate of deformation which moves the system between the two and if yes what is the most efficient strategy. The answer will depend on many factors, but also for planar bodies and infinitesimal deformations is tricky to find algebraic condition even to prove the controllability of the system. The main difficulty it is to get an analytic expression for the gauge potential, due to the complexity of the solution of the Stokes problem. Therefore the idea is to try to simplify the hydrodinamics of the problem making some approximations.

Chapter 4

Flagellar microrganisms

As explained in the previous chapter, one of the main difficulties in exploiting control theory in order to solve effectively motion planning or optimal control problems is the complexity of the hydrodynamic forces exerted by the fluid on the swimmer as a reaction to its shape changes. In the case of slender swimmers, Resistive Force Theory (RFT) [39] provides a simple and concise way to compute a local approximation of such forces, and it has been successfully used in several recent studies, see for example [13, 33]. From now on we use this approach as well, in order to obtain the forces acting on the swimmer. In addition, we simplify the kinematics of the swimmer by discretizing its body. This is represented by a chain of N rigid links moving in a plane (N-link swimmer). Thus, its motion is described by a system of ODEs that can be easily assembled and solved, hence providing a valuable tool for the quantitative description of the motion of biological micro-swimmers. The simplicity of the governing equations makes our model particularly appealing as a tool for the design of engineered devices and for the optimization of their performance as some design parameters are varied.

4.1 Mathematical setting of the problem

In this section we describe the kinematics of the N-link swimmer, a generalization of Purcell's 3-link swimmer. The angles between successive links provide a discrete representation of the swimmer's curvature, concentrated at the joints between successive links. We think of them as freely prescribed shape parameters. We then write the equations of motion (balance of total viscous force and torque) and solve for the time evolution of position and orientation of the swimmer in response to a prescribed history of (concentrated) curvatures along the swimmer's body.

4.1.1 Kinematics of the N-link swimmer

We focus here on essentially one–dimensional swimmers moving in a plane. This two-dimensional setting is suitable for the study of slender, essentially one-dimensional swimmers exploring planar trajectories. While the general case is slightly more involved because of the non-additivity of three–dimensional rotations, see e.g. [5], it can be handled with similar techniques.

Our swimmer consists of N rigid links with joints at their ends (see Fig. 4.1), moving in a plane (2d lab-frame) which is defined by the vectors $(\mathbf{e}_x, \mathbf{e}_y)$. We set $\mathbf{e}_z := \mathbf{e}_x \times \mathbf{e}_y$. The i-th link is the segment with end points $\mathbf{x}_i$ and $\mathbf{x}_{i+1}$. It has length $L_i > 0$ and makes an angle θ_i with the horizontal x-axis. The size of the sticks is chosen such that the length of the swimmer is of order of μm. We define by $\mathbf{x}_i := (x_i, y_i)$ $(i = 1, \cdots, N)$ the coordinates of the first end of each link. Note that, for $i \in \{2 \cdots N\}$, the coordinates $\mathbf{x}_i$ can be expressed as a function of $\mathbf{x}_1$, θ_k and L_k, with $k \in \{1 \cdots i-1\}$:

$$\mathbf{x}_i := \mathbf{x}_1 + \sum_{k=1}^{i-1} L_k \begin{pmatrix} \cos(\theta_k) \\ \sin(\theta_k) \end{pmatrix} . \tag{4.1}$$

The swimmer is described by two sets of variables:

- the state variables which specify the position and the orientation of one selected link, labeled as the $i*$-th one;

- the shape variables which describe the relative orientations between successive links. For each link with $i > i*$, this is the angle relative to the preceding one, denoted by $\alpha_i = \theta_i - \theta_{i-1}$, for $i* < i \leq N$. For $i < i*$ this is the the angle relative to the following one, denoted by $\alpha_i = \theta_{i+1} - \theta_i$, for $1 \leq i < i*$.

For example, if the triplet $(\mathbf{x}_1, \theta_1)$ describes the state of the swimmer then the vector $(\alpha_2 = \theta_2 - \theta_1, \cdots, \alpha_N = \theta_N - \theta_{N-1})$ represents the shape of the swimmer. This will be the default choice in the rest, with the only exception of subsection 4.2.1, where the central link is selected as the $i*$-th one, in order to exploit the symmetries of the 3-link swimmer.

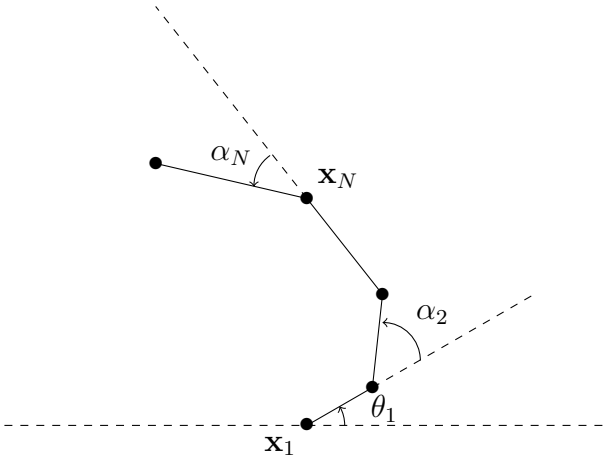

Figure 4.1: Coordinates for the N-link swimmer.

4.1.2 Equations of motion

The equations which govern the dynamics of the swimmer form a system of three ODEs, which is linear with respect to the rate of deformation, and without drift.

The dynamics of the swimmer follows from Newton laws, in which inertia is neglected. These read

$$\begin{cases} \mathbf{F} = 0\,, \\ \mathbf{e}_z \cdot \mathbf{T}_{\mathbf{x}_1} = 0\,, \end{cases} \tag{4.2}$$

where $\mathbf{F}$ is the total force exerted on the swimmer by the fluid and $\mathbf{T}_{\mathbf{x}_1}$ is the corresponding total torque computed with respect to the point $\mathbf{x}_1$.

To couple the fluid and the swimmer, we use the local drag approximation of Resistive Force Theory. We denote by s the arc length coordinate on the i-th link ($0 \leq s \leq L_i$) and by $\mathbf{v}_i(s)$ the velocity of the corresponding point. We also introduce the unit vectors $\mathbf{e}_i = \begin{pmatrix} \cos(\theta_i) \\ \sin(\theta_i) \end{pmatrix}$ and $\mathbf{e}_i^\perp = \begin{pmatrix} -\sin(\theta_i) \\ \cos(\theta_i) \end{pmatrix}$ in the directions parallel and perpendicular to the i-th link and write $\mathbf{x}_i(s) = \mathbf{x}_i + s\mathbf{e}_i$. By differentiation, we obtain,

$$\mathbf{v}_i(s) = \dot{\mathbf{x}}_i + s\dot{\theta}_i \mathbf{e}_i^\perp\,. \tag{4.3}$$

The density of the force $\mathbf{f}_i$ acting on the i-th segment is assumed to depend linearly on the velocity. It is defined by

$$\mathbf{f}_i(s) := -\xi\left(\mathbf{v}_i(s)\cdot\mathbf{e}_i\right)\mathbf{e}_i - \eta\left(\mathbf{v}_i(s)\cdot\mathbf{e}_i^\perp\right)\mathbf{e}_i^\perp, \tag{4.4}$$

where ξ and η are respectively the drag coefficients in the directions of $\mathbf{e}_i$ and $\mathbf{e}_i^\perp$ measured in $\mathrm{N\,s\,m^{-2}}$. We thus obtain

$$\begin{cases} \mathbf{F} = \displaystyle\sum_{i=1}^{N} \int_0^{L_i} \mathbf{f}_i(s)\, ds\,, \\ \mathbf{e}_z \cdot \mathbf{T}_{\mathbf{x}_1} = \mathbf{e}_z \cdot \displaystyle\sum_{i=1}^{N} \int_0^{L_i} (\mathbf{x}_i(s) - \mathbf{x}_1) \times \mathbf{f}_i(s)\, ds\,. \end{cases} \tag{4.5}$$

Using (4.3) and (4.4) into (4.5), the total force and torque can be expressed as

$$\mathbf{F} = -\sum_{i=1}^{N} L_i \xi (\dot{\mathbf{x}}_i \cdot \mathbf{e}_i)\, \mathbf{e}_i + \left(L_i \eta (\dot{\mathbf{x}}_i \cdot \mathbf{e}_i^\perp) + \frac{L_i^2}{2} \eta \dot{\theta}_i \right) \mathbf{e}_i^\perp\,, \tag{4.6}$$

and

$$\begin{aligned} \mathbf{e}_z \cdot \mathbf{T}_{\mathbf{x}_1} &= -\sum_{i=1}^{N} \frac{L_i^2}{2} \eta \left(\dot{\mathbf{x}}_i \cdot \mathbf{e}_i^\perp \right) + \frac{L_i^3}{3} \eta \dot{\theta}_i \\ &+ (\mathbf{x}_i - \mathbf{x}_1) \times \left(L_i \xi (\dot{\mathbf{x}}_i \cdot \mathbf{e}_i)\, \mathbf{e}_i + \left(L_i \eta (\dot{\mathbf{x}}_i \cdot \mathbf{e}_i^\perp) + \frac{L_i^2}{2} \eta \dot{\theta}_i \right) \mathbf{e}_i^\perp \right) \end{aligned} \tag{4.7}$$

Moreover, differentiating (4.1) gives

$$\dot{\mathbf{x}}_i = \dot{\mathbf{x}}_1 + \sum_{k=1}^{i-1} L_k \dot{\theta}_k \mathbf{e}_k^\perp, \tag{4.8}$$

an expression linear in $\dot{\mathbf{x}}_1$ and $(\dot{\theta}_k)_{1 \le k \le N}$. This entails that (4.6) and (4.7) are linear in $\dot{\mathbf{x}}_1$ and $\dot{\theta}_i$ for $i \in [1 \cdots N]$, and therefore system (4.2) reads

$$\begin{pmatrix} \mathbf{F} \\ \mathbf{e}_z \cdot \mathbf{T}_{\mathbf{x}_1} \end{pmatrix} = \mathbf{M}\,(\theta_1, \cdots, \theta_N) \begin{pmatrix} \dot{\mathbf{x}}_1 \\ \dot{\theta}_1 \\ \dot{\theta}_2 \\ \vdots \\ \dot{\theta}_N \end{pmatrix} = \begin{pmatrix} 0 \\ 0 \\ 0 \end{pmatrix}\,. \tag{4.9}$$

Observing that for all $i \in \{2, \cdots, N\}$, $\alpha_i = \theta_i - \theta_{i-1}$, equations (4.6) and (4.7) can be expressed using the angles $(\alpha_i)_{i=2,\cdots,N}$ instead of the variables

$(\theta_i)_{2\leq i\leq N}$. To this end, we introduce the matrix $\mathbf{C}$ defined by

$$\mathbf{C} = \begin{pmatrix} 1 & 0 & \cdots & \cdots & \cdots & \cdots & 0 \\ 0 & 1 & \ddots & \ddots & \ddots & \ddots & \vdots \\ 0 & 0 & 1 & \ddots & \ddots & & \vdots \\ 0 & 0 & -1 & \ddots & \ddots & & \vdots \\ \vdots & \vdots & 0 & \ddots & \ddots & & 0 \\ \vdots & \vdots & \vdots & \ddots & \ddots & \ddots & 0 \\ 0 & 0 & 0 & \cdots & 0 & -1 & 1 \end{pmatrix} \tag{4.10}$$

and obtain

$$\mathbf{C} \begin{pmatrix} \dot{\mathbf{x}}_1 \\ \dot{\theta}_1 \\ \dot{\theta}_2 \\ \vdots \\ \dot{\theta}_N \end{pmatrix} = \begin{pmatrix} \dot{\mathbf{x}}_1 \\ \dot{\theta}_1 \\ \dot{\alpha}_2 \\ \vdots \\ \dot{\alpha}_N \end{pmatrix} . \tag{4.11}$$

Therefore, by setting

$$\mathbf{N}(\theta_1, \alpha_2, \cdots, \alpha_N) := \mathbf{M}\left(\theta_1, \theta_2(\theta_1, \alpha_2, \cdots, \alpha_N), \cdots, \theta_N(\theta_1, \alpha_2, \cdots, \alpha_N)\right) \mathbf{C}^{-1}, \tag{4.12}$$

system (4.9) can be rewritten in the equivalent form

$$\mathbf{N}\left(\theta_1, \alpha_2, \cdots, \alpha_N\right) \begin{pmatrix} \dot{\mathbf{x}}_1 \\ \dot{\theta}_1 \\ \dot{\alpha}_2 \\ \vdots \\ \dot{\alpha}_N \end{pmatrix} = \begin{pmatrix} 0 \\ 0 \\ 0 \end{pmatrix} . \tag{4.13}$$

We observe that the $3 \times (N+2)$ matrix $\mathbf{N}\left(\theta_1, \alpha_2, \cdots, \alpha_N\right)$ can be block-decomposed into a 3×3 sub-matrix $\mathbf{A}\left(\theta_1, \alpha_2, \cdots, \alpha_N\right)$ and a $3 \times (N-1)$ sub-matrix $\mathbf{B}\left(\theta_1, \alpha_2, \cdots, \alpha_N\right)$, according to

$$\mathbf{N} = \left(\mathbf{A} \,|\, \mathbf{B}\right) . \tag{4.14}$$

The matrix $\mathbf{A}$ is the 'grand-resistance-matrix' of a rigid system evolving at frozen shape, i.e., with $\dot{\alpha}_i \equiv 0$, $i = 2, \ldots, N$, see [41]. It is symmetric and negative definite [41], as it can be easily verified, hence it is invertible. We can then recast the equations of motion of the swimmer as an affine system without drift. Indeed, solving (4.13) for $(\dot{\mathbf{x}}_1, \dot{\theta}_1)$ leads to

$$\begin{pmatrix} \dot{\mathbf{x}}_1 \\ \dot{\theta}_1 \end{pmatrix} = -\mathbf{A}^{-1}\left(\theta_1, \alpha_2, \cdots, \alpha_N\right) \mathbf{B}\left(\theta_1, \alpha_2, \cdots, \alpha_N\right) \begin{pmatrix} \dot{\alpha}_2 \\ \vdots \\ \dot{\alpha}_N \end{pmatrix} \tag{4.15}$$

that we rewrite in the form

$$\begin{pmatrix} \dot{\mathbf{x}}_1 \\ \dot{\theta}_1 \end{pmatrix} = \sum_{i=1}^{N-1} g_i \left(\theta_1, \alpha_2, \cdots, \alpha_N\right) \dot{\alpha}_{i+1} \,, \tag{4.16}$$

or similarly

$$\begin{pmatrix} \dot{\alpha}_2 \\ \vdots \\ \dot{\alpha}_N \\ \dot{\mathbf{x}}_1 \\ \dot{\theta}_1 \end{pmatrix} = \sum_{i=1}^{N-1} \underbrace{\begin{pmatrix} \mathbf{b}_i \\ g_i \left(\theta_1, \alpha_2, \cdots, \alpha_N\right) \end{pmatrix}}_{\mathbf{g}_i(\theta_1, \alpha_2, \cdots, \alpha_N)} \dot{\alpha}_{i+1} \,, \tag{4.17}$$

where the $N-1$ vector fields $\{g_i\}_{i=1}^{N-1}$, are the columns of the $3 \times (N-1)$ matrix $-\mathbf{A}^{-1}\mathbf{B}$, and $\mathbf{b}_i$ is the i-th vector of the canonical basis of $\mathbb{R}^{N-1}$

The equation above links the displacement (both translation and rotation) of the swimmer to its deformation. In other words, for a given history of shapes, prescribed through functions $t \mapsto (\alpha_2, \cdots, \alpha_N)(t)$, the motion of the swimmer is obtained by solving the system (4.17). Typically, in what follows a stroke is given by a time-periodic shape change, i.e., the functions $t \mapsto \alpha_i(t)$, $i = 2, \cdots, N$ are all periodic, with the same period.

In order to solve (4.17) numerically, we need to construct the vector fields $\mathbf{g}_i$ explicitly. To this end, we observe that $\mathbf{F}$ and $\mathbf{T}_{\mathbf{x}_1}$ depend linearly on $(\dot{\mathbf{x}}_i)_{1 \le i \le N}$ and $(\dot{\theta}_i)_{1 \le i \le N}$ and that these quantities depend in turn linearly on $(\dot{\mathbf{x}}_1, \dot{\theta}_1, \cdots, \dot{\theta}_N)$ in view of (4.8). Therefore, we can rewrite (4.6) and (4.7) as

$$\mathbf{F} = \mathbf{P}_1 \begin{pmatrix} \dot{\mathbf{x}}_1 \\ \vdots \\ \dot{\mathbf{x}}_N \\ -- \\ \dot{\theta}_1 \\ \vdots \\ \dot{\theta}_N \end{pmatrix} = \mathbf{P}_1 \mathbf{Q} \begin{pmatrix} \dot{\mathbf{x}}_1 \\ \dot{\theta}_1 \\ \vdots \\ \dot{\theta}_N \end{pmatrix} \,, \quad \mathbf{e}_z \cdot \mathbf{T}_{\mathbf{x}_1} = \mathbf{P}_2 \begin{pmatrix} \dot{\mathbf{x}}_1 \\ \vdots \\ \dot{\mathbf{x}}_N \\ -- \\ \dot{\theta}_1 \\ \vdots \\ \dot{\theta}_N \end{pmatrix} = \mathbf{P}_2 \mathbf{Q} \begin{pmatrix} \dot{\mathbf{x}}_1 \\ \dot{\theta}_1 \\ \vdots \\ \dot{\theta}_N \end{pmatrix} \,, \tag{4.18}$$

where

$$\mathbf{P}_1 := \begin{pmatrix} -\mathbf{m}_1 & \cdots & -\mathbf{m}_N & | & \frac{\eta}{2} L_1^2 \mathbf{e}_1^\perp & \cdots & \frac{\eta}{2} L_N^2 \mathbf{e}_N^\perp \end{pmatrix}$$

with $\mathbf{m}_i := L_i(\xi \mathbf{e}_i \otimes \mathbf{e}_i + \eta \mathbf{e}_i^\perp \otimes \mathbf{e}_i^\perp)$ for $i = 1 \cdots N$,

$$\mathbf{P}_2 := \begin{pmatrix} \cdots & -(L_i^2 \eta \mathbf{e}_i^\perp + (\mathbf{x}_i - \mathbf{x}_1) \times \mathbf{m}_i)^T & \cdots & | & \cdots & \eta L_i^2 (\frac{L_i}{3} + \frac{(\mathbf{x}_i - \mathbf{x}_1) \times \mathbf{e}_i^\perp \cdot \mathbf{e}_z}{2}) & \cdots \end{pmatrix} ,$$

and, finally,

$$\mathbf{Q} = \begin{pmatrix} 1 & 0 & 0 & 0 & \cdots & 0 \\ 1 & L_1\mathbf{e}_1^\perp & 0 & 0 & \cdots & 0 \\ 1 & L_1\mathbf{e}_1^\perp & L_2\mathbf{e}_2^\perp & 0 & \cdots & 0 \\ \vdots & \vdots & \vdots & \ddots & \cdots & 0 \\ 1 & L_1\mathbf{e}_1^\perp & L_2\mathbf{e}_2^\perp & \cdots & L_{N-1}\mathbf{e}_{N-1}^\perp & 0 \\ 0 & & & & & \\ \vdots & & & \mathbf{Id} & & \\ 0 & & & & & \end{pmatrix}.$$

We thus have

$$\mathbf{M} = \begin{pmatrix} \mathbf{P}_1\mathbf{Q} \\ \mathbf{P}_2\mathbf{q} \end{pmatrix}$$

and can compute $\mathbf{N} = \mathbf{C}^{-1}\mathbf{M}$, where $\mathbf{C}^{-1}$ is explicitly given as

$$\mathbf{C}^{-1} = \begin{pmatrix} 1 & 0 & \cdots & \cdots & \cdots & \cdots & 0 \\ 0 & 1 & \ddots & \ddots & \ddots & \ddots & \vdots \\ 0 & 0 & 1 & \ddots & \ddots & & \vdots \\ 0 & 0 & 1 & \ddots & \ddots & & \vdots \\ \vdots & \vdots & 1 & \ddots & \ddots & & 0 \\ \vdots & \vdots & \vdots & \ddots & \ddots & \ddots & 0 \\ 0 & 0 & 1 & \cdots & 1 & 1 & 1 \end{pmatrix}. \tag{4.19}$$

Matrices $\mathbf{A}$ and $\mathbf{B}$ are obtained from the columns of $\mathbf{N}$ as in (4.14) and, finally, the vectors g_i are simply the columns of $-\mathbf{A}^{-1}\mathbf{B}$.

4.1.3 Geometric aspects

In this part we want to underline the fact that making use of the Resistive Force Theory to approximate the local drag forces that the fluid exerts on the swimmer, does not effect the geometrical setting of our problem. First of all we introduce the moving frame, solidal to the swimmer $(\mathbf{e}_x^*, \mathbf{e}_y^*)$ centered in the first end of the first stick and with $\mathbf{e}_x^*$ aligned with the first stick. Thus similarly to what we have done in chapter two in the case of an ideal fluid, we can express any velocity $\mathbf{v}$ in the lab-frame, starting from the same velocity in the moving frame $\mathbf{v}^*$ according to the formula:

$$\mathbf{v} = \mathcal{R}(\theta_1)\mathbf{v}^*$$

Now it is possible to show that equation (4.15) it is of the form

$$\begin{pmatrix} \dot{\mathbf{x}}_1 \\ \dot{\theta}_1 \end{pmatrix} = -\mathcal{R}(\theta_1)\tilde{\mathbf{A}}^{-1}\left(\alpha_2, \cdots, \alpha_N\right)\tilde{\mathbf{B}}\left(\alpha_2, \cdots, \alpha_N\right)\begin{pmatrix} \dot{\alpha}_2 \\ \vdots \\ \dot{\alpha}_N \end{pmatrix} \tag{4.20}$$

indeed the matrix $\tilde{\mathbf{A}}^{-1}\tilde{\mathbf{B}}$ is the expressions of the translational and angular velocities of the swimmer expressed in the moving frame. Obviously they do not depend on θ_1 that is the angle that this frame forms with the $\mathbf{e}_x$ direction. To obtain the equations of motion in the lab frame it suffices to rotate $\tilde{\mathbf{A}}^{-1}\tilde{\mathbf{B}}$ of an angle θ_1 according to what said before.
Now we can easily recover the usual expression (1.13)

$$\frac{d\mathcal{R}}{dt} = \mathcal{R}A \tag{4.21}$$

where $\mathcal{R}$ is a rotation and A is the usual gauge potential. This fact tell us that the geometrical setting introduced in the first chapter does not depend on the way to compute the hydrodynamic forces but only on the intrinsic structure of the swimming problem.

4.2 Applications

4.2.1 Purcell's 3−link swimmer

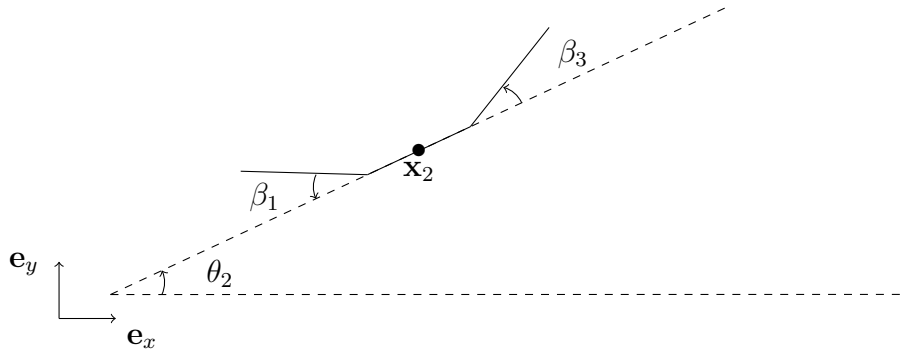

Figure 4.2: Purcell's 3-link swimmer.

We now focus on the case $N = 3$ (Purcell's 3−link swimmer). To benefit from the symmetry of the system, we use as state variables the coordinate

$\mathbf{x}_2 := (x_2, y_2)$ of the middle point of the second segment, and the angle θ_2 that it forms with the x-axis. With the notation of the preceding sections, we call $\beta_1 = \theta_2 - \theta_1$ and $\beta_3 = \theta_3 - \theta_2$ the relative angles to the central link of the left and right arms respectively, see Figure 4.14.

(*A remark on the notation: we point out that here we use as relative angles the β_1, β_3 instead of the α_2, α_3 to highlight the symmetry of the system. The relation between the two can be found in paragraph 4.5.*)

Purcell introduced this system in [70], where he predicted that it would exhibit net motion as a consequence of a suitable non-reciprocal stroke (a square loop in the (β_1, β_3) plane). He also argued by symmetry that, for a swimmer with first and third links of equal length, this symmetric stroke would produce a net displacement along the direction of the central link, but did not provide a formula to predict either the sign or the magnitude of this displacement. In the following, we show the connection between Purcell's proposed stroke and Lie brackets, a classical tool of Geometric Control Theory. This enables us to obtain a formula for the displacement induced by a Purcell-type stroke of infinitesimal amplitude. We also compute numerically the motion resulting from a Purcell-type stroke of finite amplitude and check it against the theoretical prediction.

Setting $\mathbf{X} := (\beta_1, \beta_3, x_2, y_2, \theta_2)^{\mathbf{T}}$, and using (4.16), the equations of motion become

$$\dot{\mathbf{X}} = \mathbf{g}_1(\theta_2, \beta_1, \beta_3)\dot{\beta}_1 + \mathbf{g}_2(\theta_2, \beta_1, \beta_3)\dot{\beta}_3 \,. \tag{4.22}$$

We refer to Appendix B for the explicit calculation of the coefficients appearing in (4.22). We remark that none of them depends on (x_2, y_2) as a consequence of the translational invariance of the problem.

4.2.2 Displacement for square strokes of small amplitude

Proposition 4.1. *Let $\epsilon > 0$, and consider the square stroke defined by*

$$\begin{aligned}
&(\dot{\beta}_1(t), \dot{\beta}_3(t)) = (1, 0) \text{ for } t \in (0, \epsilon),\\
&(\dot{\beta}_1(t), \dot{\beta}_3(t)) = (0, 1) \text{ for } t \in (\epsilon, 2\epsilon),\\
&(\dot{\beta}_1(t), \dot{\beta}_3(t)) = (-1, 0) \text{ for } t \in (2\epsilon, 3\epsilon),\\
&(\dot{\beta}_1(t), \dot{\beta}_3(t)) = (0, -1) \text{ for } t \in (3\epsilon, 4\epsilon).
\end{aligned} \tag{4.23}$$

Then, for small ϵ, the solution of (4.22) *with initial condition* $\mathbf{X}(0)$ *is given by*

$$\mathbf{X}(4\epsilon) - \mathbf{X}(0) = \begin{pmatrix} 0 \\ 0 \\ \epsilon^2\delta + O(\epsilon^3) \\ O(\epsilon^3) \\ O(\epsilon^3) \end{pmatrix}, \tag{4.24}$$

where

$$\delta = \frac{L_1 L_2 L_3 \left(L_1^2 + L_1(L_2+L_3) + L_3(L_2+L_3)\right)(\eta - \xi)}{(L_1+L_2+L_3)^4 \xi} \tag{4.25}$$

Proof: The first two components in (4.24) vanish, as it is obvious from direct integration of (4.23). Moreover, it is well known (see,e.g., [29]) and easy to check that the solution of (4.22) for the square stroke given by (4.23) satisfies the expansion

$$X(4\epsilon) - X(0) = \epsilon^2[\mathbf{g}_1, \mathbf{g}_2] + O(\epsilon^3)$$

where the *Lie bracket* $[\mathbf{g}_1, \mathbf{g}_2]$ is defined by

$$[\mathbf{g}_1, \mathbf{g}_2](\mathbf{y}) := (\mathbf{g}_1 \cdot \nabla)\, \mathbf{g}_2(\mathbf{y}) - (\mathbf{g}_1 \cdot \nabla)\, \mathbf{g}_2(\mathbf{y})\,. \tag{4.26}$$

The direct calculation of this Lie bracket[1] shows that

$$[\mathbf{g}_1, \mathbf{g}_2](\mathbf{y})|_{\mathbf{y}=(0,0,0)} = \begin{pmatrix} 0 \\ 0 \\ \delta \\ 0 \\ 0 \end{pmatrix}, \tag{4.27}$$

□

The proposition above provides us with an explicit formula for the net displacement which, in the symmetric case $L_1 = L_3 = L$, reads

$$\Delta\mathbf{x}_2 = \epsilon^2 \frac{L^3 L_2 (3L + 2L_2)}{(2L + L_2)^4} \left(\frac{\eta - \xi}{\xi}\right) \mathbf{e}_2 + O(\epsilon^3)\,. \tag{4.28}$$

Formula (4.28) above shows that the net displacement at leading order is along the axis of the central link and vanishes when $\eta = \xi$. As already stated

[1] We have used for this step the symbolic computation software MAPLE and the formulas given in Appendix B.

by Purcell, it can also be shown that a square stroke (4.23) on such a symmetric swimmer does not produce any global rotation or vertical displacement.

By integrating numerically the equations of motion for small angle excursion ϵ and small times 4ϵ, we have obtained the state of the swimmer, $t \mapsto (x_2(t), y_2(t), \theta_2(t))$. We have verified that after the square stroke $y_2(4\epsilon)$ and $\theta_2(4\epsilon)$ vanish, in accordance with the previous remark, and that the net displacement along the $x-$axis is given by formula (4.28) (see Figure 4.3).

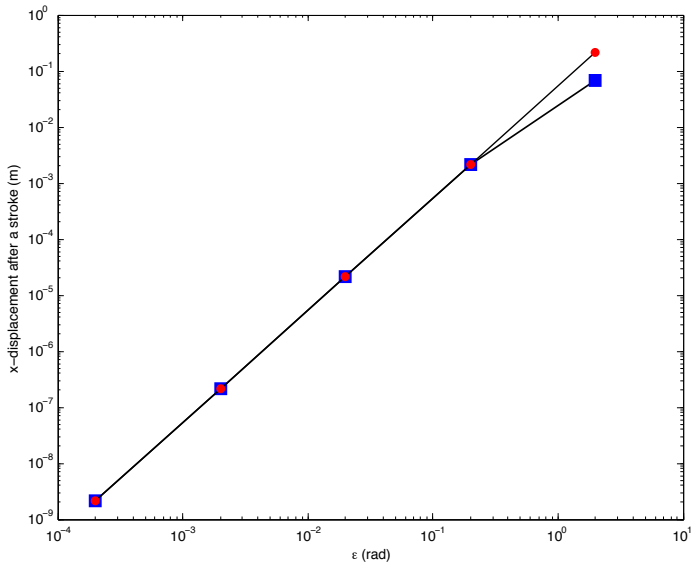

Figure 4.3: Graphs of the displacement of the 3-link-swimmer in meters after one square stroke, as a function of the angle amplitude ϵ in radians. Here $L_1 = L_3 = 1\mu\,\mathrm{m}$, $L_2 = 2\,\mu\,\mathrm{m}$, and $\eta = 2\xi\,\mathrm{N\,s\,m^{-2}}$. The blue squares are obtained by numerical integration of the equations of motion, while the red circles are obtained from the Lie bracket formula (4.28).

4.2.3 Displacement for square strokes of large amplitude

The preceding results only apply to infinitesimal strokes. For strokes of large amplitude, we can integrate the equations of motion numerically and compare our results to known results from the literature. To this aim, we use the same data as in [13], namely $L_1 = L_3 = L = 1$, $L_2 = 2$, $\xi = 1$ and $\eta = 2$, $\Delta\theta = \frac{\pi}{3}$ and the control angles given by

$$\beta_1(t) = \begin{cases} -(\frac{\Delta\theta}{2} - t) & \text{if } 0 \le t \le \Delta\theta \\ \frac{\Delta\theta}{2} & \text{if } \Delta\theta \le t \le 2\Delta\theta \\ -(t - \frac{5\Delta\theta}{2}) & \text{if } 2\Delta\theta \le t \le 3\Delta\theta \\ -\frac{\Delta\theta}{2} & \text{if } 3\Delta\theta \le t \le 4\Delta\theta \end{cases}, \quad \beta_3(t) = \begin{cases} \frac{\Delta\theta}{2} & \text{if } 0 \le t \le \Delta\theta \\ (\frac{3\Delta\theta}{2} - t) & \text{if } \Delta\theta \le t \le 2\Delta\theta \\ -\frac{\Delta\theta}{2} & \text{if } 2\Delta\theta \le t \le 3\Delta\theta \\ (t - \frac{7\Delta\theta}{2}) & \text{if } 3\Delta\theta \le t \le 4\Delta\theta \end{cases}.$$

This leads to a square stroke of amplitude $\frac{\pi}{3}$, as shown in Figure 4.2.3. Such a stroke produces the displacement of the swimmer given in Figure 4.5, which matches exactly Figure 6 in [13].

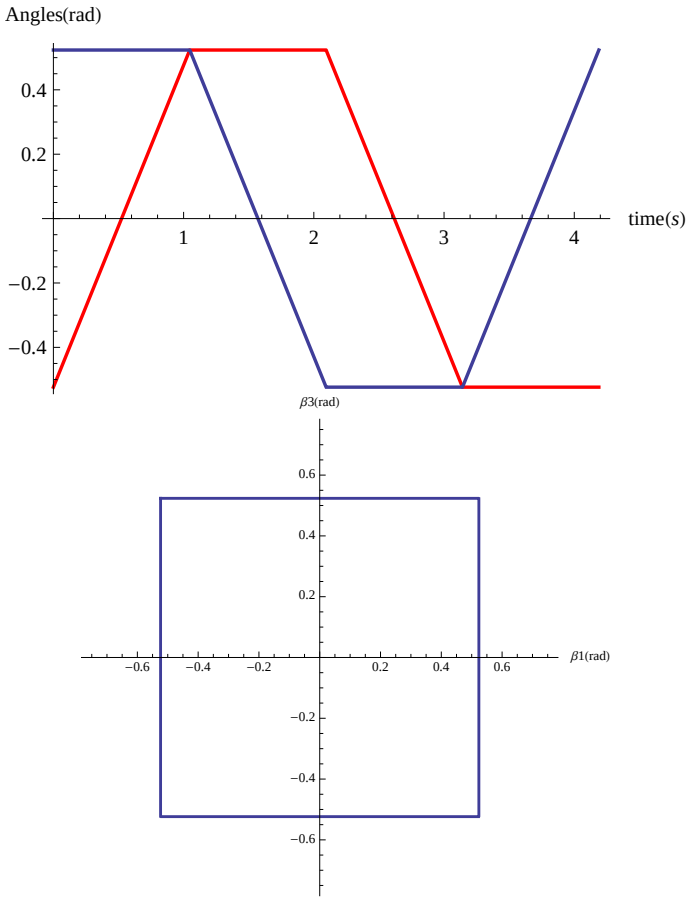

Figure 4.4: Control functions β_1 (red) and β_3 (blue) as functions of time (above), and their phase portrait (below). The square loop on the right is traced clockwise.

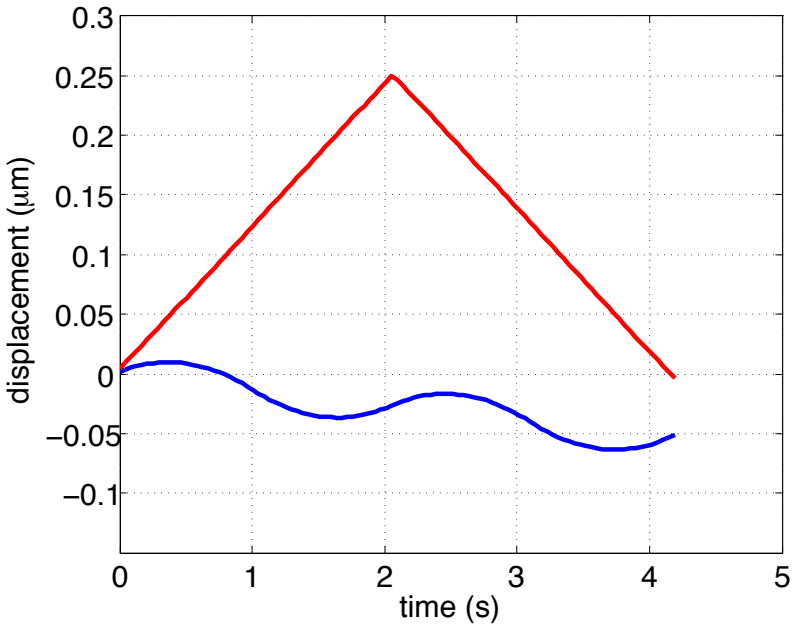

Figure 4.5: Graphs of $x_2(t)$ (blue), and $y_2(t)$ (red) as a function of time during the stroke of Figure 4.2.3. A net horizontal backward displacement is observed when the square stroke is traced clockwise, matching the results of [13].

4.2.4 $N-$link swimmers

The full $N-$link swimmer can be used as a discrete model of a flexible tail whose shape is controlled by curvature. We show how curvature control can be implemented in our model in some concrete cases reproducing the motion of Taylor's sheet [81] and the motion of a sperm cell analyzed in [33].

Curvature approximation

Here, we show how to approximate the curvature of a beating tail with a discrete N link swimmer. Let $L > 0$ be the total length of the flexible tail and let us denote by $\mathbf{r}(s,t)$ the position at time $t > 0$ of the point of arc-length coordinate $s \in [0, L]$ along the tail, in the body frame of the swimmer (see Figure 4.6). We also define $\Psi(s,t)$ as the angle between the tangent vector to the tail at the point $\mathbf{r}(s,t)$ and the $x-$axis in the lab-frame. We recall that the derivative of $\Psi(s,t)$ with respect to s is the local curvature of the curve.

We divide the swimmer into N equal parts of size $L_i = L/N$, and define the angles $(\theta_i)_{1\leq i\leq N}$ by averaging $\Psi(s,t)$ on the interval $[iL/N, (i+1)L/N]$

$$\theta_i(t) = \frac{N}{L}\int_{\frac{(i-1)L}{N}}^{\frac{iL}{N}} \Psi(s,t)\,ds\,, \quad i = 1\dots N\,. \tag{4.29}$$

Finally, we differentiate (4.29) with respect to time to get $\dot\theta_i$, $i = 1, \cdots, N$,

$$\dot\theta_i(t) = \frac{N}{L}\int_{\frac{(i-1)L}{N}}^{\frac{iL}{N}} \frac{\partial\Psi(s,t)}{\partial t}\,ds\,, \quad i = 1\dots N\,. \tag{4.30}$$

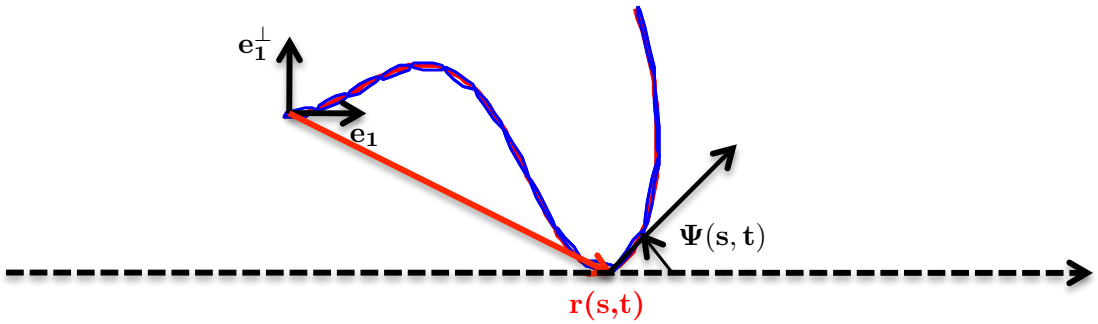

Figure 4.6: A prescribed continuous wave (red curve) and its discrete approximation by the N-link swimmer (blue curve), $N = 15$.

4.2.5 N-link approximation of Taylor's swimming sheet

We now use our discretization method to compute the displacement and velocity of the so-called Taylor sheet [81]. To that aim, we describe a sinusoidal wave propagating along the tail in its frame by

$$\mathbf{r}(s(x,t),t) = b\sin(kx - \sigma t) + b\sin(\sigma t) \tag{4.31}$$

where the arclength s and x are linked by

$$s(x,t) = \int_0^x \sqrt{1 + b^2k^2(\cos(ku - \sigma t))^2}\,du\,. \tag{4.32}$$

(Notice that $\mathbf{r}(0,t) = 0$, which keeps the origin fixed in the swimmer's frame.)

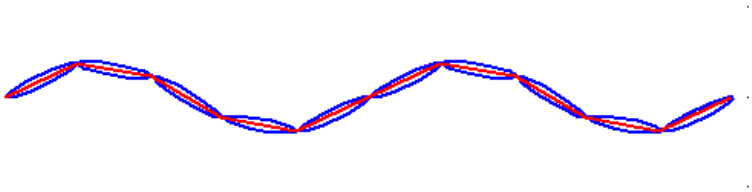

Figure 4.7: A sinusoidal wave (red) and its $N-$link approximation (blue) with $N = 10$

Using Resistive Force Theory, Gray and Hancock give in [39] the following formula for the velocity of the sheet in the horizontal direction:

$$V_x = \sigma k b^2 \left(\frac{\xi - \eta}{\eta} \right) , \tag{4.33}$$

from which one can recover Taylor's formula

$$V_x = -\frac{1}{2} k \sigma b^2 \tag{4.34}$$

by setting $\xi = 1$ and $\eta = 2$. The net displacement of the swimmer after a period $T = \frac{2\pi}{\sigma}$ is therefore

$$\Delta x = V_x T = \sigma k b^2 \left(\frac{\xi - \eta}{\eta} \right) T \, . \tag{4.35}$$

We have solved numerically the equations of motion choosing as parameters

$\sigma = 1\,\mathrm{rad\,s^{-1}}$, $k = 4\,\mathrm{rad\,\mu m^{-1}}$, and $N = 50$ links to describe the swimmer, and drag coefficients $\xi = 1\mathrm{N\,s\,\mu m^{-2}}$ and $\eta = 2\,\mathrm{N\,s\,\mu m^{-2}}$. The displacement in the parallel direction after one period is plotted in Figure 4.8, together with the the one predicted by (4.35), for a wave amplitude $b = 0.001\,\mu\mathrm{m}$.

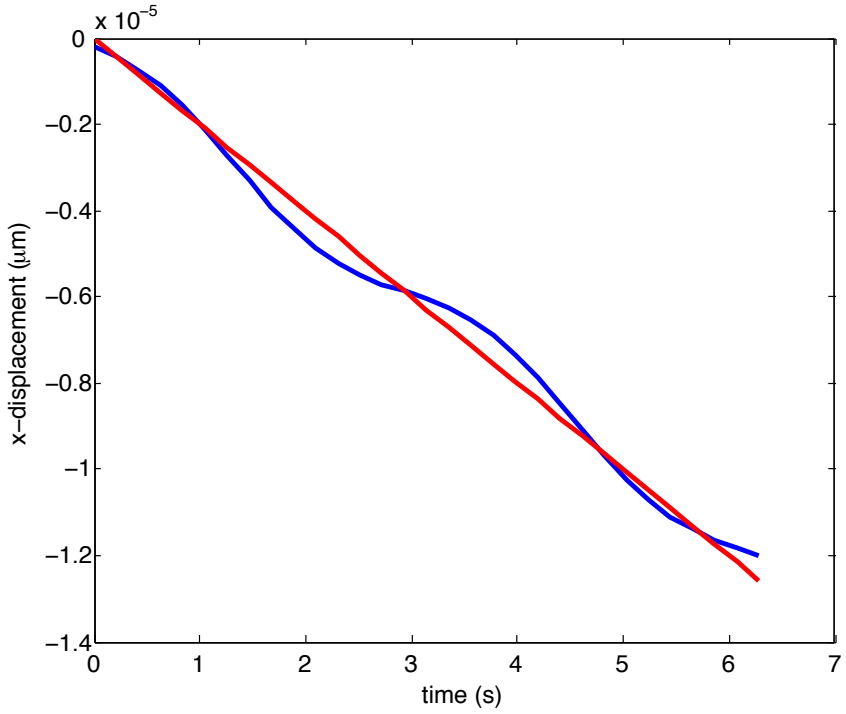

Figure 4.8: Graphs of the displacement of Taylor's sheet for $b = 1 \cdot 10^{-3}\,\mu$m. The blue curve is the one obtained by numerical integration of the equations of motion while the red one is the one predicted by (4.35)

.

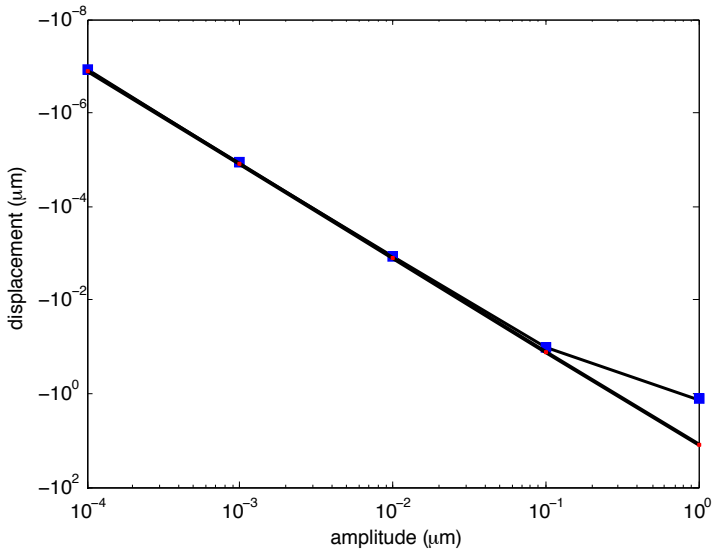

Figure 4.9: Logarithmic plot of the x-displacement as a function of the amplitude b (blue squares) compared with the one obtained from (4.35) (red dots).

The dependence of the displacements on the amplitude b is shown in Figure 4.9. The graph shows that formula (4.35) gives an accurate prediction for an amplitude of the wave b smaller than $1 \cdot 10^{-1}$.

4.2.6 N-link approximation of sperm cell swimmer

We now turn to the simulation of the motion of a sperm cell and compare to the one reported in [33]. To that aim, we modify the first segment of the $N-$link swimmer to take into account the presence of the head of the sperm cell, which possesses its own translational and rotational viscous drag. Indeed, we call $\mathbf{x}_1$ the position of the center of the head and θ_1 the angle that the direction $\mathbf{e}_1$ of first segment (attached to the head) makes with the horizontal axis. We assume that the viscous force and torque generated by a movement of the head are given by

$$\mathbf{F}_{\text{head}} = -\xi_{\text{head}}(\dot{\mathbf{x}}_1 \cdot \mathbf{e}_1)\mathbf{e}_1 - \eta_{\text{head}}(\dot{\mathbf{x}}_1 \cdot \mathbf{e}_1^{\perp})\mathbf{e}_1^{\perp}\,, \tag{4.36}$$

and

$$\mathbf{T}_{\text{head}} \cdot \mathbf{e}_z = -\zeta_{\text{head}}\dot{\theta}_1\,. \tag{4.37}$$

We also assume that the head length is $L_{\text{head}} = 10\,\mu$m and we call again L the length of the tail which is fixed to one of the extremities of the head segment. The wave profile along the tail of the sperm cell was obtained from experimental data, keeping only the two first Fourier modes as suggested in [73] and we use the method described in section 4.2.4 to approximate the motion of the tail.

More precisely, we describe the wave shape shown in Fig. 4.10 by

$$\mathbf{r}(s,t) = \frac{L_{\text{head}}}{2}\,\mathbf{e}_1(t) + \int_0^s \cos(\Psi(u,t))\mathbf{e}_1(t) + \sin(\Psi(u,t)\mathbf{e}_1^{\perp}(t)du\,. \qquad (4.38)$$

where

$$\Psi(s,t) = K_0 s + 2A_0 s\cos(\omega t - \frac{2\pi s}{\lambda})\,. \qquad (4.39)$$

In the preceding equations, K_0 is the mean flagellar curvature while ω, λ and A_0 are respectively the frequency, the wave-length and the amplitude of the wave. Following [33], in the numerical simulations below we use the following values for the wave parameters: $A_0 = 15.2 \cdot 10^3\,\text{rad}\,\text{m}^{-1}$, $K_0 = 19.1 \cdot 10^3\,\text{rad}\,\text{m}^{-1}$, $\omega = 200\,\text{rad}\,\text{s}^{-1}$ and $\lambda = 71.6 \cdot 10^{-6}\,\text{m}$.

Apart from the first segment, the rest of the tail is discretized with $N-1$ segments of extremities $(\mathbf{x}_i, \mathbf{x}_{i+1})$ for $i = 2, \cdots, N$. We discretize the beating wave using the method described in section 4.2.4, and obtain the shapes shown in Figure 4.11 for one period ($0 \le t \le \frac{2\pi}{\omega}$).

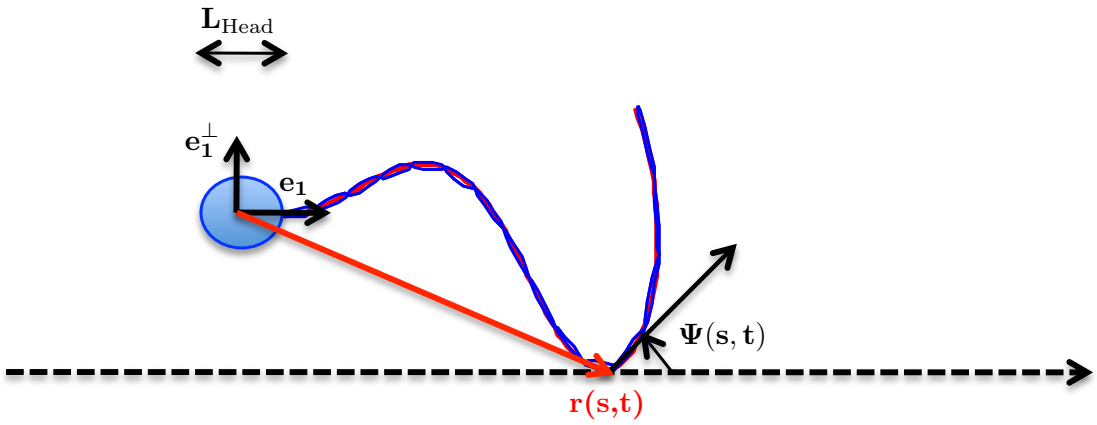

Figure 4.10: The prescribed continuous wave (red curve) and its discrete approximation by the N-link swimmer (blue curve), $N = 15$.

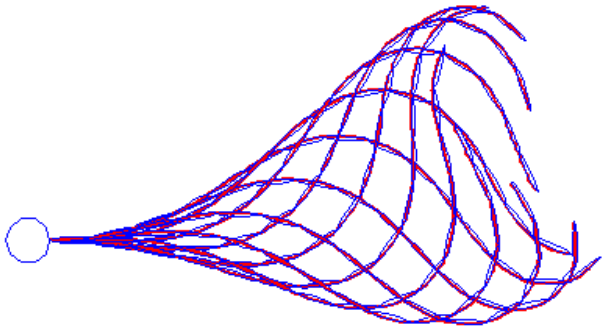

Figure 4.11: Flagellar beating during one period. The red curve represents the tail as described by formula (4.38) while the blue links describe the tail according to our discrete approximation.

With the notation above, the equations of motion become

$$\begin{cases} \mathbf{F} = \mathbf{F}_{\text{head}} + \sum_{i=1}^{N} \int_0^{L_i} \mathbf{f}_i(s)\, ds\,, \\ \mathbf{T}_{\mathbf{x}_1} = \mathbf{T}_{\text{head}} + \sum_{i=1}^{N} \int_0^{L_i} \mathbf{f}_i(s) \times (\mathbf{x}_i(s) - \mathbf{x}_1)\, ds\,. \end{cases} \tag{4.40}$$

where $L_i = L/N$ is the length of each segment $(\mathbf{x}_i, \mathbf{x}_{i+1})$ for $i = 2, \cdots, N$, while the first segment, also of size $L_1 = L/N$ is given by $(\mathbf{x}_1 + \frac{L_{\text{head}}}{2}\mathbf{e}_1, \mathbf{x}_2)$.

Thanks to the fact that the two previous formulas (4.40) are linear in $\dot\theta_1$ and $\dot{\mathbf{x}}_1$, we get the same compact expression of the equations of motion as in (4.16). More in detail, the matrix $\mathbf{P}_1$ and $\mathbf{P}_2$ defined the system (4.18) are replaced by

$$\mathbf{P}_1^{\text{head}} := \left(-\xi_{\text{head}}\mathbf{e}_1 \otimes \mathbf{e}_1 + \eta_{\text{head}}\mathbf{e}_1^\perp \otimes \mathbf{e}_1^\perp \quad -\mathbf{m}_1 \quad \cdots \quad -\mathbf{m}_N \quad | \quad \tfrac{\eta}{2}L_1^2\mathbf{e}_1^\perp \quad \cdots \quad \tfrac{\eta}{2}L_N^2\mathbf{e}_N^\perp\right)$$

and

$$\mathbf{P}_2^{\text{head}} := \left(-p_1 \quad \cdots \quad -p_N \quad | \quad -\zeta_{\text{head}} + q_1 \quad q_2 \quad \cdots \quad q_N\right),$$

with $\mathbf{m}_i := L_i(\xi \mathbf{e}_i \otimes \mathbf{e}_i + \eta \mathbf{e}_i^\perp \otimes \mathbf{e}_i^\perp)$ for $i = 1 \cdots N$, and $p_i := (L_i^2 \eta \mathbf{e}_i^\perp + (\mathbf{x}_i - \mathbf{x}_1) \times \mathbf{m}_i)^T$, $q_i := \eta L_i^2(\frac{L_i}{3} + \frac{(\mathbf{x}_i - \mathbf{x}_1)\times \mathbf{e}_i^\perp \cdot \mathbf{e}_z}{2})$, for $i = 1 \cdots N$.
We use the following values for the drag coefficients

- for the head, $\xi_{\text{head}} = 40.3 \cdot 10^3\,\text{pN}\,\text{s}\,\text{m}^{-1}$, $\eta_{\text{head}} = 46.1 \cdot 10^3\,\text{pN}\,\text{s}\,\text{m}^{-1}$, and $\zeta_{\text{head}} = 0.84 \cdot 10^{-6}\,\text{pN}\,\text{s}\,\text{m}$

- for the links representing the tail, $\xi = 0.38 \cdot 10^9\,\mathrm{pN\,s\,m^{-2}}$, $\frac{\eta}{\xi} = 1.89$.

Our results, summarized by the graphs in Figures 4.12 and 4.13 below, are in perfect agreement with those of [33] (see Figure 3 for the trajectory and Figure 4 for the various speeds).

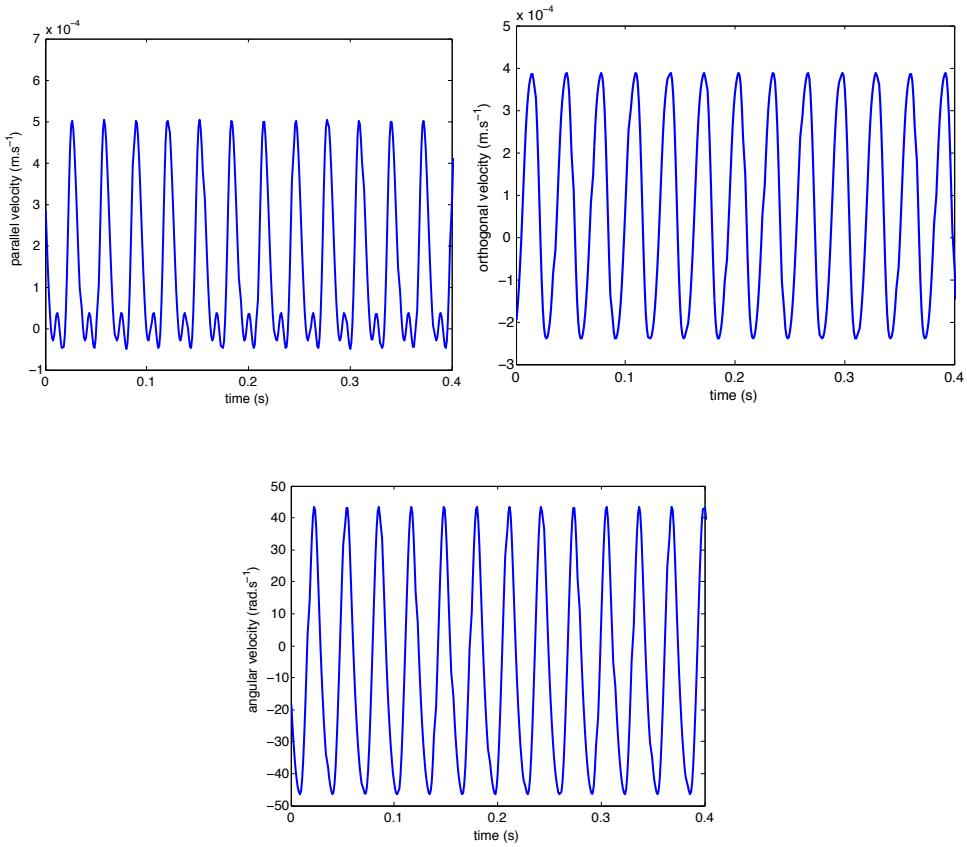

Figure 4.12: Above translational speed of the swimmer head in the tangent and perpendicular directions, and below rotational speed.

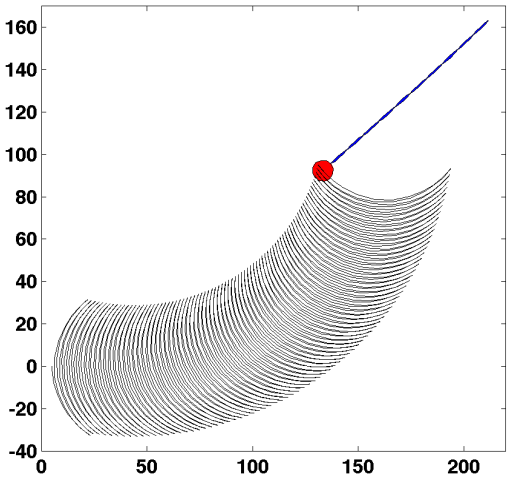

Figure 4.13: Trajectory of the head of the sperm-cell during one period.

4.3 Controllability

In this section we present a controllability result for the N-link swimmer, and a new optimal stroke for displacement in minimum time. First, we prove by geometrical control techniques that for $N \geq 3$ sticks, the N-link swimmer is capable to reach any configuration in the plane. More precisely, we show that for almost any swimmer (i.e. for almost every set of sticks length) and for any initial configuration, the swimmer can reach any final position with a fixed final configuration. The global controllability result proved here shows the existence of a suitable shape deformation which leads the swimmer the desired final state. As a direct consequence, we show that the optimal swimming problem, that is to minimize the time to reach a given configuration, is well posed. Therefore, there exists an optimal strategy which leads to the set final position and configuration in minimum time. Finally, we perform some numerical simulations for the Purcell swimmer ($N = 3$), without any assumptions on the structure of the optimal strategy. Our results suggest that the optimal swimming motion is indeed periodic, and we show that the stroke we obtain gives a displacement 20% better than the Purcell one.

Theorem 4.1. *Consider the N-link swimmer described in Section 4.1 evolving in the space $\mathbf{R}^2$. Then for almost any length of sticks $(L_i)_{i=1,\cdots,N}$ and for any initial configuration*

$(\mathbf{x}_1^i, \theta_1^i, \alpha_2^i, \cdots, \alpha_N^i) \in \mathbb{R}^2 \times [0, 2\pi]^N$, any final configuration $(\mathbf{x}_1^f, \theta_1^f, \alpha_2^f, \cdots, \alpha_N^f)$ and any final time $T > 0$, there exists a shape function $(\alpha_2, \cdots, \alpha_N) \in \mathcal{W}^{1,\infty}([0, T])$, satisfying $(\alpha_2, \cdots, \alpha_N)(0) = (\alpha_2^i, \cdots, \alpha_N^i)$ and $(\alpha_2, \cdots, \alpha_N)(T) = (\alpha_2^f, \cdots, \alpha_N^f)$ and such that if the self-propelled swimmer starts in position $(\mathbf{x}_1^i, \theta_1^i)$ with the shape $(\alpha_2^i, \cdots, \alpha_N^i)$ at time $t = 0$, it ends at position $(\mathbf{x}_1^f, \theta_1^f)$ and shape $(\alpha_2^f, \cdots, \alpha_N^f)$ at time $t = T$ by changing its shape along $(\alpha_2, \cdots, \alpha_N)(t)$.

Proof: The proof of the theorem is divided into three steps. First, we deal with the analyticity of the dynamics vector fields. Then, we prove the controllability of the Purcell 3-link swimmer, exploiting the Chow theorem and the Orbit theorem. Finally, we generalize the result to the N-link swimmer.

4.3.1 Regularity

The first step is to prove that the vector fields of the motion equation of the swimmer are analytic on $\mathcal{M}$.

As a direct consequence of (4.6) and (4.7), the linear maps $\mathbf{A}$ and $\mathbf{B}$ belong to the set of matrices whose entries are analytic functions on $[0, 2\pi]^N$. The family of vector $(\tilde{\mathbf{g}}_i(\theta_1, \alpha_2, \cdots, \alpha_N))_{i=1,\cdots,N-1}$ is obtained by the multiplication of $\mathbf{A}^{-1}$ by $\mathbf{B}$. Since the coefficients of $\mathbf{A}^{-1}$ are obtained by multiplication and division of those of $\mathbf{A}$, and because the determinant of $\mathbf{A}$ is never null, the entries of inverse matrix $\mathbf{A}^{-1}$ remain analytic functions on $[0, 2\pi]^N$. Thus, the family of vector fields $(\tilde{\mathbf{g}}_i)_{i=1,\cdots,N}$ are analytic on $[0, 2\pi]^N$.

4.3.2 Controllability of the Purcell Swimmer (N=3)

Now we prove the controllability of the Purcell's swimmer. By replacing $N = 3$ in (4.17), the Purcell's dynamics reads

$$\begin{pmatrix} \dot{\alpha}_2 \\ \dot{\alpha}_3 \\ \dot{x}_1 \\ \dot{y}_1 \\ \dot{\theta}_1 \end{pmatrix} = \mathbf{g}_1(\theta_1, \alpha_2, \alpha_3)\dot{\alpha}_2 + \mathbf{g}_2(\theta_1, \alpha_2, \alpha_3)\dot{\alpha}_3 \,. \tag{4.41}$$

We now express the Lie algebra of the vector fields $\mathbf{g}_1$ and $\mathbf{g}_2$ for any $\theta_1 \in [0, 2\pi]$ at the point $(\alpha_2, \alpha_3) = (0, 0)$, for a swimmer whose sticks have

same length $L > 0$.

The two vectors $\mathbf{g}_1(\theta_1, 0, 0)$ and $\mathbf{g}_2(\theta_1, 0, 0)$ are

$$\mathbf{g}_1(\theta_1,0,0) = \begin{pmatrix} 1 \\ 0 \\ \frac{2L\sin\theta_1}{27} \\ -\frac{2L\cos\theta_1}{27} \\ \frac{20}{27} \end{pmatrix}, \qquad \mathbf{g}_2(\theta_1,0,0) = \begin{pmatrix} 0 \\ 1 \\ -\frac{5L\sin\theta_1}{54} \\ \frac{5L\cos\theta_1}{54} \\ -\frac{7}{27} \end{pmatrix}.$$

Then, the iterated Lie brackets are equals to

$$[\mathbf{g}_1,\mathbf{g}_2](\theta_1,0,0) = \begin{pmatrix} 0 \\ 0 \\ \frac{5L(\eta-\xi)\cos\theta_1}{81\xi} \\ \frac{5L(\eta-\xi)\sin\theta_1}{81\xi} \\ 0 \end{pmatrix},$$

$$[\mathbf{g}_1,[\mathbf{g}_1,\mathbf{g}_2]](\theta_1,0,0) = \begin{pmatrix} 0 \\ 0 \\ -\frac{L(85\eta^2-58\eta\xi+21\xi^2)\sin\theta_1}{2187\xi\eta} \\ \frac{L(85\eta^2-58\eta\xi+21\xi^2)\cos\theta_1}{2187\xi\eta} \\ -\frac{22\eta^2-28\eta\xi+22\xi^2}{729} \end{pmatrix},$$

$$[\mathbf{g}_2,[\mathbf{g}_1,\mathbf{g}_2]](\theta_1,0,0) = \begin{pmatrix} 0 \\ 0 \\ \frac{L(47\eta^2-110\eta\xi+111\xi^2)\sin\theta_1}{2187\eta\xi} \\ -\frac{L(47\eta^2-110\eta\xi+111\xi^2)\cos\theta_1}{2187\eta\xi} \\ \frac{22\eta^2-28\eta\xi+22\xi^2}{729} \end{pmatrix}.$$

The determinant of the matrix whose columns are the previous vector fields is equal to

$$\begin{aligned} &\Big|\Big(\mathbf{g}_1\ \mathbf{g}_2\ [\mathbf{g}_1,\mathbf{g}_2]\ [\mathbf{g}_1,[\mathbf{g}_1,\mathbf{g}_2]]\ [\mathbf{g}_2,[\mathbf{g}_1,\mathbf{g}_2]]\Big)(\theta_1,0,0)\Big| \\ &= \tfrac{20L^2(\eta-\xi)^2(19\eta+45\xi)(11\eta^2-14\xi\eta+11\xi^2)}{129140163\eta^2\xi^2}. \end{aligned} \tag{4.42}$$

Since ξ and η are both strictly positive and anisotropic, the determinant is never null. Thus for any $\theta_1 \in [0, 2\pi]$, the Lie algebra of the vector fields $\mathbf{g}_1$

and $\mathbf{g}_2$ is fully generated at the point $(\theta_1, \alpha_2, \alpha_3) = (\theta_1, 0, 0)$. Remark that any point $(\alpha_2, \alpha_3, \mathbf{x}_1, \theta_1) \in [0, 2\pi]^2 \times \mathbf{R}^2 \times [0, 2\pi]$ belongs to the orbit of the point $(0, 0, \mathbf{x}_1, \theta_1)$. Since the vector fields are analytic, Orbit Theorem (cfr 1.2) guarantees that the Lie algebra of $\mathbf{g}_1$ and $\mathbf{g}_2$ is fully generated everywhere in the manifold $[0, 2\pi]^2 \times \mathbf{R}^2 \times [0, 2\pi]$.

To conclude, by Chow Theorem 1.1 we get the controllability of the Purcell's swimmer whose sticks have same length.

4.3.3 Controllability of the N-link swimmer

The third step is to generalize the previous controllability result to the N-link swimmer.

The dynamics of this swimmer is described by the ODE (4.17). By construction, the family of vector fields $\mathbf{g}_i$ generates the tangent space of the manifolds $[0, 2\pi]^{N-1}$,

$$\mathrm{Span}(\mathbf{g}_1, \cdots, \mathbf{g}_{N-1}) = \mathbb{R}^{N-1}\,. \tag{4.43}$$

The two vector fields $\mathbf{g}_1$ and $\mathbf{g}_2$ are related to the Purcell's one defined in (4.41): we add $N-2$ rows of zeroes, take sticks of null length $L_i = 0$ for $4 \leq i \leq N-1$, while keeping the three sticks $L_1 = L_3 = L$ and $L_2 = 2L$ unchanged.

In this case, for any $(\mathbf{x}_1, \theta_1) \in \mathbb{R}^2 \times [0, 2\pi]$ Subsection 4.3.2 shows that the vectors $\mathbf{g}_1(\theta_1, 0, \cdots 0)$, $\mathbf{g}_2(\theta_1, 0, \cdots 0)$ and their iterated Lie brackets $[\mathbf{g}_1, \mathbf{g}_2](\theta_1, 0, \cdots 0)$, $[\mathbf{g}_1, [\mathbf{g}_1, \mathbf{g}_2]](\theta_1, 0, \cdots 0)$, and $[\mathbf{g}_2, [\mathbf{g}_1, \mathbf{g}_2]](\theta_1, 0, \cdots 0)$ are linearly independent.

Therefore, the Lie algebra of the family $(\mathbf{g}_i)_{i=1,\cdots,N-1}$ at the point $(\theta_1, 0, \cdots, 0)$ is equal to the tangent space $T_{(0,\cdots,0,\mathbf{x}_1,\theta_1)}\mathcal{M}$.

Then, by analyticity of the vector fields $\mathbf{g}_i$, Orbit Theorem 1.2 states that the Lie algebra is fully generated everywhere for a swimmer whose the length of sticks verify $L_1 = L_3 = L$, $L_2 = 2L$ and $L_i = 0$, for $4 \leq i \leq N-1$.

Notice that the vector fields of the motion equation depend analytically also on the sticks length L_i, $i = 1, \cdots, N$. We define by $D^{(0,\cdots,0)}$, the function which associates to the $N-$uplet of the sticks lengths the determinant of the vectors $\mathbf{g}_1(0, \cdots, 0), \cdots, \mathbf{g}_{N-1}(0, \cdots, 0)$ and their iterated Lie brakets at the point $(0, \cdots, 0)$.

Since the dependance on L_i of vector fields $\mathbf{g}_i$ is analytic, we get the analyticity of the function $D^{(0,\cdots,0)}$. Thus for any $L > 0$, the value of $D^{(0,\cdots,0)}$ at

the point $(L, 2L, L, 0 \cdots 0)$ is not null. Then, by analyticity it remains non null almost everywhere in $\mathbb{R}^N$. Therefore, we obtain that the Lie algebra is fully generated for almost every swimmer.

Finally, by using Chow Theorem 1.1, we get the controllability stated in the Theorem 4.1.

4.4 Minimum time optimal control problem for the N-Link swimmer

This Section describes the minimum time optimal control problem for the N-link swimmer. The problem is defined in 4.4.1, and is well defined, from the controllability result proven in 4.3. Then in 4.4.2 we present the optimization strategy we used to find a solution to this optimal control problem.

4.4.1 Optimal Time Control Problem Statement

For any time $t > 0$, let us denote the state of the swimmer by $\mathbf{z}(t) := (\dot{\alpha}_2, \cdots, \dot{\alpha}_N, \dot{\mathbf{x}}_1, \dot{\theta}_1)(t)^T$, the control function by $\mathbf{u}(t) := (\dot{\alpha}_2, \cdots, \dot{\alpha}_N)(t)$ and the dynamics by $\mathbf{f}(\mathbf{z}(t), \mathbf{u}(t)) = \sum_{i=1}^{N-1} \mathbf{g}_i(\mathbf{z}(t))\, \dot{\alpha}_i(t)$.
In the following we assume that the swimmer starts at the initial configuration $\mathbf{z}^i$ and we set a final state $\mathbf{z}^f$. We want to find an optimal swimming strategy which minimizes the time to reach the final configuration, i.e.,

$$(OCP) \begin{cases} \inf\ T \\ \dot{\mathbf{z}}(t) = f(\mathbf{z}(t), \mathbf{u}(t))\ ,\ \forall t \in [0, T] \\ \mathbf{u}(t) \in \mathbf{U} := [-1, 1]^N\ ,\ \forall t \in [0, T] \\ \mathbf{z}(0) = \mathbf{z}^i \\ \mathbf{z}(T) = \mathbf{z}^f \end{cases}$$

By rescaling the dynamics (4.17), from the controllability result 4.1 the following statement holds.

Corollary 4.1. *Consider the N-link swimmer described in Section 4.1 evolving in $\mathbf{R}^2$. Then for almost any sticks lengths $(L_i)_{i=1,\cdots,N}$ and for any initial configuration $(\mathbf{x}_1^i, \theta_1^i, \alpha_2^i, \cdots, \alpha_N^i)$, any final configuration $(\mathbf{x}_1^f, \theta_1^f, \alpha_2^f, \cdots, \alpha_N^f)$ and any final time $T > 0$, there exists a function $(\alpha_2, \cdots, \alpha_N) \in \mathcal{W}^{1,\infty}([0, T])$ such that $(\dot{\alpha}_2, \cdots, \dot{\alpha}_N) \in \mathbf{U}$, satisfying $(\alpha_2, \cdots, \alpha_N)(0) = (\alpha_2^i, \cdots, \alpha_N^i)$ and $(\alpha_2, \cdots, \alpha_N)(T) = (\alpha_2^f, \cdots, \alpha_N^f)$ and such that if the self-propelled swimmer starts in position $\mathbf{x}_1^i, \theta_1^i$ with the shape $\alpha_2^i, \cdots, \alpha_N^i$ at time $t = 0$, it ends at*

position $(\mathbf{x}_1^f, \theta_1^f)$ *and shape* $\alpha_2^f, \cdots, \alpha_N^f$ *at time* $t = T$ *by changing its shape along* $(\alpha_2, \cdots, \alpha_N)(t)$.

This corollary means that the displacement of the swimmer does not depend of the speed of the shape changes of the swimmer. By applying Filippov-Cesary Theorem (as stated in [82]), there exist a minimal time such that the constraints are satisfied, and the optimal problem reads

$$(OCP) \begin{cases} \min\ T \\ \dot{\mathbf{z}}(t) = f(\mathbf{z}(t), \mathbf{u}(t))\ ,\ \forall t \in [0,T] \\ \mathbf{u}(t) \in \mathbf{U} := [-1,1]^N\ ,\ \forall t \in [0,T] \\ \mathbf{z}(0) = \mathbf{z}^i \\ \mathbf{z}(T) = \mathbf{z}^f \end{cases} \tag{4.44}$$

4.4.2 Optimization Strategy

In order to solve this optimal control problem, we use a so-called direct approach. The direct approach transforms the infinite dimensional optimal control problem (OCP) into a finite dimensional optimization problem (NLP). This is done by a discretization in time applied to the state and control variables, as well as the dynamics equation. These methods are usually less precise than indirect methods based on Pontryagin's Maximum Principle, but more robust with respect to the initialization. Also, they are more straightforward to apply, hence they are widely used in industrial applications.

Summary of the time discretization:

$t \in [0,T]$	$\rightarrow$	$\{t_0 = 0, \ldots, t_N = T\}$
$z(\cdot), u(\cdot)$	$\rightarrow$	$X = \{z_0, \ldots, z_N, u_0, \ldots, u_{N-1}, T\}$
Criterion	$\rightarrow$	$\min\ T$
Dynamics	$\rightarrow$	$(ex: Euler)\ z_{i+i} = z_i + hf(z_i, u_i)$
Adm. Cont.	$\rightarrow$	$-1 \leq u_i \leq 1$
Bnd. Cond.	$\rightarrow$	$\Phi(z_0, z_N) = 0$

We therefore obtain a nonlinear programming problem on the discretized state and control variables

$$(NLP) \begin{cases} \min\ F(z) = T \\ LB \leq C(z) \leq UB \end{cases}$$

All tests were run using the software Bocop[2] ([17]). The discretized nonlinear optimization problem is solved by the well-known solver Ipopt ([83])

[2]http://bocop.org

with MUMPS ([10, 9]), while the derivatives are computed by sparse automatic differentiation with Adol-C ([84]) and ColPack ([35]). In the numerical experiments, we used a Midpoint (implicit 2nd order) discretization with 1000 time steps. Execution times on a Xeon 3.2GHz CPU were a few minutes.

4.5 Numerical simulations for the Purcell swimmer ($N = 3$)

In this Section, we present the numerical simulations associated with the problem (4.44) in the case of N=3 sticks (Purcell's swimmer). We observe that while we did not make any assumptions on the structure of the optimal trajectory, the solution given by the direct solver Bocop shows a periodic structure. We extract a stroke from these solutions, and check that we obtain a better displacement better than the one of Purcell ([70], [13]).

In the rest, we reformulate the system in order to match the state variables used in the literature for the Purcell swimmer ([13]), as we have done in the previuous section. Following [13], we take the sticks lengths $L_1 = L_3 = 1$ and $L_2 = 2$. For the sake of clarity we recall that, the state of the swimmer (see Fig 4.14) is described by

- the position (x_2, y_2) of the center of the second stick, and $\theta_2 := \theta_1 - \alpha_2$ the angle between the x-axis and the second stick
- the shape of the swimmer, defined by the two angles $\beta_1 := -\alpha_2$ and $\beta_3 := \alpha_3$.

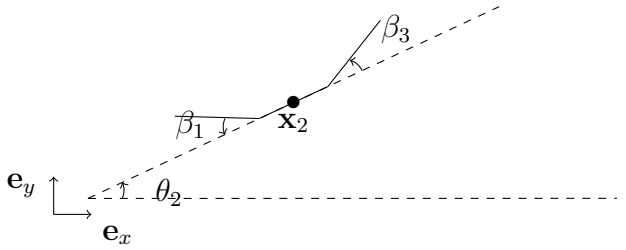

Figure 4.14: Purcell's 3-link swimmer.

The time derivative of the new variables which describe the swimmer are

linear in the previous ones,

$$\begin{pmatrix} \dot{\beta}_1 \\ \dot{\beta}_3 \\ \dot{\mathbf{x}}_2 \\ \dot{\theta}_2 \end{pmatrix} = \mathbf{M}\left(\theta_2, \beta_1\right) \begin{pmatrix} \dot{\alpha}_2 \\ \dot{\alpha}_3 \\ \dot{\mathbf{x}}_1 \\ \dot{\theta}_1 \end{pmatrix} ,$$

where the matrix $\mathbf{M}\left(\theta_2, \beta_1\right)$ is defined by,

$$\mathbf{M}\left(\theta_2, \beta_1\right) = \begin{pmatrix} -1 & 0 & 0 & 0 & 0 \\ 0 & 1 & 0 & 0 & 0 \\ \sin(\theta_2) + \cos(\beta_1) & 0 & 1 & 0 & -\sin(\theta_2) \\ -\cos(\beta_1) - \cos(\theta_2) & 0 & 0 & 1 & \cos(\theta_2) \\ -1 & 0 & 0 & 0 & 1 \end{pmatrix} .$$

As a result, the dynamics (4.17) reads in this case

$$\begin{pmatrix} \dot{\beta}_1 \\ \dot{\beta}_3 \\ \dot{\mathbf{x}}_2 \\ \dot{\theta}_2 \end{pmatrix} = \tilde{\mathbf{f}}_1\left(\theta_2, \beta_2, \beta_3\right)\ \dot{\beta}_1 + \tilde{\mathbf{f}}_2\left(\theta_2, \beta_2, \beta_3\right)\ \dot{\beta}_3 \tag{4.45}$$

where for $i = 1, 2$

$$\tilde{\mathbf{f}}_i\left(\theta_2, \beta_1, \beta_3\right) = \mathbf{M}\left(\theta_2, \beta_1, \right) \mathbf{g}_i\left(\theta_1, \alpha_2, \alpha_3\right) . \tag{4.46}$$

Since the variables which describe the swimmer are the image of the previous one by a one-to-one mapping, it is clear that the controllability result proved in Section 4.3.2 holds for the ODE (4.45).

4.5.1 The classical Purcell stroke

Here, we recall the Purcell Stroke given in [70] and studied in more detail in [13]. Moreover in order to compare better the results Let us denote by $\Delta\theta$, the angular excursion of β_1 and β_3, meaning that for all time $\beta_1(t)$ and $\beta_3(t)$ belong to the interval $[-\frac{\Delta\theta}{2}, \frac{\Delta\theta}{2}]$. Calling T the interval of time in which the swimmer performs the stroke, the Purcell stroke is defined by the following periodic cycle of deformation,

$$\beta_1(t) = \begin{cases} \dfrac{4\Delta\theta}{T}t - \dfrac{\Delta\theta}{2} & \text{if } 0 \le t \le \frac{T}{4} \\ \dfrac{\Delta\theta}{2} & \text{if } \frac{T}{4} \le t \le \frac{T}{2} \\ -\dfrac{4\Delta\theta}{T}t + \dfrac{5\Delta\theta}{2} & \text{if } \frac{T}{2} \le t \le \frac{3T}{4} \\ -\dfrac{\Delta\theta}{2} & \text{if } \frac{3T}{4} \le t \le T \end{cases} ,$$

and

$$\beta_3(t) = \begin{cases} \dfrac{\Delta\theta}{2} & \text{if } 0 \le t \le \frac{T}{4} \\ -\dfrac{4\Delta\theta}{T}t + \dfrac{3\Delta\theta}{2} & \text{if } \frac{T}{4} \le t \le \frac{T}{2} \\ -\dfrac{\Delta\theta}{2} & \text{if } \frac{T}{2} \le t \le \frac{3T}{4} \\ \dfrac{4\Delta\theta}{T}t - \dfrac{7\Delta\theta}{2} & \text{if } \frac{3T}{4} \le t \le T \end{cases} .$$

In the following, we call the "classical" Purcell stroke the one corresponding to $\Delta\theta = \frac{\pi}{3}$.

4.5.2 Comparison of the optimal stroke with the classical Purcell stroke

For the comparison, we take the initial position $\mathbf{x}_2 = (0, 0)$ and $\theta_2 = 0$ and the final position $\mathbf{x}_2 = (-0.25, 0)$ and $\theta_2 = 0$. We also constrain the angles $\beta_1(t)$ and $\beta_3(t)$ to vary between $-\frac{\pi}{6}$ and $\frac{\pi}{6}$ for all time $t > 0$. We recompute the displacement produced by the classical Purcell's stroke, integrating the dynamics (4.45) with a classical fourth order Runge-Kutta method. Solving the minimum time problem with the direct method gives us a periodic solution from which we extract a candidate for the time optimal stroke.
We describe this stroke in more details, and show its displacement versus the Purcell one.

Solving the optimal problem (4.44) we observe that the solution is periodic, as show the graphs on Fig. 4.15 for the angles functions β_1, β_3 and the x-displacement.

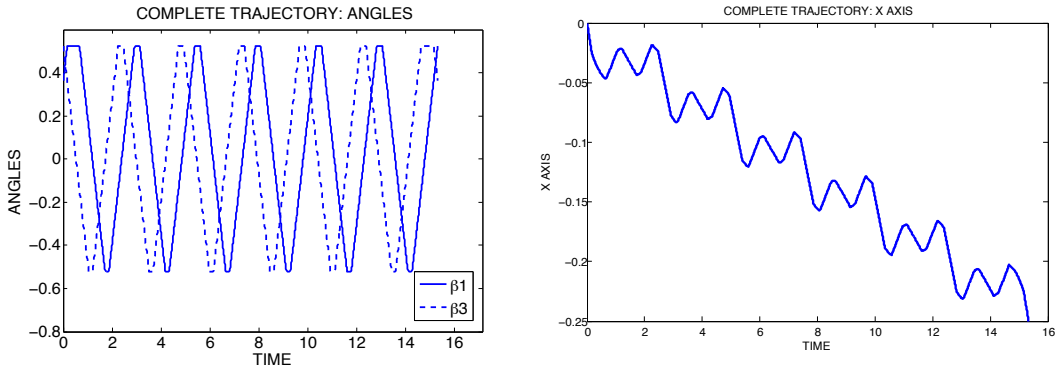

Figure 4.15: Angles and x-displacement for a whole periodic trajectory.

From the plots above it is evident that the optimal controls have a periodic structure and perform more than one period in the optimal interval of time. In order to compare the results for the displacement with the Purcell's ones, we need to select only one period (i.e. one stroke). Moreover we chose the period T of the classical Purcell stroke equal to the period of the optimal stroke. We show on Fig. 4.5.2 the angles functions β_1 and β_3. Moreover, Fig. 4.17 represents the phase portrait for both the classical Purcell stroke and our selected optimal stroke in the same period T.

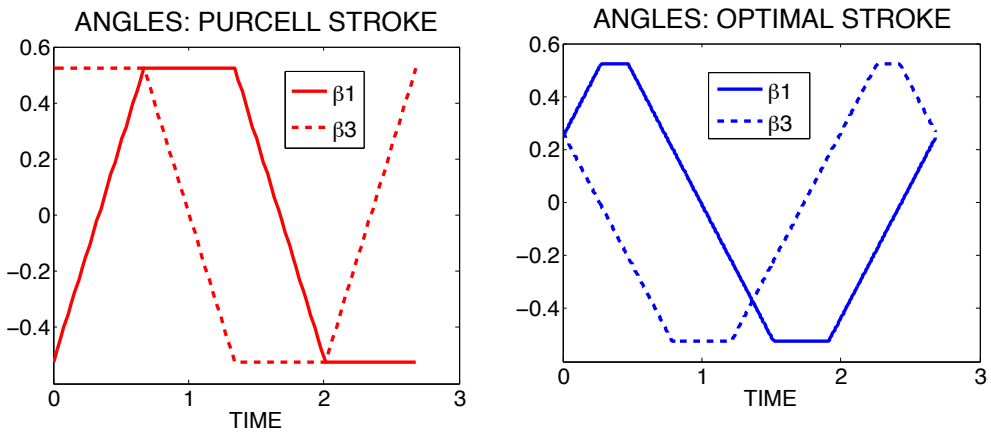

Figure 4.16: Angles of Purcell stroke and optimal stroke.

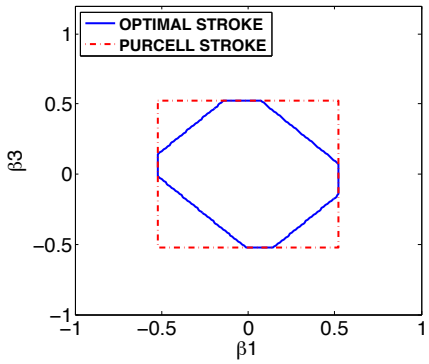

Figure 4.17: Phase portrait of Purcell stroke and optimal stroke.

We show now the shape changes in the (X,Y) plane for the Purcell and optimal stroke. Figure 4.18 shows the Purcell swimmer in four different

times during the classical Purcell stroke, and figure 4.19 shows the swimmer performing the selected optimal stroke.

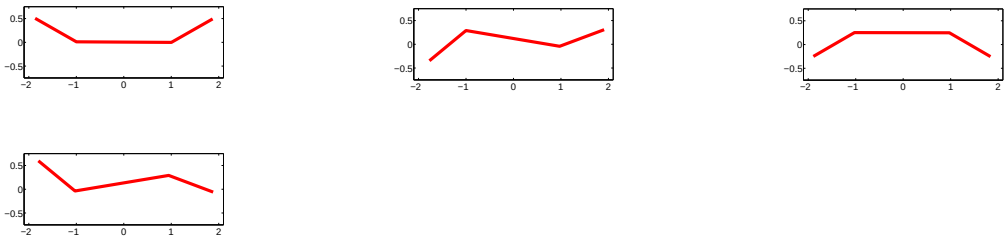

Figure 4.18: Shape changes for the Purcell's stroke.

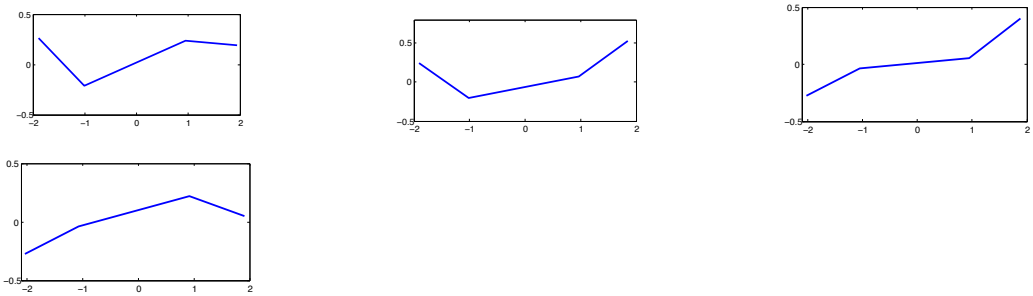

Figure 4.19: Shape changes for the optimal stroke.

We draw on Fig. 4.20 the displacement of the point (x_2, y_2) during one classical Purcell stroke and one optimal stroke. The final displacement observed for the Purcell stroke matches the results of [13]. We observe that our optimal stroke allows the swimmer to move 20% further in the x-direction.

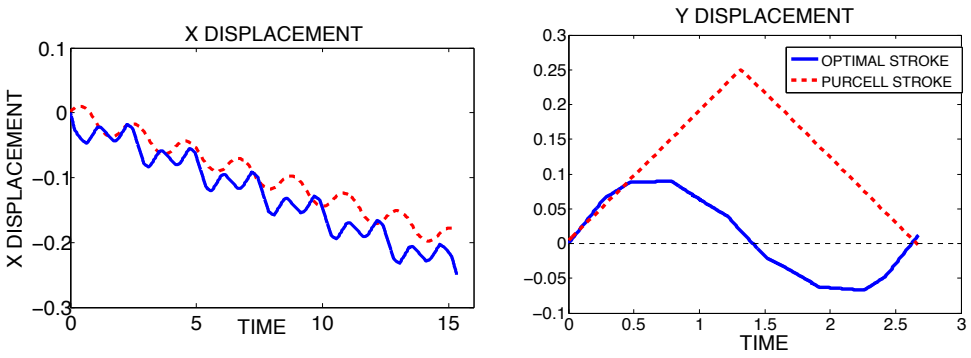

Figure 4.20: On the left the x displacement for the Purcell swimmer and the optimal one in the time of 6 Purcell strokes. On the right y displacement for one Purcell and one optimal stroke.

We study now for both strokes the x-displacement with respect to the angular excursion, as shown on Fig. 4.21. In both cases, we see that a larger interval of angular excursion gives a greater displacement. The results we find for the Purcell stroke results match the ones in [13]. Here again, it is obvious that the strokes given by our optimization strategy produce a greater x-displacement than the Purcell, one for any range of angular excursion.

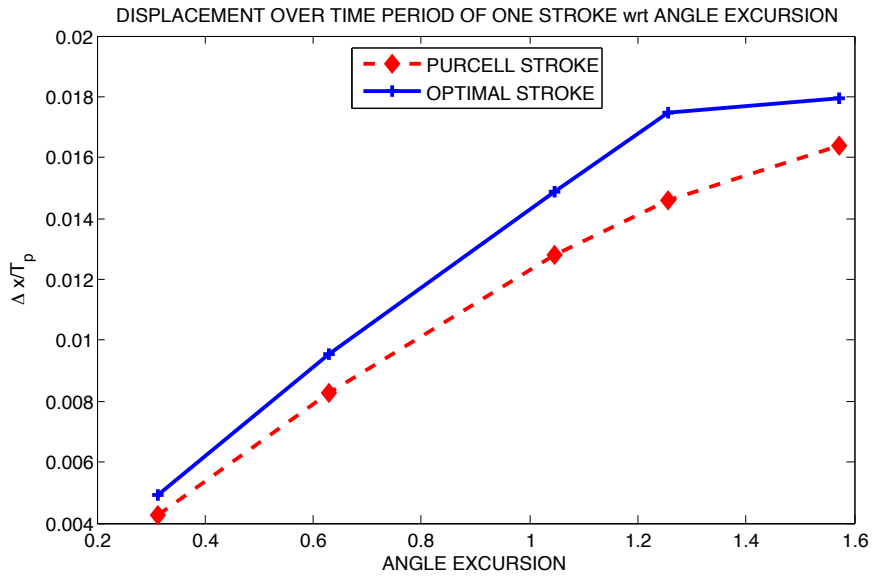

Figure 4.21: x displacement wrt angular excursion, Purcell and optimal stroke.

4.5.3 Optimization of other movements: y-displacement and rotation

We try here different final conditions, $(0, 1, 0)$ for a displacement along the y-axis, and $(0, 0, \pi/4)$ for a rotation at the origin. The angular excursion is here $2\pi/3$, i.e. the angles β_1 and β_3 are in $[-\pi/3, \pi/3]$.

First numerical simulations indicate periodic movements for both y-displacement and rotations, and the strokes have different shapes than in the x displacement case. The y-displacement case is shown on Fig. 4.22 and Fig. 4.23, we note that the distance covered in one "stroke" is lesser than in the x-displacement case. This would be consistent with the fact that the drag force of the fluid is greater in this direction.

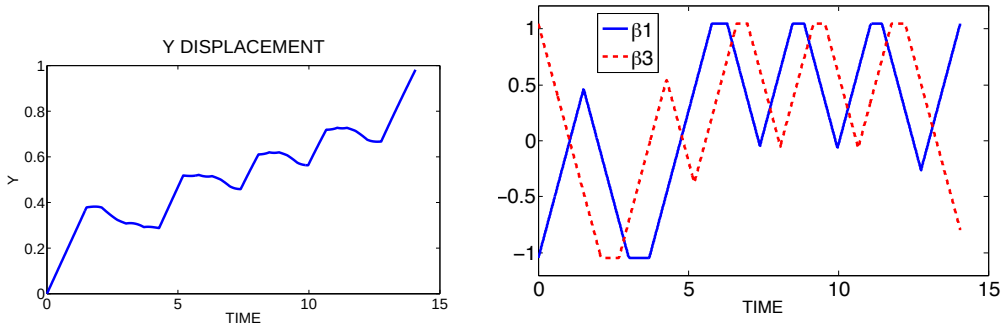

Figure 4.22: Y-displacement: Y, angles

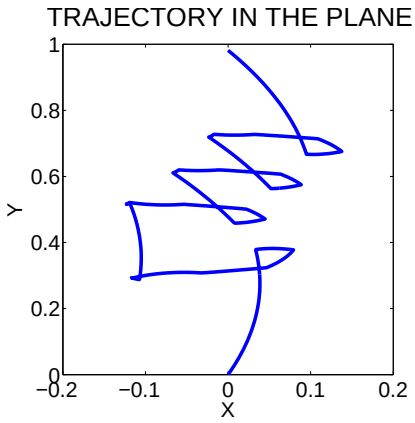

Figure 4.23: Y-displacement: trajectory in the plane

Fig. 4.24 shows the solution for a rotation of the angle θ_2. Fig. 4.25 is the associated displacement in the plane around the origin before returning

to $(0, 0)$. Is would seem that rotations cannot be performed while staying at the same (x,y) coordinates all the time, which would need to be confirmed by a formal study of the dynamics.

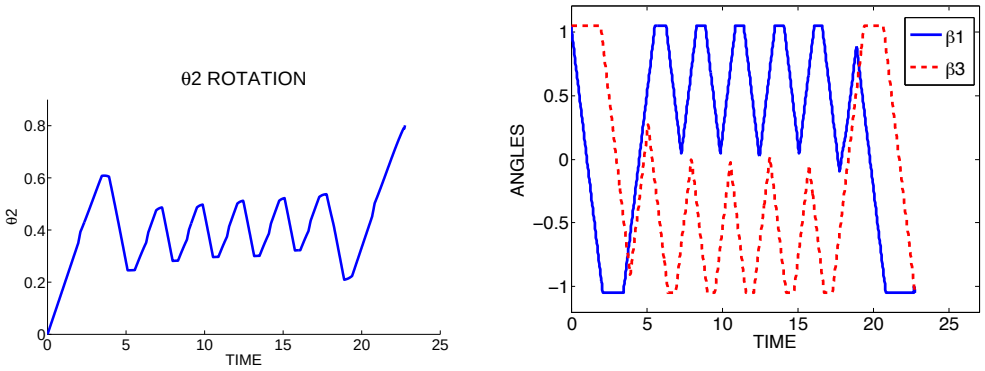

Figure 4.24: θ_2-rotation: θ_2, angles

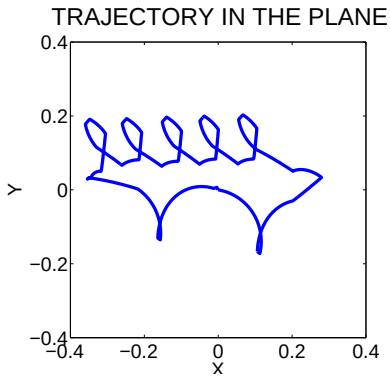

Figure 4.25: θ_2-rotation: trajectory in the plane

4.6 Optimal design of the three link Purcell swimmer

In this subsection we address the question of the optimal design for the Purcell 3-link swimmer presented in the previous section. More precisely we investigate the best link length ratio which maximizes its displacement. Among a set of optimal strategies of deformation (strokes), we provide an asymptotic estimate of the displacement for small deformations, from which we derive the optimal link ratio.

To this end we recall throughout a picture the variables by which we describe our system

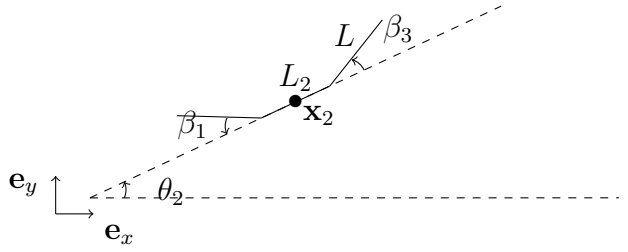

Figure 4.26: Purcell's 3-link swimmer with variable stick's length.

Notice that we denote by L and L_2 the length of the two external arms and central link whose optimal ration we wish to determine.

4.6.1 Optimal strokes

We are interested in finding a periodic sequence of deformations which maximizes the displacement of the swimmer along the x-axis. More precisely, we optimize both the link length ratio L_2/L and the deformation of the swimmer over time. Taking the deformation speed $\dot{\beta}_{1|3}$ as control functions, we obtain the optimal control problem

$$(OCP)\begin{cases} \max\ x_2(T)\ \text{ s.t.} \\ \dot{\mathbf{z}}(t) = f(\mathbf{z}(t), \dot{\beta}_1, \dot{\beta}_3) \quad \forall t \in [0,T]\,, \\ \dot{\beta}_{1|3} \in \mathbf{U} = [-b,b] \quad \forall t \in [0,T]\,, \\ \beta_{1|3}(t) \in [-a,a] \quad \forall t \in [0,T]\,, \\ x_2(0) = y_2(0) = \theta_2(0) = 0, y_2(T) = \theta_2(T) = 0\,, \\ \beta_{1|3}(0) = \beta_{1|3}(T), \\ 2L + L_2 = c. \end{cases}$$

We set the constraints a and b over the amplitude and deformation speed, as well as the total length c of the swimmer. The final time T is fixed, and the constraint $\beta_{1|3}(0) = \beta_{1|3}(T)$ ensures that the swimmer is in the same configuration at the initial and final time. Note that this condition can be satisfied by either a single stroke or a sequence of strokes. From [36], numerically solving (OCP) typically gives a periodic sequence of identical strokes. Their phase portrait is octagonal, as illustrated on Fig.4.27, and we will detail how this shape is consistent with optimal control theory.

We would like also to recall here the Pontryagin Maximum Principle (PMP) as it gives some insight on the shape of optimal strokes. This theorem in optimal control introduced by Pontryagin et al. in [16] gives necessary conditions for local optimality. More information on the PMP can be found in [2, 82]. The PMP is characterized by an Hamiltonian function H that formally depends on the state variables $\mathbf{z}$, the control functions $\dot{\beta}_{1|3}$, and so-called *costate* variables noted $\mathbf{p}$. While originally inspired by the Hamiltonian in mechanics, in the context of optimal control H does not actually correspond to the energy of the system. The costate variables play the part of the generalized velocities in Lagrangian mechanics, and they can be interpreted as Lagrange multipliers (in the sense of constrained optimization) related to the dynamics of the system. Let the Hamiltonian be

$$H(\mathbf{z}, \mathbf{p}, \dot{\beta}_1, \dot{\beta}_3) = \langle \mathbf{p}, \mathbf{g}_1(\mathbf{z}) \rangle \, \dot{\beta}_1 + \langle \mathbf{p}, \mathbf{g}_2(\mathbf{z}) \rangle \, \dot{\beta}_3. \tag{4.47}$$

Under the assumption that $\mathbf{g}_{1|2}$ are continuous and C^1 with respect to $\mathbf{z}$, the PMP states that:
if $(\mathbf{z}^*, \dot{\beta}_1^*, \dot{\beta}_3^*)$ is a solution of (OCP) then there exists $\mathbf{p}^* \neq 0$ absolutely continuous such that $\dot{\mathbf{z}}^* = H_p(\mathbf{z}^*, \mathbf{p}^*, \dot{\beta}_1^*, \dot{\beta}_3^*)$, $\dot{\mathbf{p}}^* = -H_z(\mathbf{z}^*, \mathbf{p}^*, \dot{\beta}_1^*, \dot{\beta}_3^*)$, $\mathbf{p}^*(T)$ is orthogonal to the cotangent cone of the final conditions at $\mathbf{z}^*(T)$ and $(\dot{\beta}_1^*, \dot{\beta}_3^*)$ maximizes the Hamiltonian for almost every time $t \in [0, T]$.
The Hamiltonian in (4.47) is linear in the controls $\dot{\beta}_{1|3}$. If we assume $\langle \mathbf{p}, \mathbf{g}_i(\mathbf{z}) \rangle \neq 0$ for $i = 1, 2$ over a time interval, then the optimal control $\dot{\beta}_{1|3^*}$ that maximizes H must be on the boundary of $U = \{(-b, -b), (-b, b), (b, -b), (b, b)\}$. In terms of phase portrait, this corresponds to diagonal lines.
Moreover, we have the constraints on the joint angles $\beta_{1|3}(t) \in [-a, a]$. When one of them is active and $|\beta_i| = a$, the corresponding control $\dot{\beta}_i = 0$. In terms of phase portrait, this gives horizontal or vertical lines.

Finally as stated in [80], we expect optimal strokes to be symmetric with respect to the diagonal axes $\beta_1 = \beta_3$ and $\beta_1 = -\beta_3$. This comes from the equations of motion being linear and time independent. From the linearity, optimal strokes should be invariant by reflection with respect to the axis of the swimmer's body. From time independence, the stroke should be invariant when inverting the arms movement and going backwards in time.

4.6.2 Optimal swimmer design

In this section, we express the leader term of the swimmer's displacement for a stroke of small perimeter which satisfies all properties stated in the previous section. We represent the stroke by a closed octagonal curve γ in the phase portrait (β_1, β_3), see Fig. 4.27.

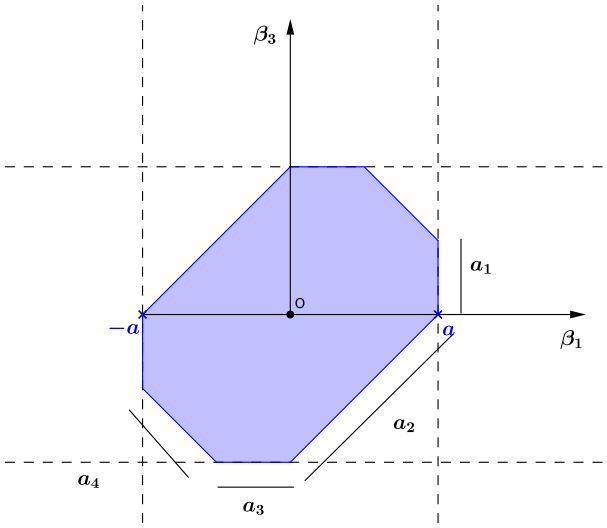

Figure 4.27: Phase portrait (β_1, β_3) of the octagonal stroke considered for the expansion of the displacement.

As a consequence of neglecting inertia forces, velocities appear linearly in the dynamic, and time can be rescaled without changing the dynamics. Thus the displacement of the swimmer after one stroke does not depend on the speed along the curve γ, but only on the shape of the stroke. From now on, we parametrize γ by the arc-length s. Using a similar approach to [29], we express the swimmer's displacement along the x-axis (i.e., $x(T) - x(0)$) as an asymptotic expansion for small length a_i, $i = 1, \cdots, 4$.

Displacement over the arc $s \in [0, a_1]$.
On this part, according to Fig. 4.27, we set $\mathbf{u} = (\dot{\beta}_1, \dot{\beta}_3) = (0, -1)$. The dynamics of the swimmer is therefore given by $\dot{\mathbf{z}} = -\mathbf{g}_2$, and the time expansion at order two is given by

$$\begin{aligned} \mathbf{z}(a_1) = \quad & \mathbf{z}(0) - a_1 \mathbf{g}_2(\mathbf{z}(0)) \\ & + \frac{a_1^2}{2} \frac{\partial \mathbf{g}_2}{\partial \mathbf{z}}(\mathbf{z}(0)) \left(\mathbf{g}_2(\mathbf{z}(0))\right) + o(a_1^3)\,. \end{aligned} \tag{4.48}$$

Displacement over the arc $s \in [a_1, a_1 + a_2]$.
Similarly, the position of the swimmer at $s = a_1 + a_2$ can be expressed as

$$\begin{aligned} \mathbf{z}(a_1 + a_2) = \quad & \mathbf{z}(a_1) - \frac{a_2\sqrt{2}}{2} \mathbf{h}(\mathbf{z}(a_1)) \\ & + \frac{a_2^2}{4} \frac{\partial \mathbf{h}}{\partial \mathbf{z}}(\mathbf{z}(a_1)) \left(\mathbf{h}(\mathbf{z}(a_1))\right) + o(a_2^3)\,, \end{aligned} \tag{4.49}$$

where $\mathbf{h} := \mathbf{g}_1 + \mathbf{g}_2$. Plugging the value of $\mathbf{z}(a_1)$ from (4.48) into (4.49) and

neglecting the terms of order greater than two, we get

$$\begin{aligned}\mathbf{z}(a_1+a_2) = \quad & \mathbf{z}(0) + c_1(\mathbf{g}_1,\mathbf{g}_2,\mathbf{z}(0),a_1,a_2) \\ & + c_2(\mathbf{g}_1,\mathbf{g}_2,\mathbf{z}(0),a_1,a_2) \\ & + o(a_1^3) + o(a_2^3) \end{aligned} \tag{4.50}$$

with

$$\begin{aligned} c_1(\mathbf{f},\mathbf{g},\mathbf{z},a_1,a_2) = \quad & -\frac{\sqrt{2}a_2}{2}\mathbf{f}(\mathbf{z}) \\ & + (-a_1 - \frac{\sqrt{2}a_2}{2})\mathbf{g}(\mathbf{z}), \\ c_2(\mathbf{f},\mathbf{g},\mathbf{z},a_1,a_2) = \quad & \frac{a_2^2}{4}\frac{\partial \mathbf{f}}{\partial \mathbf{z}}(\mathbf{z})\left(\mathbf{f}(\mathbf{z})\right) + \frac{a_2^2}{4}\frac{\partial \mathbf{g}}{\partial \mathbf{z}}(\mathbf{z})\left(\mathbf{f}(\mathbf{z})\right) \\ & + \left(\frac{a_1 a_2\sqrt{2}}{2} + \frac{a_2^2}{4}\right)\frac{\partial \mathbf{f}}{\partial \mathbf{z}}(\mathbf{z})\left(\mathbf{g}(\mathbf{z})\right) \\ & + \left(\frac{a_1 a_2\sqrt{2}}{2} + \frac{a_2^2}{4} + \frac{a_1^2}{2}\right)\frac{\partial \mathbf{g}}{\partial \mathbf{z}}(\mathbf{z})\left(\mathbf{g}(\mathbf{z})\right). \end{aligned}$$

Displacement over the complete stroke.
Iterating the computations along each arc and noting by $P = 2(a_1 + a_2 + a_3 + a_4)$ the stroke perimeter, the expansion of the total displacement for the octagonal stroke is finally obtained as

$$\mathbf{z}(T) - \mathbf{z}(0) = C\ [\mathbf{g}_1,\mathbf{g}_2](\mathbf{z}(0)) + o(a_i^3)_{i=1-4}\,, \tag{4.51}$$

where

$$C = \frac{a_1 a_2\sqrt{2}}{2} + a_1 a_3 + \frac{a_2 a_3\sqrt{2}}{2} + \frac{a_1 a_4\sqrt{2}}{2} + a_2 a_4 + \frac{a_3 a_4\sqrt{2}}{2}$$

and

$$[\mathbf{g}_1,\mathbf{g}_2](\mathbf{z}(0)) = \nabla\mathbf{g}_2(\mathbf{z}(0))\cdot\mathbf{g}_1(\mathbf{z}(0)) - \nabla\mathbf{g}_1(\mathbf{z}(0))\cdot\mathbf{g}_2(\mathbf{z}(0))$$

is the Lie brackets of $\mathbf{g}_1$ and $\mathbf{g}_2$ at point $\mathbf{z}(0)$. Choosing the starting point $\mathbf{z}(0)$ such that $\theta(0) = \beta_1(0) = \beta_3(0) = 0$, we compute the Lie bracket with a formal calculus tool

$$[\mathbf{g}_1,\mathbf{g}_2](0,0,x,y,0) = \begin{pmatrix} 0 \\ 0 \\ \frac{\eta-\xi}{\xi}\frac{L^3 L_2(3L+2L_2)}{(2L+L_2)^4} \\ 0 \\ 0 \end{pmatrix}. \tag{4.52}$$

Consequently, the x-displacement after one stroke is approximated by

$$x(T) - x(0) = C\left(\frac{\eta - \xi}{\xi}\right)\left(\frac{L^3 L_2(3L + 2L_2)}{(2L + L_2)^4}\right) + o(a_i^3)_{i=1-4} \tag{4.53}$$

Setting the total length of the swimmer by a constant equal to c, i.e., $2L + L_2 = c$, we find that (4.53) has a unique maximum at

$$L^* = c\Big(1 - \sqrt{\frac{2}{5}}\Big)\,, \quad L_2^* = c\Big(2\sqrt{\frac{2}{5}} - 1\Big)\,, \tag{4.54}$$

which gives an optimal ratio of

$$\left(\frac{L_2}{L}\right)^* = \frac{\sqrt{10} - 1}{3} \sim 0.721\,. \tag{4.55}$$

Remark: in [80] an optimal ratio of 0.747 is given for an efficiency-type criterion. The small gap may be due to the difference in models, or the change of the objective function.

4.6.3 Numerical simulations

We solve now the optimal control problem (OCP) numerically, in order to determine the optimal swimming strategy and link ratio. Simulations are performed with the toolbox Bocop ([17]) that implements a direct transcription method. This approach uses a time discretization to transform the continuous (OCP) into a finite-dimensional optimization problem (nonlinear programming). We refer to [14] for more details on these methods. We use here an implicit midpoint discretization with 100 to 2500 time steps. Note that this method does not use the PMP.

As stated in (OCP), the criterion is to maximize the total displacement along the x-axis over a fixed time T. The initial state of the swimmer is set as $x(0) = y(0) = \theta_2(0) = 0$, with the final conditions $y(T) = \theta_2(T) = 0$. The initial shape angles are left free, with the periodicity conditions $\beta_i(0) = \beta_i(T), i = 1, 3$. We set the total length $c = 4$ for an easier comparison with the classical Purcell swimmer ($L = 1, L_2 = 2$).

We explore different values for the bounds a, b on the shape angles and deformation speed and see their influence on the optimal stroke and link ratio. For practical applications, the values for a and b should reflect the physical characteristics of the studied swimmer. It should be pointed out

that the period of the optimal stroke is not known a priori. We arbitrarily set $T = 1$ in the first set of simulations, and $T = 25$ when studying the larger amplitudes. In the latter case we find that the swimming strategy consists in a periodic sequence of identical strokes, as previously observed in [36].

Small amplitudes, influence of speed limits

We start with small amplitudes by setting $a = \pi/20$ and solve (OCP) for different values of the speed limit b. Here we set $T = 1$ and use 250 time steps for the discretization. Optimizations take about one minute on a standard laptop. Results are given in Table.4.1, with the phase portraits for the shape angles β_1, β_3 on Fig.4.28.

First, we observe that the optimal ratio L_2/L is very close to its theoretical value of 0.721 from (4.55), regardless of b. The speed bound does however have an influence on the shape of the optimal stroke, and its displacement. Displacement increases with higher speeds, and we find the following empirical relation between b and the stroke shape, confirmed by simulations with other values of a:
- for $b < 4a/T$: diamond stroke, which touches the bound a for the limit case $b = 4a/T$.
- for $4a/T < b < 8a/T$: octagonal stroke.
- for $b = 8a/T$: classical Purcell stroke (square).
- for $b > 8a/T$: sequence of several strokes.

The three strokes observed (diamond, octagon, square) match the discussion from subsection 4.6.1. They include only diagonal lines (bang arcs saturating the speed limit b) and horizontal/vertical lines (constrained arcs for the amplitude limit a). Note also that the square and diamond strokes are particular cases of the octagonal one, by setting the appropriate arc lengths to 0.

Remark 4.1. *This empirical relation can also be interpreted in terms of the period T, with the two limit values $T = 8a/b$ for the Purcell stroke and $T = 4a/b$ for the diamond touching a.*

Table 4.1: Small amplitude ($a = \pi/20$).

b	$x(T)$	L_2/L	stroke
0.5	2.68E-3	0.719	diamond
$\pi/5$	4.23E-3	0.719	diamond
0.75	5.70E-3	0.719	octagon
1	7.73E-3	0.719	octagon
$2\pi/5$	8.42E-3	0.717	square
1.5	1.14E-2	0.719	octagon (x2)
2	1.55E-2	0.719	octagon (x2)

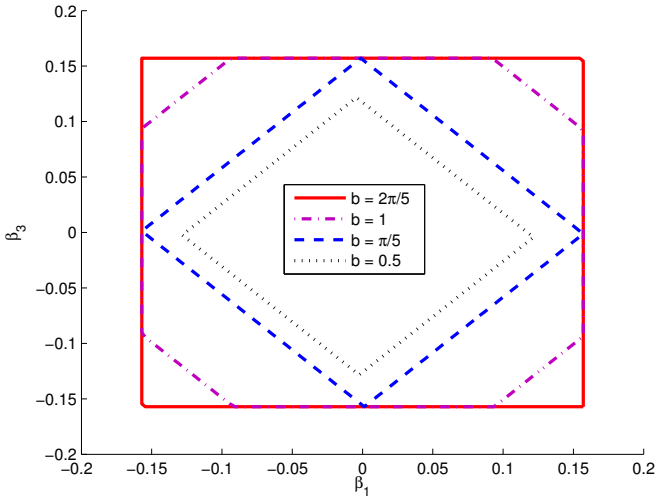

Figure 4.28: Phase portraits of the strokes for small amplitudes, $a = \pi/20$. The shapes observed are consistent with the discussion in subsection 4.6.1.

Comparison with the classical Purcell swimmer

Now we compare the performance of the optimal swimmer with respect to the classical Purcell swimmer defined by $L = 1, L_2 = 2$, meaning a ratio of 2. For this comparison we set $a = \pi/6$ (thus a stroke amplitude of $\pi/3$) and $b = \pi/3, 2\pi/3, \pi, 4\pi/3$ and $T = 1$. The optimization for the Purcell swimmer is done by setting $L = 1$ instead of letting it free. The results are summed up in Table.4.2 and Fig.4.29. We see that the shape of the stroke matches the empirical law, and that the optimal link ratio stays close to its theoretical value. We also observe a consistent gain in displacement that seems to increase with the speed limit, up to 64% for the classical Purcell stroke (square).

Table 4.2: Optimal swimmer vs Purcell swimmer.

b	x(T)	L_2/L	stroke	$x_{Purcell}(T)$	gain
$pi/3$	1.17E-2	0.717	diamond	7.373E-3	51%
$2\pi/3$	4.57E-2	0.708	diamond	2.848E-2	60%
π	7.82E-2	0.699	octagon	4.806E-2	63%
$4\pi/3$	8.80E-2	0.695	square	5.359E-2	64%

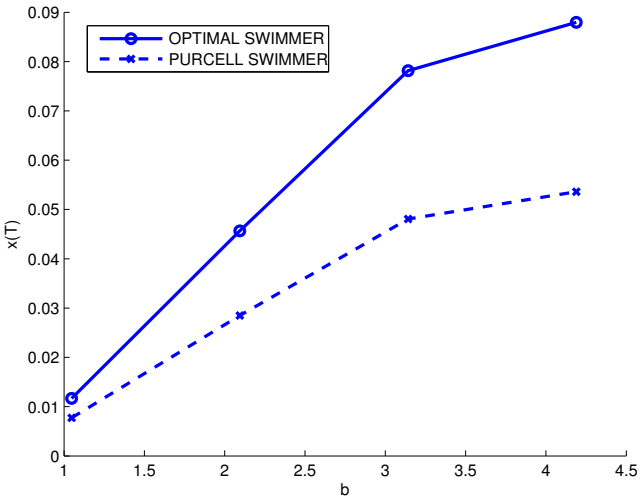

Figure 4.29: Displacement for the optimal/Purcell swimmer.

Large amplitudes, influence of angle limits

Now we study the influence of the maximal amplitude of the stroke, set by the bound a. In this last part we set the deformation speed limit $b = 1$ to focus on the amplitude. Since we would like to study only the true optimal strokes, whose period is not known, we also take a longer final time $T = 25$. We expect to obtain trajectories that exhibit a sequence of several identical strokes with a period $T^* < T$. The number of time steps is raised accordingly to 2500, which increases the computational time up to half an hour. Another way of finding the optimal stroke directly could be to leave the final time T free in the optimization, while maximizing the average speed of the stroke

$x(T)/T$ instead of the displacement $x(T)$.

The results are illustrated in Table.4.3 and Figs.4.30-4.31. First, the simulations confirm that the optimal strategy is a periodic sequence of identical strokes. The shape of the optimal stroke is always octagonal until it becomes unconstrained for very large values of a. We observe that the central symmetry observed for small amplitudes is lost for larger a, however symmetry w.r.t both diagonal axes still holds as expected.

In the unconstrained case, we see arcs that are neither bang arcs (diagonal) or constrained arcs (horizontal/vertical), but rather appear as smooth curves (see Fig.4.30) . These are characteristic of so-called *singular arcs*, namely the case where $\langle p, g_i(z)\rangle = 0$ in the PMP. More details on the analysis of singular arcs can be found in [82], unfortunately here the complexity of the g_i makes further study quite difficult.

The total displacement $x(T)$ increases with a, first almost linearly when $a < \pi/3$ (see Fig.4.31). From $a \approx 1.95$ and above, we obtain the same, unconstrained solution. The improvement in displacement appears to be marginal between $a = \pi/3$ and the unconstrained case. Note that since the displacement is expected to be a monotone increasing function of a, we see that for $a = 1.5$, the optimization converged to a local solution.

The optimal ratio L_2/L shows a steady decrease with a, starting quite close to the value 0.721 computed for small amplitudes, the seemingly reaching a limit value of 2/3 in the unconstrained case (i.e. $L = 1.5, L_2 = 1$). We recall that the classical Purcell swimmer has a link ratio of 2 ($L = 1, L_2 = 2$).

a	x(T)	L_2/L	stroke
$\pi/20$	0.192	0.719	octagon x26
$\pi/10$	0.384	0.712	octagon x13
$\pi/6$	0.593	0.697	octagon x7
0.75	0.811	0.676	octagon x5
$\pi/3$	1.088	0.660	octagon x4
1.25	1.266	0.660	octagon x4
1.5	1.263	0.660	octagon x3
1.75	1.329	0.667	octagon x3
$2\pi/3$	1.335	0.667	unconstrained x3
2.5	1.335	0.667	unconstrained x3

Table 4.3: Larger amplitudes: optimal link ratio and stroke. Solutions become unconstrained about $a = 1.95$.

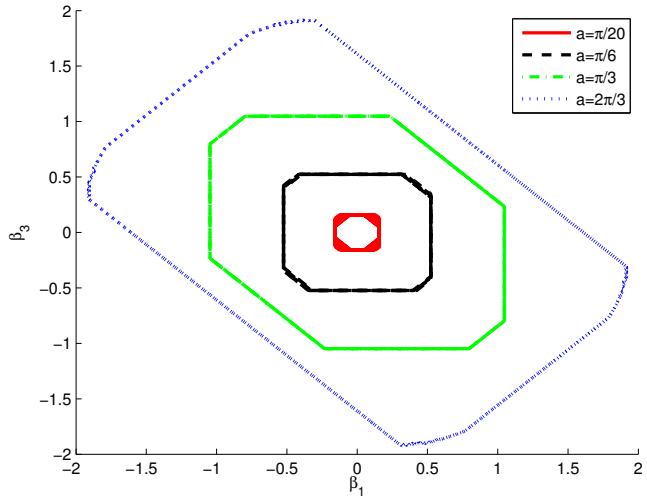

Figure 4.30: Larger amplitudes - Phase portrait (with several superposed strokes for each trajectory).

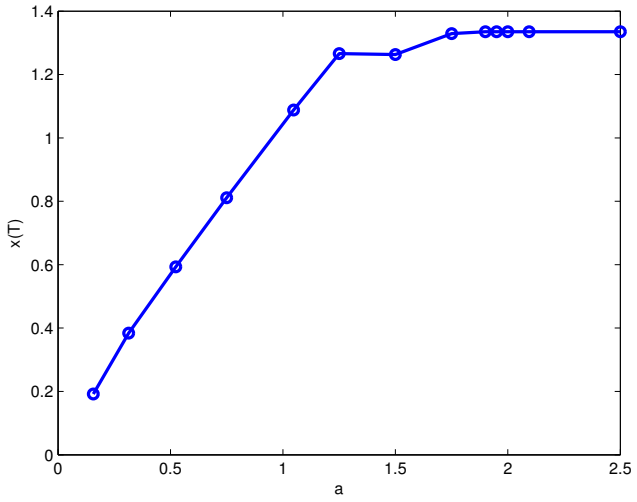

Figure 4.31: Larger amplitudes - Overall displacement. Note that since the displacement is expected to be a strictly increasing function of a, we see that for $a = 1.5$, the optimization converged to a local solution.

Chapter 5

Magneto-elastic flagellar microswimmer

While the idea of building artificial devices emulating these motile capabilities is quite natural, much remains to be done for this to be practical. Learning skills from biological organisms requires, in particular, that we learn how to move and control continuously deformable objects such as filaments, cilia, and flagella. This is, in fact, an instance of bio-inspired soft robotics, where novel designs are inspired by the study of how animals exploit soft materials to move effectively in complex and unpredictable natural environments [11, 12, 42, 53, 59, 69]. Artificial devices mimicking sperm cells, in which the payload could be contained in a relatively large head, and propulsion forces could be extracted from the beating of a long, thin tail, is a natural concept which has been pioneered in [31]. The idea is particularly attractive also because it may lend itself to diverse micro-fabrication techniques. For example, one may consider functionalized magnetic multi-layers (MMLs) originally conceived for spintronics applications, an idea explored in [30]. The flexibility in the fabrication procedure could be exploited to target diverse biotechnological applications, by including different functional components. In addition, it could be used to tune the magnetic and elastic properties in order to optimize performance, controllability, manoeuvrability. For the time being, attention is mostly focused on actuation with an externally applied magnetic field, but autonomous self-propelled systems can also be envisaged by using built-in motors, such as muscle cells like in [32], or by using active materials, such as in [75].

Having in mind the applications discussed above, in this chapter we present and discuss a computational tool for the simulation of the behaviour of a model magneto-elastic swimmer, consisting of a head and of a tail made of a film of permanent magnetic material, and activated by an oscillating

magnetic field. This system is inspired by the pioneering concept explored in [31], based on a magnetic filament consisting of super-paramagnetic beads, and thoroughly analyzed in [34] and [74]. Recent work on a simpler system made of two rigid magnetic segments [40] is also relevant to our analysis. Our aim is to provide a feasibility study for the concept of a magneto-elastic swimmer based on MML fabrication techniques. The main specific questions we address are whether, by restricting oneself to the small parameter window of magnetic, elastic, and geometric parameters that are realistic for MMLs, and to magnetic field amplitude and actuation frequencies achievable in a laboratory, reasonable swimming speeds can be obtained and, if so, thanks to which swimming gaits. Our answers to these questions are based on a simplified model that makes the problems of control and motion planning tractable. The problem is complex, and inherently multiphysics. Indeed, it combines magnetism, elasticity, and fluid dynamics in a single system where magnetic torques drive the shape changes of an elastic flagellum which, in turn, produce a propulsive force through the interaction with a surrounding viscous fluid. While a full description of the system via three coupled systems of partial differential equations is, in principle, feasible, our aim is here to develop an agile numerical tool that may help the design, optimization, and motion planning stages. Our simplifying assumptions reduce the governing equations of our magneto-elastic swimmer to a system of ordinary differential equations (ODEs). Solving these does not require the complex three-dimensional meshing necessary for the numerical solution of the coupled system of partial differential equations of elasticity, magnetostatics, and hydrodynamics. By contrast, our system of ODEs can be easily and quickly solved on a small laptop computer. So, exploring the effect of varying geometric, material, and actuation parameters becomes a feasible task. Given the length scales involved, the induced flows are characterized by very low Reynolds numbers. Accordingly, and in view of the slenderness of the tails, we use the local drag approximation of Resistive Force Theory [39]. Bending of the tail is rendered by concentrating the elasticity on a finite number of points, so that the tail is modeled as a sequence of (many) rigid segments joined by angular springs. Finally, the magnetic behaviour of the segments is modeled by assuming that their magnetization is always parallel to the segment, and with fixed magnitude, and that stray fields can be neglected. In future work, we will remove some of the simplifying assumptions leading to the reduced model, as this may be required to resolve some finer details. The main results of our work are the following. First, we show that by actuating a system made of a non-magnetic head and an MML tail with a magnetic field composed of a constant longitudinal component and an oscillatory transversal one, one can propel it along the longitudinal axis achieving

swimming speeds comparable to those observed for bull sperm cells in [33], and using magnetic fields that are easily attainable in a laboratory. We use for the magnetic film the material parameters of Permalloy, and geometric parameters that are in the range of current manufacturing techniques. This proves that the MML swimmer is a viable concept, at least in principle. In addition, we compare the swimming gait of our MML swimmer with that of other natural and artificial micro-swimmers and, in particular, with sperm cells, whose behaviour is well known from the exisiting literature. It turns out that the mechanisms underlying the motility of MML swimmers and of sperm cells are radically different. Sperm cells propel themselves by propagating bending waves along the flagellum. Similarly, the behaviour of the model swimmer in [31] can be understood as arising from the propagation of bending waves between free and tethered ends, and it is shown in [74] that the resulting gait is intermediate between that of eukaryotic sperm cells and the one of a waggled elastic rod. By contrast, our MML swimmer moves in the absence of bending waves, through a mechanism similar to the one propelling the two-link system studied in [40]. The main difference is that, in our case, the two rigid links with an angular elastic joint are replaced by a flexible magnetic tail which exhibits a time-dependent spatially constant curvature. Finally, we show that the transversal magnetic field can be used as a steering device, and that by varying its direction one can guide the magneto-elastic swimmer along curved trajectories and even sharply curved pipes.

5.1 Formulation of the problem

Following the line of thought of chapter 4, we think of our swimmer as composed by N segments $(L_i)_{1\leq i\leq N}$, which move in the plane $z = 0$. The first segment is special, as it describes the non-magnetic 'head' where the payload is located. Accordingly, it experiences different hydrodynamic drag, as described below. The other segments are characterised by thickness t_i (in direction perpendicular to the filament axis), width w_i (in direction perpendicular to the plane $z = 0$), and length l_i (along the filament axis) such that $t_i \ll w_i \ll l_i$. We take $l_1 = l_{head}$, $t_1 = t_{head}$, $w_1 = w_{head}$, and $l_i = l_{tail}$, $w_i = w_{tail}$, $t_i = t_{tail}$ for $i = 2, \ldots, N$. The actual values used for these geometric parameters in the concrete examples analysed in Section 5.2 are given in Table 5.1.

The position at time t of segment L_i is specified by the position of its first end $\mathbf{x}_i = (x_i, y_i, 0)$, and the angle θ_i that L_i makes with the $x-$axis. We also denote by $\mathbf{e}_{i,\parallel} = (\cos(\theta_i), \sin(\theta_i), 0)$ (resp. $\mathbf{e}_{i,\perp} = (-\sin(\theta_i), \cos(\theta_i), 0)$)

the unit vector along (resp. orthogonal to) the axis of segment L_i.

The segments are linked together, so that the first end of L_{i+1} coincides with the second end of L_i, namely, $\mathbf{x}_{i+1} = \mathbf{x}_i + l_i \mathbf{e}_{i,\parallel}$. We rewrite these kinematic constraints in the explicit form

$$\begin{cases} x_{i+1} &= x_i + l_i \cos(\theta_i)\,, \\ y_{i+1} &= y_i + l_i \sin(\theta_i)\,. \end{cases} \tag{5.1}$$

The three different physical mechanisms governing the motion of our magneto-elastic swimmer are rendered in the way described below.

5.1.1 Elasticity

We account for the elasticity of the structure by using a discrete beam theory. At the junction between the segments L_i and L_{i+1}, a torsional spring with spring constant κ independent of i, is assumed to be present. The spring exerts a torque with the same magnitude $\mathbf{T}^{el}_{i,\mathbf{x}_i} = \kappa(\theta_{i+1} - \theta_i)\mathbf{e}_z$, but with opposite signs, on each of the two neighboring segments L_i and L_{i+1} of the swimmer. The spring constant is given by

$$\kappa = \frac{(EJ)_{tail}}{l_{tail}} \tag{5.2}$$

where E is Young's modulus and J is the moment of inertia of the cross-section of the tail segments

$$J = \frac{1}{12} w_{tail} t^3_{tail}\,. \tag{5.3}$$

The actual values used in Section 5.2 for these geometric and material parameters are given in Table 5.1.

5.1.2 Hydrodynamics

We assume that the swimmer is immersed in water, that it is neutrally buoyant, and that its size and the actuation frequency are such that the induced flows are governed by low Reynolds number hydrodynamics [26]. We model the interaction with the surrounding fluid by using the local drag approximation of Resistive Force Theory [39]. This assumes a linear dependence between the hydrodynamic drag force per unit length acting on the swimmer at a point $\mathbf{x}$ and the velocity at that point through the relation

$$\mathbf{f}^h(\mathbf{x}) = -\xi_i \mathbf{u}_\parallel(\mathbf{x}) - \eta_i \mathbf{u}_\perp(\mathbf{x})\,. \tag{5.4}$$

Here $\mathbf{x}$ is the current location of a point on the $i-$th link, while $\mathbf{u}_{\|}(\mathbf{x})$ and $\mathbf{u}_{\perp}(\mathbf{x})$ stand for the components of the velocity vector of the swimmer at $\mathbf{x}$ (and thus of the fluid at the same point $\mathbf{x}$, due to the no-slip boundary condition) along $\mathbf{e}_{i,\|}$ and $\mathbf{e}_{i,\perp}$ respectively.

The shortcomings of the local drag approximation are well known. In particular, the relation (5.4) being local, hydrodynamic interactions between the different elements of the swimmer are neglected. Nevertheless, it gives satisfactory results, which are often in striking agreement with experiments, at least for very slender filaments in low Reynolds number flows (see e.g. [33]).

Noticing that at $\mathbf{x} = \mathbf{x}_i + s\mathbf{e}_{i,\|}$ we have $\mathbf{u}(\mathbf{x}) = \dot{\mathbf{x}}_i + s\dot{\theta}_i\mathbf{e}_{i,\perp}$, we can compute the total hydrodynamic force on L_i which is given by

$$\mathbf{F}_i^h = \int_{L_i} \mathbf{f}^h(\mathbf{x})\, d\mathbf{x} = -l_i\xi_i(\dot{\mathbf{x}}_i \cdot \mathbf{e}_{i,\|})\mathbf{e}_{i,\|} - \left(l_i\eta_i(\dot{\mathbf{x}}_i \cdot \mathbf{e}_{i,\perp}) + \frac{l_i^2}{2}\eta_i\dot{\theta}_i \right) \mathbf{e}_{i,\perp}\,. \quad (5.5)$$

Similarly, the (component perpendicular to the plane $z = 0$ of the) torque with respect to any point $\mathbf{x}_0$ is given by

$$\begin{aligned} \mathbf{e}_z \cdot \mathbf{T}^h_{i,\mathbf{x}_0} &= \mathbf{e}_z \cdot \int_{L_i} (\mathbf{x} - \mathbf{x}_0) \times \mathbf{f}^h(\mathbf{x})\, d\mathbf{x} \\ &= -\frac{l_i^2}{2}\eta_i(\dot{\mathbf{x}}_i \cdot \mathbf{e}_{i,\perp}) + \frac{l_i^3}{3}\eta_i\dot{\theta}_i \\ &\quad + (\mathbf{x}_i - \mathbf{x}_0) \times \left(l_i\xi_i(\dot{\mathbf{x}}_i \cdot \mathbf{e}_{i,\|})\mathbf{e}_{i,\|} + \left(l_i\eta_i(\dot{\mathbf{x}}_i \cdot \mathbf{e}_{i,\perp}) + \frac{l_i^2}{2}\eta_i\dot{\theta}_i \right) \mathbf{e}_{i,\perp} \right) \cdot \mathbf{e}_z\,. \end{aligned} \quad (5.6)$$

For simplicity, we will assume that the drag coefficients are constant along the tail and set $\xi_i = \zeta_{tail,\|}$, $\eta_i = \zeta_{tail,\perp}$, for $i = 2, \ldots, N$. The first segment describing the 'head' is special, and we take $\xi_1 = \eta_1 = \zeta_{head}$ The actual values used in Section 5.2 for these material parameters are given in Table 5.1.

5.1.3 Magnetism

We assume that each segment, excluding only the first one describing the head, is constantly magnetized, and we make the simplifying assumption that the magnetization on each segment stays permanently aligned with the segment axis. We also neglect the magneto-static coupling between different segments, in particular through the stray-field induced by the magnetic distribution along the swimmer. The only magnetic interaction we consider is that with an external applied field: we assume that each segment experiences a (magnetic) torque due to the external magnetic field that is imposed to the

swimmer. For the $i-$th segment, this torque takes the form

$$\mathbf{T}_i^m = \mathbf{M}_i \times \mathbf{B} \tag{5.7}$$

where $\mathbf{M}_i$ is the (total) magnetization of the $i-$th segment, $\mathbf{B}$ the external magnetic field, and i ranges from 2 to N. In view of our assumptions, the magnetization of the $i-$th segment can be written as

$$\mathbf{M}_i = M\, l_i\, \mathbf{e}_{i,\parallel}\,. \tag{5.8}$$

Here M is for the magnetization per unit length of each segment, which is given by

$$M = M_s t_{tail} w_{tail}\,, \tag{5.9}$$

where M_s is the saturation magnetization. The actual values used in Section 5.2 for these material parameters are given in Table 5.1.

5.1.4 Governing equations

It remains to assemble the equations governing the motion of the magneto-elastic swimmer, by putting together the various contributions to forces and torques described above.

We start by observing that the swimmer is completely described - both for its position and shape - by the $3N$ variables $(x_i, y_i, \theta_i)_{1\le i\le N}$ satisfying the $2(N-1)$ constraints (5.1). Therefore, we need to write $N+2$ additional equations. To that aim, and recalling that the motion takes place in the plane $z=0$, we write the total balance of horizontal forces (2 equations) and a balance of the torque components perpendicular to $z=0$ with respect to $\mathbf{x}_k$ on each of the subsystems consisting of all the segments from k to N, for $k=1,\cdots,N$ (N equations). Since inertia is assumed to be negligible, and since the (spatially uniform) external magnetic field exerts no forces but only torques on the various parts of the swimmer, these equations take the form

$$\left\{\begin{array}{l} \mathbf{F} = \sum_{i=1}^N \mathbf{F}_i^h = 0\,, \\ \mathbf{e}_z \cdot \sum_{i=1}^N \left(\mathbf{T}_{i,\mathbf{x}_1}^h + \mathbf{T}_i^m\right) = 0\,, \\ \mathbf{e}_z \cdot \sum_{i=2}^N \left(\mathbf{T}_{i,\mathbf{x}_2}^h + \mathbf{T}_i^m\right) = -\kappa(\theta_2-\theta_1)\,, \\ \vdots \\ \mathbf{e}_z \cdot \sum_{i=k}^N \left(\mathbf{T}_{i,\mathbf{x}_k}^h + \mathbf{T}_i^m\right) = -\kappa(\theta_k-\theta_{k-1})\,, \\ \vdots \\ \mathbf{e}_z \cdot \left(\mathbf{T}_{N,\mathbf{x}_N}^h + \mathbf{T}_N^m\right) = -\kappa(\theta_N-\theta_{N-1})\,. \end{array}\right. \tag{5.10}$$

In view of equations (5.5), (5.6), (5.7) and (5.8), we see that all quantities appearing in system (5.10) above depend linearly on the rate of positional and

orientational changes $(\dot{x}_i, \dot{y}_i, \dot{\theta}_i)_{1\leq i\leq N}$. Therefore, if we append to equations (5.10) above the time derivative of the $2(N-1)$ constraints (5.1), namely,

$$\left\{ \begin{array}{rcl} \dot{x}_{i+1} - \dot{x}_i + l_i \sin(\theta_i)\dot{\theta}_i & = & 0\,, \\ \dot{y}_{i+1} - \dot{y}_i - l_i \cos(\theta_i)\dot{\theta}_i & = & 0\,, \end{array} \right. \tag{5.11}$$

then we end up with a system of ODEs which completely determines the evolution of the magneto-elastic swimmer. This system takes the form

$$\mathbf{A} \begin{pmatrix} \dot{x}_1 \\ \vdots \\ \dot{x}_N \\ \dot{y}_1 \\ \vdots \\ \dot{y}_N \\ \dot{\theta}_1 \\ \vdots \\ \dot{\theta}_N \end{pmatrix} = \mathbf{F}_0 + \mathbf{F}_1 B_x(t) + \mathbf{F}_2 B_y(t)\,. \tag{5.12}$$

The explicit expressions of the matrix $\mathbf{A}$ and of the vector-fields $\mathbf{F}_0$, $\mathbf{F}_1$, and $\mathbf{F}_2$ are given in the Appendix. Assembling and solving this system numerically, for a given external field $\mathbf{B}(t) = (B_x(t), B_y(t))$ is a relatively straightforward task, see e.g.[3].

5.2 A case study

We consider the swimmer depicted in Fig. 1, which consists of a large (say, disk-shaped) head linked to a tail composed of 10 segments. Each segment, including the head, is $10\mu m$ long, so that the length of the whole system is $110\,\mu m$. For the head, we take $w_{head} = l_{head}$ and $t_{head} = t_{tail}$. In order to represent a continuous tail made of a Permalloy thin film, we use the following values for the magneto-elastic parameters: $E = 10^{11} Nm^{-2}$ and $M_s = 8 \cdot 10^5\, A\, m^{-1}$. As for the drag coefficients, we follow [33] and take $\zeta_{tail,\parallel} = 6.2 \cdot 10^{-3}\ Nsm^{-2}$, $\zeta_{tail,\perp} = 12.4 \cdot 10^{-3}\ Nsm^{-2}$, $\zeta_{head} = 0.05 Nsm^{-2}$. The values for the other parameters used in the numerical simulations are given in Tab. 5.1.

5.2.1 Straight swimming

We first consider the case where the swimmer, originally in the horizontal position, is excited by a magnetic field with a constant horizontal component

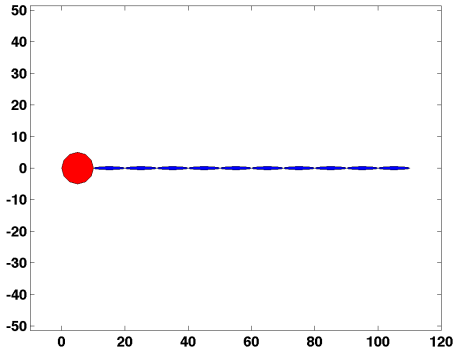

Figure 5.1: The magneto-elastic swimmer: initial configuration, before the application of the external magnetic field. Lengths are in μm.

and an oscillating vertical one

$$\mathbf{B}(t) = (B_x, B_y \sin(\omega t))^t \tag{5.13}$$

where B_x, B_y have the (fixed) values given in Tab. 5.1. These values have been selected on a trial-and-error basis, as field strengths of magnitude achievable in a laboratory and producing interesting performance. Notice that the presence of a nonzero value of B_x proved necessary to obtain stable net motion along the horizontal axis.

We explore the dynamics of the swimmer by varying the driving frequency $\omega/2\pi$ in the range 3-70 Hz. We see from Fig. 5.2 that the net horizontal displacement per cycle is maximised at about 8 Hz, while the maximal swimming speed is attained around 50 Hz. The value of this maximal displacement is close to 5 μm, while the maximal swimming speed is around 70μm/s.

The evolving shape of the swimmer is well characterised by the angle $\Psi(s,t)$ between the horizontal axis and the tangent to the swimmer at arc-length distance s from the external end of the head segment. Following [33], we compute the Fourier coefficients of $\Psi(s,\cdot)$

$$\hat{\Psi}_n(s) = \int_0^{\frac{2\pi}{\omega}} \Psi(s,t) \exp(in\omega t)\, dt$$

in order to capture its periodic behavior, and remark that only the term $\hat{\Psi}_1(s)$ corresponding to the smaller frequency (i.e. the frequency of the magnetic field) is non negligible. We plot in Fig. 5.3 the complex values of $\hat{\Psi}_1(s)$ normalized in such a way that $\hat{\Psi}_1(0)$ is real (in other words, we plot $\frac{\hat{\Psi}_1(s)\overline{\hat{\Psi}_1(0)}}{|\hat{\Psi}_1(0)|}$). These graphs, shown for the three frequencies highlighted in

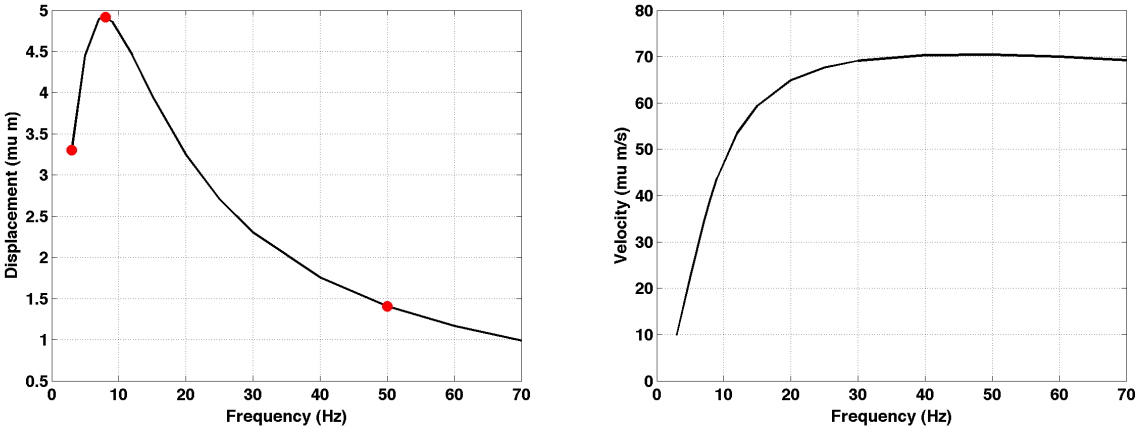

Figure 5.2: Horizontal displacement during one period of the external field (left) and velocity of the swimmer (right). Very small and very high frequencies are not effective and a maximum displacement is obtained for a frequency of about 8 Hz. Three bullets indicate the frequencies 3, 8 and 50 Hz that are used in the sequel for a more thorough analysis.

Fig. 2, clearly show that $\hat{\Psi}_1(s)$ is well approximated by a function of the type $\hat{\Psi}_1(s) = \lambda + \mu s \exp(i\phi)$ which indicates a behaviour of $\Psi(s,t)$ that is well approximated by the function

$$\begin{aligned} \Psi(s,t) &\sim Re(\hat{\Psi}_1(s)\exp(i\omega t)) \\ &\sim \lambda\cos(\omega t) + \mu s\cos(\omega t + \phi)\,. \end{aligned} \tag{5.14}$$

The deformation of the swimmer is thus composed of a global rotation (the spatially constant term) and of a term describing bending with a spatially constant curvature (the term linear in s), which both oscillate in time with angular frequency ω and a phase shift ϕ.

According to (5.14), there is no travelling wave of curvature propagating along the tail of the swimmer. Therefore, this swimming mechanism is very different from the one observed in sperm cells in [33], but also from the one observed in the artificial system described in [31], which is also actuated by an external oscillating magnetic field. In particular, notice that by differentiating (5.14) with respect to s, we obtain that the curvature remains constant along the tail of the swimmer (i.e., s-independent) at every time, while being modulated by a time-dependent amplitude.

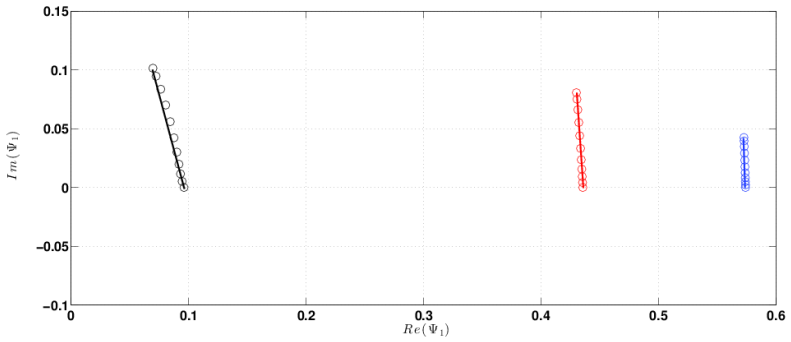

Figure 5.3: The Fourier mode $\hat{\Psi}_1(s)$ corresponding to the three frequencies 50 Hz (black), 8 Hz (red), and 3 Hz (blue). The circles, represented in the complex plane, correspond to the data obtained from the numerical simulations, and we have interpolated them with straight lines. This linear approximation leads to formula (5.14).

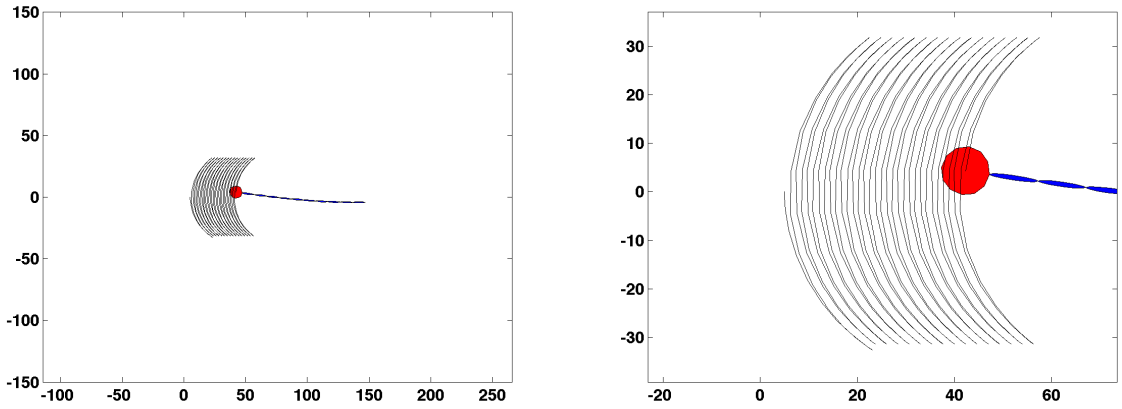

Figure 5.4: Trajectory of the head of the swimmer with the magnetic field given by (5.13) with $\omega = 8$ Hz. The close-up view in the right panel emphasizes the oscillations in the head movement. Lengths are in μm.

5.2.2 Swimming in circles

The previous section shows that, as it was pointed out already in [31], the constant horizontal component of the magnetic field (which is parallel to the

M_s	$8 \cdot 10^5\, A\, m^{-1}$
E	$10^{11} N m^{-2}$
l_{head}	$10\ \mu m$
l_{tail}	$10\ \mu m$
w_{tail}	$1\ \mu m$
t_{tail}	$0.1\ \mu m$
ζ_{head}	$0.05 N s m^{-2}$
$\zeta_{tail,\perp}$	$12.4 \cdot 10^{-3}\, N s m^{-2}$
$\zeta_{tail,\parallel}$	$6.2 \cdot 10^{-3}\, N s m^{-2}$
B_x	$0.01\, T$
B_y	$0.02\, T$

Table 5.1: Values of the parameters used in the numerical simulations.

initial straight configuration of the magnetic tail, and then parallel to its average orientation during the motion), acts in a stabilising way, keeping the average orientation of the swimmer always aligned with it. Indeed, the swimmer oscillates, following the oscillations of the transversal component of the applied field, but its average motion is that of a translation along the average direction of the oscillating magnetic field, which is horizontal.

If we now consider an external magnetic field which is obtained by superposing fast transversal oscillations with frequency ω on a slowly varying longitudinal field, oscillating at frequency $\omega' \ll \omega$, we expect that we can use the direction of the slowly varying field to steer the swimmer. As an example, consider an external magnetic field of the form

$$\mathbf{B} = B_{\parallel} \mathbf{e}_{\theta(t)} + B_{\perp} \sin(\omega t) \mathbf{e}^{\perp}_{\theta(t)} \tag{5.15}$$

where $\mathbf{e}_{\theta(t)}$ is the unit vector forming an angle $\theta(t)$ with the horizontal axis given by

$$\theta(t) = 2\pi t / T_{\max}\,, \tag{5.16}$$

and $B_{\parallel}$ and $B_{\perp}$ have the same values of B_x and B_y, respectively, given in Table 5.1. Here, in order to have a clear separation of the time scales associated with fast and slow oscillations, we take $\omega/2\pi = 8\, Hz$, and $T_{\max} = 40\, s$, which, in view of (5.16) leads to a frequency $\omega'/2\pi = 0.025\, Hz \ll \omega/2\pi$.

The swimmer traces now a circular trajectory, and its average orientation follows the slow modulations of the applied magnetic field (see Fig. 5.5, where only the part of the trajectory following one quarter of a circle is shown).

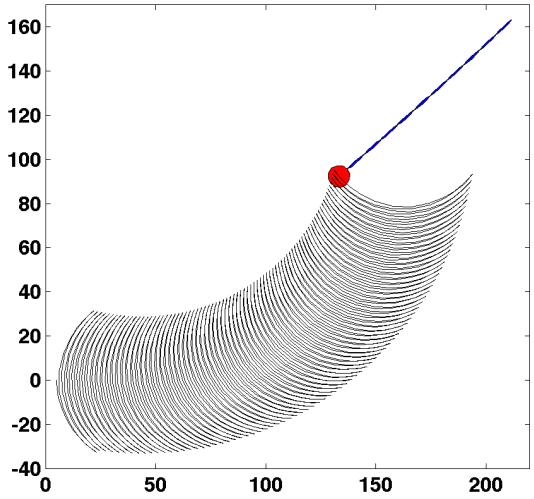

Figure 5.5: Trajectory of the head of the swimmer with the magnetic field given by equations (5.15, 5.16). The average direction of the magnetic field experiences a low frequency circular motion together with a high frequency oscillation. The swimmer follows the slow modulations of the applied magnetic field by tracing a circular trajectory. Lengths are in μm.

5.2.3 Turning abruptly

In this last section we push further the idea developed in the previous section. Indeed, we take the same parameters as before, given in Tab. 5.1, and use now a magnetic field given by (5.15) which oscillates around an average orientation $\mathbf{e}_{\theta(t)}$ that now varies in time according to

$$\theta(t) = \frac{\pi}{4}\left(1 + \tanh\left(30\left(\frac{t}{T_{\max}} - \frac{1}{2}\right)\right)\right) . \tag{5.17}$$

Notice that $\theta(t)$ experiences a sudden jump from 0 to $\frac{\pi}{2}$ around $t = \frac{T_{\max}}{2}$. The result we obtain is displayed in Fig. 5.6 and shows clearly a sudden change in the swimming direction which would allow the swimmer to navigate along an elbow in a pipe. Here, we are tacitly assuming that the pipe is wide enough with respect to the size of the swimmer so that the hydrodynamics effects of the walls can be neglected. Enriching the model to consider explicitly the confining effects due to the pipe walls would be interesting, also in view of recent results in [8], but will not be done here.

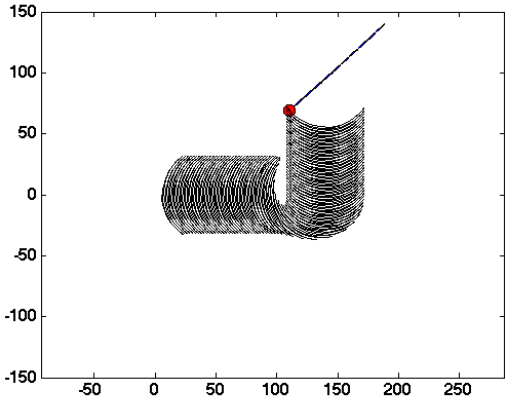

Figure 5.6: Trajectory of the head of the swimmer with the magnetic field given by equations (5.15, 5.17) where we have used $\omega/2\pi = 8\,Hz$ and $T_{\max} = 10\,s$. The sudden rotation of the axis along which the magnetic field oscillates induces a sudden change in the swimming direction that could allow the swimmer to navigate along the elbow of a pipe (not shown). Lengths are in μm.

5.2.4 The swimming mechanism: propagation of bending waves along the tail is not necessary for propulsion

In order to shed light on the mechanism propelling our swimmer, it is useful to introduce the angles $\theta_R := \theta_N$ and $\theta_L := \theta_1$ giving the orientations of the right-most and of the left-most segments, respectively. Figure 5.7 shows that the dynamics is such that the point $(\theta_L(t), \theta_R(t))$ traces a loop. By contrast, the orientation of the second link is always very near the one of the first link, and the corresponding loop (shown in red in Figure 5.7) is close to a single line. The right panel shows snapshots of the swimming stroke along the beat cycle and the dots in the left panel locate them along the loop in the (θ_L, θ_R) plane.

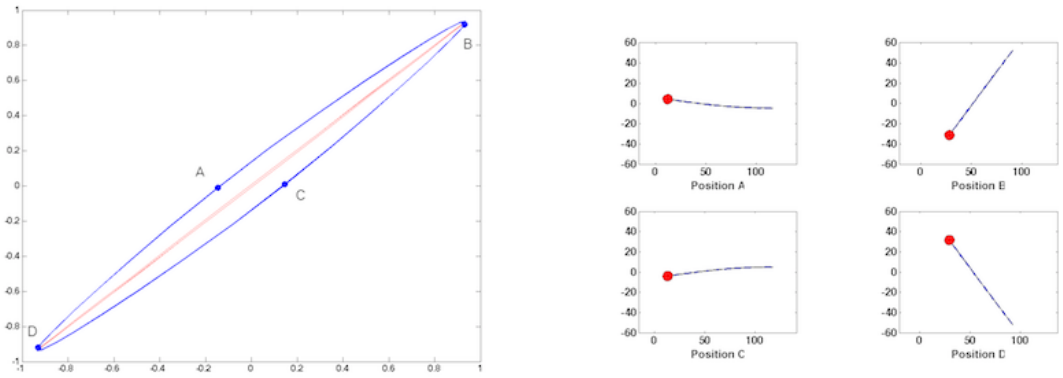

Figure 5.7: Left − The loop in the (θ_L, θ_R) traced by the MML swimmer is indicated in blue. The curve described by (θ_L, θ_2) is given in red. Right - Snapshots of the swimming stroke along the beat cycle corresponding to points A, B, C and D.

The presence of a loop in the (θ_L, θ_R) plane shows that the dynamics of the swimmer is not time reversible: net motion in the horizontal direction arises precisely from this lack of time reversibility. In order to make this statement clearer and more quantitative, we compare the swimming gait of our swimmer with the one of a simplified system consisting of two rigid magnetic links joined by an elastic spring where all the bending elasticity is concentrated. A somewhat similar system has been analyzed in [40] In our case, the first link has also a passive head attached, and hence experiences hydrodynamic forces and torques different from those acting on the second link. The total length and the magnetic properties of the two swimmers are otherwise identical. The length of each link is $5l$, the one of the head is l. The drag coefficient of the head is ζ_{head} and the ones for the tail are $\zeta_{tail,||}$ and $\zeta_{tail,\perp}$. We derive the equations of motion for this system from (5.12) by setting $N = 3$ and $\theta_2 = \theta_1$. The last assumption is made to fix the orientation of head to be equal to the one of the first segment. Figure 8 shows that the behaviour of the simpler two-link system reproduces the one of our original system, made of a stiff but deformable magnetoelastic tail.

Figure 8

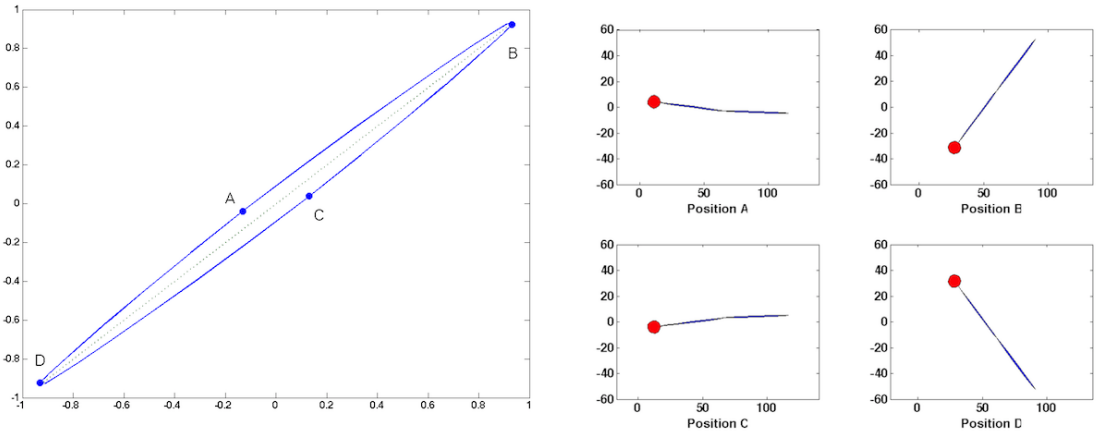

Figure 5.8: Left - The loop in the (θ_L, θ_R) plane traced by the 2-link swimmer is indicated in blue. The dashed curve gives the corresponding picture when no passive head is attached to the first link. Right - Snapshots of the swimming stroke along the beat cycle corresponding to points A, B, C and D.

5.8 also shows that no loop is generated in the two-link system when the passive head is removed (dashed curve). Indeed, in this case the the two links are subject to the same hydrodynamic forces and no net displacement is produced, as expected.
The dynamics of the simpler two-link system can be easily analyzed. Considering the subsystem made by the first 2 rows of (5.12) and by noticing that the 2 first components of vector fields $\mathbf{F}_0$, $\mathbf{F}_1$ and $\mathbf{F}_2$ are null, we get

$$\mathbf{M}\begin{pmatrix}\dot{x}_1\\ \dot{y}_1\end{pmatrix} = (\mathbf{G}_L, \mathbf{G}_R)\begin{pmatrix}\dot{\theta}_L\\ \dot{\theta}_R\end{pmatrix} \tag{5.18}$$

where $\mathbf{M}$ is a symmetric matrix defined by

$$\mathbf{M} = \begin{pmatrix} m_{11} & m_{12}\\ m_{12} & m_{22}\end{pmatrix}$$

with

$$m_{11} = 5l(\zeta_{tail,\perp} - \zeta_{tail,||}))(\cos^2\theta_L + \cos^2\theta_R) - 10\zeta_{tail,\perp}l - \zeta_{head}l$$
$$m_{12} = 5l(\zeta_{tail,\perp} - \zeta_{tail,||}))(\sin\theta_L\cos\theta_L + \sin\theta_R\cos\theta_R)$$
$$m_{2,2} = -5l(\zeta_{tail,\perp} - \zeta_{tail,||}))(\cos^2\theta_L + \cos^2\theta_R) - 10\zeta_{tail,\perp}l - \zeta_{head}l$$

Here $\mathbf{G}_i = (G_i^1, G_i^2)$ with $i = L, R$, are the two column vectors whose expression is

$$G_L^1 = -30l^2\cos\theta_R(\zeta_{tail,\perp} - \zeta_{tail,||})(\sin\theta_L\cos\theta_R - \sin\theta_R\cos\theta_L) + \frac{1}{2}l^2\sin\theta_L(95\zeta_{tail,\perp} + \zeta_{head})$$
$$G_L^2 = -30l^2\cos\theta_R(\zeta_{tail,\perp} - \zeta_{tail,||})(\sin\theta_L\cos\theta_R - \sin\theta_R\cos\theta_L) - \frac{1}{2}l^2\cos\theta_L(\zeta_{head} + 35\zeta_{tail,\perp} + 60\zeta_tail,||)$$
$$G_R^1 = \frac{25}{2}\zeta_{tail,\perp}\sin\theta_R l^2$$
$$G_R^2 = -\frac{25}{2}\zeta_{tail,\perp}\cos\theta_R l^2$$

The first component of system (5.18) is

$$\dot{x} = g_L(\theta_L, \theta_R)\dot{\theta}_L + g_R(\theta_L, \theta_R)\dot{\theta}_R$$

Integrating this equation over a swimming cycle, and using Stokes theorem, we obtain

$$\Delta x = -\iint_\gamma curl(g_L, g_R)(\theta_L, \theta_R)\, d\theta_L\, d\theta_R$$

where γ denotes the region enclosed by the closed loop traced by (θ_L, θ_R) during the cycle. The minus sign comes from the fact that the loops are traced clockwise (in the direction ABCD in Figures 5.7 and 5.8). Assuming that the amplitudes of the two angles are sufficiently small, the leading order term of Δx becomes

$$\Delta x \approx -Area(\gamma)curl(g_L, g_R)(0,0) \tag{5.19}$$

We can therefore conclude that the net horizontal displacement is proportional to the area of the loop, with a non-vanishing factor given by

$$curl(g_L, g_R)(0,0) = -\frac{5}{2}\frac{l(\zeta_{tail,\perp} - \zeta_{tail,||})(50\zeta_{tail,\perp} + 11\zeta_{tail,||})}{(10\zeta_{tail,||} + \zeta_{head})(10\zeta_{tail,\perp} + \zeta_{head})}$$

Conclusions and perspectives

In this thesis we have investigated the geometric nature of the swimming problem of a 2-dimensional deformable body immersed in a fluid. In the first part we suppose it immersed in an ideal incompressible and irrotational fluid. We faced a new problem: the study of the controllability properties of a dynamical system which can start with a non zero initial impulse. Reinterpreting the hydrodynamic forces exerted by the fluid on the body, as kinetic terms, and describing the shape changes with a finite number of parameters, we derive the equations of motion of the system. Using classical techniques in control theory [29, 49] we are able to gain some interesting results for the controllability of this kind of system.
If it starts with zero initial impulse we recover results present in the literature, we are always able to find a suitable rate of deformation which makes the swimmer moving between two different fixed configurations. If instead the body starts with an initial impulse different from zero, the swimmer can self-propel in almost any direction if it can undergo shape changes without any bound on their velocity.
The fact that we take into account the presence of an initial impulse not null, and the analysis of the controllability of this system seems innovative and makes the study of the self-propulsion of deformable bodies in an ideal fluid more accurate and complete.
The approach described here can be extended in a number of natural ways. To begin with, we have restricted our attention to planar swimmers. The general 3-dimensional case is conceptually straightforward, even though the way of describing the shape changes is rather different.
The study of bodies that change their shape using only a finite number of parameters is the initial point of a more complex study of controlling the deformation by diffeomorphisms. Future work will also explore the optimal control problem associated to these kind of systems, especially in the case of non zero initial impulse.

In the second part of the work we set a general kinematic framework for

discussing self-propulsion in a fluid at low Reynolds number. We have formulated this problem in terms of a gauge potential A, which gives the net rigid motion resulting from an arbitrary change of shape [76, 77]. Finite motions due to a sequence of changes of shape are given by a path-ordered exponential integral of A along a path in shape space, and cyclic infinitesimal swimming motions are described by the covariant curl F of A. We have discussed an algorithm for determining A at shapes related to the circle by a conformal map of finite degree, and evaluated A explicitly for all deformations of conformal degree two.

In order to study deeper the implication that the controllability of microswimmers can have on the design of bio-inspired replicas, we build up a new model for slender swimmers which is more manageable [3]. We have presented a discrete model of a slender swimmer which swims by propagating bending waves along its body, and in which hydrodynamic interactions are treated with the local drag approximation of Resistive Force Theory. The model is easy to assemble and to solve, and surprisingly accurate, as shown by the comparison with some benchmark examples such as the measured trajectories of sperm cells reported in [33]. Moreover we prove that for N greater than 3 and for almost any N-uplet of sticks lengths, the swimmer is globally controllable in the whole plane. Then, we focus on finding a swimming strategy that leads the N-link swimmer from an fixed initial position to a given final position, in minimum time. As a consequence of the controllability result, we show that there exists a shape change function which allows to reach the final state in a minimal time. Instead of using the approach of the minimum time function [27, 28], we formulate this optimal control problem and solve it with a direct approach (BOCOP) for the case $N = 3$ (Purcell swimmer). Without any assumption on the structure of the trajectory, we obtain a periodic solution, from which we identify an optimal stroke. Comparing this optimal stroke with the Purcell one confirms that it is better and gives a speed greater by about 20%.

Current work includes solving the optimal control problem for more complex displacements (along the y axis, rotations) and for the optimal design, i.e. the optimization of the link ratio of the three-link swimmer for maximal displacement. We provide an estimate of the displacement based on an expansion for small deformations, which gives a theoretical optimal link ratio. Numerical simulations are consistent with this theoretical ratio for small amplitudes of deformation. We also observe that the optimal ratio changes for large amplitudes of deformation, with a limit value of 0.667 in the unconstrained case versus a theoretical ratio of 0.721 obtained for small amplitudes of deformation. For an amplitude of $\pi/3$, the displacement gain is about 60% compared with the classical Purcell swimmer design. A possible

continuation of this work is the comparison of different objective functions, such as speed or efficiency.

Also, noticing that the N-link swimmer was introduced in [3] in the perspective of approximating the motion of several living micro organisms, an interesting extension of this model is to generalize the simulations to greater values of N. Of course, comparing the candidate for the optimal motion strategy with the one used by real micro organism could be a more tricky issue. On the other hand, another interesting direction is to study formally the existence of the periodic solution for the optimal problem.

Finally we made a feasibility study for the engineering of microscopic artificial swimmers consisting of a cargo head and of a flexible thin film tail made of a permanent magnetic material, and propelled by an external oscillating magnetic field. Our results indicate that for a system characterized by geometric parameters consistent with those achievable by current manufacturing techniques, and by realistic values of the magneto-elastic parameters (consistent with those of Permalloy), interesting swimming performance can be achieved by using magnetic fields that are easily attainable in a laboratory (field magnitude of a few tens of mT, frequencies of a few tens of Hz). Our analysis shows that the magneto-elastic swimmer we have described in this work propels itself with a mechanism, which is very different from the ones previously reported in the literature for flexible magneto-elastic filaments. Indeed, the deformation of the swimmer is composed of a global rotation and of a bending deformation with a spatially constant curvature, which both oscillate in time at the same frequency of the external magnetic field, but with a phase shift. By contrast, sperm cells and artificial swimmers exploiting control of their curvature propel themselves by propagating internally activated waves of bending along the flagellum [3, 33]. This mechanism can be understood in terms of the classical swimming sheet model of G.I. Taylor [81], since the flagellum is able to produce traveling waves of bending, propagating from tail to head.

Contrary to the behaviour of sperm cells, our swimmer swims tail first. Also the steering mechanism we use to produce curved trajectories differs from the one used by sperm cells. Our swimmer curves by maintaining the alignment between its average orientation and the average orientation of the external magnetic field. Sperm cells (and, similarly, artificial bio-mimetic devices based on internal actuation providing curvature control) can turn by actuating their tails with waves of curvature with non-zero spatial average, producing trajectories whose curvatures are proportional to the average curvature of the tail, see [3, 33].

Appendix A

The vector Fields g_i and their Lie brackets of the first order mentioned in theorem 2.3 are

$$g_1 = \epsilon^2 \begin{pmatrix} \mathcal{R}(\theta) \begin{pmatrix} -(1-\mu)s_2 \\ -(1-\mu)s_3 \\ 0 \end{pmatrix} \\ 1 \\ 0 \\ 0 \end{pmatrix} \quad g_2 = \epsilon^2 \begin{pmatrix} \mathcal{R}(\theta) \begin{pmatrix} -s_1 \\ 0 \\ -\frac{2\pi\rho s_3}{M} \end{pmatrix} \\ 0 \\ 1 \\ 0 \end{pmatrix}$$
$$g_3 = \epsilon^2 \begin{pmatrix} \mathcal{R}(\theta) \begin{pmatrix} 0 \\ -s_1 \\ -\frac{2\pi\rho s_2}{M} \end{pmatrix} \\ 0 \\ 0 \\ 1 \end{pmatrix} \tag{5.20}$$

The Lie brackets generated by these vector fields are

$$
\begin{aligned}
[g_1, g_2] &= \epsilon^4 \begin{pmatrix} \frac{2\pi s_2 s_3(\mu-1)\rho\sin(\theta)-\cos(\theta)\left(M\mu-2\pi s_3^2(\mu-1)\rho\right)}{M} \\ \frac{\sin(\theta)\left(2\pi s_3^2(\mu-1)\rho-M\mu\right)-2\pi s_2 s_3(\mu-1)\rho\cos(\theta)}{M} \\ 0 \\ 0 \\ 0 \\ 0 \end{pmatrix} \\
[g_1, g_3] &= \epsilon^4 \begin{pmatrix} \frac{\sin(\theta)\left(M\mu-2\pi s_2^2(\mu-1)\rho\right)-2\pi s_2 s_3(\mu-1)\rho\cos(\theta)}{M} \\ -\frac{\cos(\theta)\left(M\mu-2\pi s_2^2(\mu-1)\rho\right)+2\pi s_2 s_3(\mu-1)\rho\sin(\theta)}{M} \\ 0 \\ 0 \\ 0 \\ 0 \end{pmatrix} \\
[g_2, g_3] &= \epsilon^4 \begin{pmatrix} \frac{2\pi s_1\rho(s_2\sin(\theta)+s_3\cos(\theta))}{M} \\ \frac{2\pi s_1\rho(s_3\sin(\theta)-s_2\cos(\theta))}{M} \\ -\frac{4\pi\rho}{M} \\ 0 \\ 0 \\ 0 \end{pmatrix}
\end{aligned}
\tag{5.21}
$$

The vector fields that we need to compute the Lie algebra generated by

$\mathbf{g}_i$ in theorem 2.5 are

$$\mathbf{g}_1 = \epsilon^2 \begin{pmatrix} \mathcal{R}(\theta) \begin{pmatrix} -(1-\mu)s_2 \\ -(1-\mu)s_3 \\ 0 \end{pmatrix} \\ 0 \\ 0 \\ -(1-\mu)(s_3 p_1^* + s_2 p_2^*) \\ 1 \\ 0 \\ 0 \end{pmatrix} \quad \mathbf{g}_2 = \epsilon^2 \begin{pmatrix} \mathcal{R}(\theta) \begin{pmatrix} -s_1 \\ 0 \\ -\frac{2\pi\rho s_3}{M} \end{pmatrix} \\ \frac{2\pi\rho s_3 p_2^*}{M} \\ -\frac{2\pi\rho s_3 p_1^*}{M} \\ s_1 p_2^* \\ 0 \\ 1 \\ 0 \end{pmatrix}$$

$$\mathbf{g}_3 = \epsilon^2 \begin{pmatrix} \mathcal{R}(\theta) \begin{pmatrix} 0 \\ -s_1 \\ -\frac{2\pi\rho s_2}{M} \end{pmatrix} \\ -\frac{2\pi\rho s_2 p_2^*}{M} \\ \frac{2\pi\rho s_2 p_1^*}{M} \\ -s_1 p_2^* \\ 0 \\ 0 \\ 1 \end{pmatrix} \tag{5.22}$$

Their Lie brackets of the first order are

$$
\begin{aligned}
[\mathbf{g}_1,\mathbf{g}_2] &= \epsilon^4 \begin{pmatrix} \frac{2\pi s_2 s_3(\mu-1)\rho\sin(\theta)-\cos(\theta)\left(M\mu-2\pi s_3^2(\mu-1)\rho\right)}{M} \\ \frac{\sin(\theta)\left(2\pi s_3^2(\mu-1)\rho-M\mu\right)-2\pi s_2 s_3(\mu-1)\rho\cos(\theta)}{M} \\ 0 \\ 0 \\ 0 \\ \frac{2\pi s_3(\mu-1)\rho(p_1^* s_2-p_2^* s_3)-Mp_2^*(\mu-2)}{M} \\ 0 \\ 0 \\ 0 \end{pmatrix} \\
[\mathbf{g}_1,\mathbf{g}_3] &= \epsilon^4 \begin{pmatrix} \frac{\sin(\theta)\left(M\mu-2\pi s_2^2(\mu-1)\rho\right)-2\pi s_2 s_3(\mu-1)\rho\cos(\theta)}{M} \\ -\frac{\cos(\theta)\left(M\mu-2\pi s_2^2(\mu-1)\rho\right)+2\pi s_2 s_3(\mu-1)\rho\sin(\theta)}{M} \\ 0 \\ 0 \\ 0 \\ \frac{\left(2\pi s_2(\mu-1)\rho(p_1^* s_2+p_2^* s_3)-M(p_1^*(\mu-1)+p_2^*)\right)}{M} \\ 0 \\ 0 \\ 0 \end{pmatrix} \\
[\mathbf{g}_2,\mathbf{g}_3] &= \epsilon^4 \begin{pmatrix} \frac{2\pi s_1\rho(s_2\sin(\theta)+s_3\cos(\theta))}{M} \\ \frac{2\pi s_1\rho(s_3\sin(\theta)-s_2\cos(\theta))}{M} \\ -\frac{4\pi\rho}{M} \\ -\frac{4\pi\rho\left(Mp_2^*-2\pi p_1^* s_2 s_3\rho\right)}{M^2} \\ -\frac{8\pi^2 p_2^* s_2 s_3\rho^2}{M^2} \\ \frac{2\pi p_1^* s_1\rho(s_2+s_3)}{M} \\ 0 \\ 0 \\ 0 \end{pmatrix}
\end{aligned}
\tag{5.23}
$$

Finally the only non zero brackets of the second order are

$$
\begin{aligned}
[\mathbf{g}_1,[\mathbf{g}_2,\mathbf{g}_3]] &= \epsilon^6 \begin{pmatrix} -\frac{2\pi(2\mu-3)\rho(s_2\sin(\theta)+s_3\cos(\theta))}{M} \\ \frac{2\pi(2\mu-3)\rho(s_2\cos(\theta)-s_3\sin(\theta))}{M} \\ 0 \\ 0 \\ 0 \\ \frac{2\pi\rho\left(M(p_1^*(s_2+s_3)+2p_2^*s_3(\mu-1))+4\pi s_2s_3(\mu-1)\rho(p_2^*s_2-p_1^*s_3)\right)}{M^2} \\ 0 \\ 0 \\ 0 \end{pmatrix} \\
[\mathbf{g}_2,[\mathbf{g}_2,\mathbf{g}_3]] &= \epsilon^6 \begin{pmatrix} \frac{2\pi s_1\rho\left(\sin(\theta)\left(3M-2\pi s_3^2\rho\right)+2\pi s_2s_3\rho\cos(\theta)\right)}{M^2} \\ \frac{2\pi s_1\rho(2\pi s_3\rho(s_2\sin(\theta)+s_3\cos(\theta))-3M\cos(\theta))}{M^2} \\ 0 \\ \frac{16\pi^2s_3\rho^2\left(Mp_1^*+2\pi p_2^*s_2s_3\rho\right)}{M^3} \\ -\frac{16\pi^2s_3\rho^2\left(Mp_2^*-2\pi p_1^*s_2s_3\rho\right)}{M^3} \\ \frac{2\pi s_1\rho\left(Mp_1^*+2\pi p_2^*s_3\rho(3s_2+s_3)\right)}{M^2} \\ 0 \\ 0 \\ 0 \end{pmatrix} \\
[\mathbf{g}_3,[\mathbf{g}_2,\mathbf{g}_3]] &= \epsilon^6 \begin{pmatrix} \frac{2\pi s_1\rho\left(\cos(\theta)\left(3M-2\pi s_2^2\rho\right)+2\pi s_2s_3\rho\sin(\theta)\right)}{M^2} \\ \frac{2\pi s_1\rho(3M\sin(\theta)-2\pi s_2\rho(s_2\sin(\theta)+s_3\cos(\theta)))}{M^2} \\ 0 \\ \frac{16\pi^2s_2\rho^2\left(Mp_1^*-2\pi p_2^*s_2s_3\rho\right)}{M^3} \\ -\frac{16\pi^2s_2\rho^2\left(Mp_2^*-2\pi p_1^*s_2s_3\rho\right)}{M^3} \\ \frac{2\pi s_1\rho\left(Mp_1^*-2\pi p_2^*s_2\rho(s_2+3s_3)\right)}{M^2} \\ 0 \\ 0 \\ 0 \end{pmatrix}
\end{aligned}
\tag{5.24}
$$

To use the theorem 1.4 at the point q_0 we need also the Lie brackets of

the vector fields $\mathbf{g}_i$ with the drift that are:

$$[\mathbf{f},\mathbf{g}_1](q_0) = \begin{pmatrix} \frac{16p_1^*(\mu-1)}{8M+11\pi\epsilon\rho} \\ 0 \\ -\frac{8p_1^*\left(8M(\epsilon-\mu+1)+\pi\left((34-23\mu)\epsilon^2+8(\mu-1)\epsilon-4\mu+4\right)\rho\right)}{\epsilon(8M+11\pi\epsilon\rho)^2} \\ 0 \\ -\frac{8(p_1^*)^2\left(8M(\epsilon-\mu+1)+\pi\left((34-23\mu)\epsilon^2+8(\mu-1)\epsilon-4\mu+4\right)\rho\right)}{\epsilon(8M+11\pi\epsilon\rho)^2} \\ 0 \\ 0 \\ 0 \\ 0 \end{pmatrix} \tag{5.25}$$

$$[\mathbf{f},\mathbf{g}_2](q_0) = \begin{pmatrix} 0 \\ \frac{16p_1^*\left(-4\left(\epsilon^2-1\right)M^2+2\pi\left(3\epsilon^2+6\epsilon+1\right)\rho M+11\pi^2\epsilon^2\rho^2\right)}{M(8M+11\pi\epsilon\rho)(8M+\pi(23\epsilon^2+8\epsilon+4)\rho)} \\ 0 \\ -\frac{32(p_1^*)^2\pi\rho}{8M^2+11\pi\epsilon\rho M} \\ 0 \\ -\frac{16(p_1^*)^2\left(4\left(\epsilon^2+1\right)M^2+\pi\left(17\epsilon^2-4\epsilon+2\right)\rho M-11\pi^2\epsilon^2\rho^2\right)}{M(8M+11\pi\epsilon\rho)(8M+\pi(23\epsilon^2+8\epsilon+4)\rho)} \\ 0 \\ 0 \\ 0 \end{pmatrix} \tag{5.26}$$

$$[\mathbf{f},\mathbf{g}_3](q_0) = \begin{pmatrix} -\frac{8p_1^*}{8M+11\pi\epsilon\rho} \\ 0 \\ -\frac{8p_1^*}{8M+11\pi\epsilon\rho} \\ 0 \\ -\frac{8(p_1^*)^2}{8M+11\pi\epsilon\rho} \\ \frac{8(p_1^*)^2}{8M+11\pi\epsilon\rho} \\ 0 \\ 0 \\ 0 \end{pmatrix} \tag{5.27}$$

Appendix B

The forces $\mathbf{F}_i$, $i = 1, 2, 3$ acting on each segment of Purcell's 3-link swimmer, introduced in Subsection 4.2.1 are given by

$$\begin{aligned}
\mathbf{F}_1 = \; & -\xi L_1(\dot{x}_2 \cos(\theta_2 + \beta_1) + \dot{y}_2 \sin(\theta_2 + \beta_1) - \tfrac{L_2}{2} \sin\beta_1 \dot{\theta}_2)\mathbf{e}_1 \\
& -\eta(-L_1 \dot{x}_2 \sin(\theta_2 + \beta_1) + L_1 \dot{y}_2 \cos(\theta_2 + \beta_1) - \tfrac{L_1 L_2}{2} \cos\beta_1 \dot{\theta}_2 \\
& -\tfrac{L_1^2}{2}(\dot{\theta}_2 + \dot{\beta}_1))\mathbf{e}_1^{\perp}\,, \\
\mathbf{F}_2 = \; & -\xi L_2(\dot{x}_2 \cos\theta_2 + \dot{y}_2 \sin\theta_2)\mathbf{e}_2 - \eta L_2(-\dot{x}_2 \sin\theta_2 + \dot{y}_2 \cos\theta_2)\mathbf{e}_2^{\perp}\,, \\
\mathbf{F}_3 = \; & -\xi L_3(\dot{x}_2 \cos(\theta_2 + \beta_3) + \dot{y}_2 \sin(\theta_2 + \beta_3) + \tfrac{L_2}{2} \sin\beta_3 \dot{\theta}_2)\mathbf{e}_3 \\
& \eta(-L_3 \dot{x}_2 \sin(\theta_2 + \beta_3) + L_3 \dot{y}_2 \cos(\theta_2 + \beta_3) + \tfrac{L_3 L_2}{2} \cos\beta_3 \dot{\theta}_2 + \\
& + \tfrac{L_3^2}{2}(\dot{\theta}_2 + \dot{\beta}_3))\mathbf{e}_3^{\perp}\,,
\end{aligned} \tag{5.28}$$

while the total torque, obtained by using formula (4.5), is given by

$$\begin{aligned}\mathbf{T}_{\mathbf{x}_2}\cdot\mathbf{e}_z =&\dot{x}_2(\xi\frac{L_1L_2}{2}\sin\beta_1\cos(\theta_2+\beta_1)-\eta\frac{L_1L_2}{2}\cos\beta_1\sin(\theta_2+\beta_1)\\&-\eta\frac{L_1^2}{2}\sin(\theta_2+\beta_1)-\xi\frac{L_3L_2}{2}\sin\beta_3\cos(\theta_2+\beta_3)\\&+\eta\frac{L_3L_2}{2}\cos\beta_3\sin(\theta_2+\beta_3)+\eta\frac{L_3^2}{2}\sin(\theta_2+\beta_3))\\&\dot{y}_2(\xi\frac{L_1L_2}{2}\sin\beta_1\sin(\theta_2+\beta_1)+\eta\frac{L_1L_2}{2}\cos\beta_1\cos(\theta_2+\beta_1)\\&+\eta\frac{L_1^2}{2}\cos(\theta_2+\beta_1)-\xi\frac{L_3L_2}{2}\sin\beta_3\sin(\theta_2+\beta_3)\\&-\eta\frac{L_3L_2}{2}\cos\beta_3\cos(\theta_2+\beta_3)-\eta\frac{L_3^2}{2}\cos(\theta_2+\beta_3))\\&\dot{\theta}_2(-\xi\frac{L_1L_2^2}{4}\sin^2\beta_1-\eta L_1(\frac{L_1}{2}+\frac{L_2}{2}\cos\beta_1)^2+\eta\frac{L_1^3}{12}\\&-\xi\frac{L_3L_2^2}{4}\sin^2\beta_3-\eta L_1(\frac{L_3}{2}+\frac{L_2}{2}\cos\beta_3)^2+\eta\frac{L_3^3}{12})\\&+\dot{\beta}_1(-\eta(\frac{L_1^3}{3}+\frac{L_1^2L_2}{4}\cos\beta_1))+\dot{\beta}_3(-\eta(\frac{L_3^3}{3}+\frac{L_3^2L_2}{4}\cos\beta_3))\,.\end{aligned}\tag{5.29}$$

We now write the equations of motion of the system. Since we are neglecting inertia these reduce to $F=0$ and $M=0$. These scalar equations can be seen as ODEs in the unknown functions $x_2(t)$, $y_2(t)$ and $\theta_2(t)$. Explicitly, they read as

$$\begin{aligned}F_x =&\,\dot{x}_2(-\xi L_1(\cos(\theta_2+\beta_1))^2-\eta L_1(\sin(\theta_2+\beta_1))^2-\xi L_2(\cos(\theta_2))^2\\&-\eta L_2(\sin(\theta_2))^2-\xi L_3(\cos(\theta_2+\beta_3))^2-\eta L_3(\sin(\theta_2+\beta_3))^2)\\&+\dot{y}_2(-\xi L_1\cos(\theta_2+\beta_1)\sin(\theta_2+\beta_1)+\eta L_1\cos(\theta_2+\beta_1)\sin(\theta_2+\beta_1)\\&-\xi L_2\sin(\theta_2)\cos(\theta_2)+\eta L_2\cos(\theta_2)\sin(\theta_2)\\&-\xi L_3\sin(\theta_2+\beta_3)\cos(\theta_2+\beta_3)+\eta L_3\sin(\theta_2+\beta_3)\cos(\theta_2+\beta_3))+\\&+\dot{\theta}_2(\xi L_1\frac{L_2}{2}\sin(\beta_1)\cos(\theta_2+\beta_1)-\eta L_1\frac{L_2}{2}\cos(\beta_1)\sin(\theta_2+\beta_1)\\&-\eta L_1(\frac{L_1}{2})\sin(\theta_2+\beta_1)-\xi L_3\frac{L_2}{2}\sin(\beta_3)\cos(\theta_2+\beta_3)\\&+\eta L_3\frac{L_2}{2}\cos(\beta_3)\sin(\theta_2+\beta_3)+\eta L_3(\frac{L_3}{2})\sin(\theta_2+\beta_3)\\&+\dot{\beta}_1(-\eta\frac{L_1^2}{2}\sin(\theta_2+\beta_1))+\dot{\beta}_3(\eta\frac{L_3^2}{2}\sin(\theta_2+\beta_3))=0\,.\end{aligned}\tag{5.30}$$

$$
\begin{aligned}
F_y = \dot{x}_2(&-\xi L_1 \cos(\theta_2+\beta_1)\sin(\theta_2+\beta_1) + \eta L_1 \cos(\theta_2+\beta_1)\sin(\theta_2+\beta_1)\\
&- \xi L_2 \sin(\theta_2)\cos(\theta_2) + \eta L_2 \cos(\theta_2)\sin(\theta_2)\\
&- \xi L_3 \sin(\theta_2+\beta_3)\cos(\theta_2+\beta_3) + \eta L_3 \sin(\theta_2+\beta_3)\cos(\theta_2+\beta_3)) +\\
&+ \dot{y}_2(-\xi L_1(\sin(\theta_2+\beta_1))^2 - \eta L_1(\cos(\theta_2+\beta_1))^2 - \xi L_2(\sin(\theta_2))^2\\
&- \eta L_2(\cos(\theta_2))^2 - -\xi L_3(\sin(\theta_2+\beta_3))^2 - \eta L_3(\cos(\theta_2+\beta_3))^2) +\\
&+ \dot{\theta}_2(\xi L_1 \frac{L_2}{2}\sin(\beta_1)\sin(\theta_2+\beta_1) + \eta L_1 \frac{L_2}{2}\cos(\beta_1)\cos(\theta_2+\beta_1)\\
&+ \eta L_1(\frac{L_1}{2})\cos(\theta_2+\beta_1) - \xi L_3 \frac{L_2}{2}\sin(\beta_3)\sin(\theta_2+\beta_3)\\
&- \eta L_3 \frac{L_2}{2}\cos(\beta_3)\cos(\theta_2+\beta_3) - \eta L_3(\frac{L_3}{2})\cos(\theta_2+\beta_3))\\
&+ \dot{\beta}_1(\eta \frac{L_1^2}{2}\cos(\theta_2+\beta_1)) + \dot{\beta}_3(-\eta \frac{L_3^2}{2}\cos(\theta_2+\beta_3)) = 0\,.
\end{aligned}
\tag{5.31}
$$

$$
\begin{aligned}
T_{\mathbf{x}_2} = \dot{x}_2(&\xi L_1 \frac{L_2}{2}\sin(\beta_1)\cos(\theta_2+\beta_1) - \eta L_1 \frac{L_2}{2}\cos(\beta_1)\sin(\theta_2+\beta_1)\\
&- \eta L_1(\frac{L_1}{2})\sin(\theta_2+\beta_1) - \xi L_3 \frac{L_2}{2}\sin(\beta_3)\cos(\theta_2+\beta_3)\\
&+ \eta L_3 \frac{L_2}{2}\cos(\beta_3)\sin(\theta_2+\beta_3) + \eta L_3(\frac{L_3}{2})\sin(\theta_2+\beta_3))\\
\dot{y}_2(&\xi L_1 \frac{L_2}{2}\sin(\beta_1)\sin(\theta_2+\beta_1) + \eta L_1 \frac{L_2}{2}\cos(\beta_1)\cos(\theta_2+\beta_1)\\
&+ \eta L_1(\frac{L_1}{2})\cos(\theta_2+\beta_1) - \xi L_3 \frac{L_2}{2}\sin(\beta_3)\sin(\theta_2+\beta_3)\\
&- \eta L_3 \frac{L_2}{2}\cos(\beta_3)\cos(\theta_2+\beta_3) - \eta L_3(\frac{L_3}{2})\cos(\theta_2+\beta_3)\\
\dot{\theta}_2(&-\xi L_1 \frac{(L_2)^2}{4}(\sin(\beta_1))^2 + \frac{\eta}{3}((\frac{L_2}{2}\cos(\beta_1))^3 - (\frac{L_2}{2}\cos(\beta_1) + L_1)^3)\\
&- \eta(\frac{L_2^3}{12}) - \xi L_3 \frac{(L_2)^2}{4}(\sin(\beta_3))^2 - \frac{\eta}{3}((\frac{L_2}{2}\cos(\beta_3) + L_3)^3\\
&- (\frac{L_2}{2}\cos(\beta_3))^3)) + \dot{\beta}_1(-\eta(\frac{L_1^3}{3} + \frac{L_1^2 L_2}{4}\cos\beta_1))\\
&+ \dot{\beta}_3(-\eta(\frac{L_3^3}{3} + \frac{L_3^2 L_2}{4}\cos\beta_3)) = 0\,.
\end{aligned}
\tag{5.32}
$$

These equations lead to the system

$$
A(\theta_2,\beta_1,\beta_3)\begin{pmatrix}\dot{x}_2\\ \dot{y}_2\\ \dot{\theta}_2\end{pmatrix} + \mathbf{b}_1(\theta_2,\beta_1,\beta_3)\dot{\beta}_1 + \mathbf{b}_2(\theta_2,\beta_1,\beta_3)\dot{\beta}_3 = 0\,, \tag{5.33}
$$

where

$$A = \begin{pmatrix} a_{1\,1} & a_{1\,2} & a_{1\,3} \\ a_{1\,2} & a_{2\,2} & a_{2\,3} \\ a_{1\,3} & a_{2\,3} & a_{3\,3} \end{pmatrix} \tag{5.34}$$

is a symmetric matrix with

$$\begin{aligned}
a_{1\,1} &= -\xi L_1 \cos(\theta_2+\beta_1)\sin(\theta_2+\beta_1) + \eta L_1 \cos(\theta_2+\beta_1)\sin(\theta_2+\beta_1) \\
&\quad - \xi L_2 \sin(\theta_2)\cos(\theta_2) + \eta L_2 \cos(\theta_2)\sin(\theta_2) - \xi L_3 \sin(\theta_2+\beta_3)\cos(\theta_2+\beta_3) \\
&\quad + \eta L_3 \sin(\theta_2+\beta_3)\cos(\theta_2+\beta_3)\,, \\
a_{1\,2} &= -\xi L_1 \cos(\theta_2+\beta_1)\sin(\theta_2+\beta_1) + \eta L_1 \cos(\theta_2+\beta_1)\sin(\theta_2+\beta_1) \\
&\quad - \xi L_2 \sin(\theta_2)\cos(\theta_2) + \eta L_2 \cos(\theta_2)\sin(\theta_2) - \xi L_3 \sin(\theta_2+\beta_3)\cos(\theta_2+\beta_3) \\
&\quad + \eta L_3 \sin(\theta_2+\beta_3)\cos(\theta_2+\beta_3)\,, \\
a_{1\,3} &= (\xi L_1 \frac{L_2}{2} \sin(\beta_1)\cos(\theta_2+\beta_1) - \eta L_1 \frac{L_2}{2} \cos(\beta_1)\sin(\theta_2+\beta_1) \\
&\quad - \eta L_1 (\frac{L_1}{2}) \sin(\theta_2+\beta_1) - \xi L_3 \frac{L_2}{2} \sin(\beta_3)\cos(\theta_2+\beta_3) \\
&\quad + \eta L_3 \frac{L_2}{2} \cos(\beta_3)\sin(\theta_2+\beta_3) + \eta L_3 (\frac{L_3}{2}) \sin(\theta_2+\beta_3)\,, \\
a_{2\,2} &= -\xi L_1 (\sin(\theta_2+\beta_1))^2 - \eta L_1 (\cos(\theta_2+\beta_1))^2 - \xi L_2 (\sin(\theta_2))^2 \\
&\quad - \eta L_2 (\cos(\theta_2))^2 - \xi L_3 (\sin(\theta_2+\beta_3))^2 - \eta L_3 (\cos(\theta_2+\beta_3))^2\,, \\
a_{2\,3} &= (\xi L_1 \frac{L_2}{2} \sin(\beta_1)\sin(\theta_2+\beta_1) + \eta L_1 \frac{L_2}{2} \cos(\beta_1)\cos(\theta_2+\beta_1) \\
&\quad + \eta L_1 (\frac{L_1}{2}) \cos(\theta_2+\beta_1) - \xi L_3 \frac{L_2}{2} \sin(\beta_3)\sin(\theta_2+\beta_3) \\
&\quad - \eta L_3 \frac{L_2}{2} \cos(\beta_3)\cos(\theta_2+\beta_3) - \eta L_3 (\frac{L_3}{2}) \cos(\theta_2+\beta_3))\,, \\
a_{3\,3} &= (-\xi L_1 \frac{(L_2)^2}{4} (\sin(\beta_1))^2 + \frac{\eta}{3} ((\frac{L_2}{2}\cos(\beta_1))^3 - (\frac{L_2}{2}\cos(\beta_1) + L_1)^3) \\
&\quad - \eta (\frac{L_2^3}{12}) - \xi L_3 \frac{(L_2)^2}{4} (\sin(\beta_3))^2 - \frac{\eta}{3} ((\frac{L_2}{2}\cos(\beta_3) + L_3)^3 - (\frac{L_2}{2}\cos(\beta_3))^3))\,.
\end{aligned}$$

The vector $\mathbf{b}_1$ (resp. $\mathbf{b}_2$) is the vector of total force and torque due to a rotation of the left (resp. right) arm $\dot{\beta}_1 = 1$ (resp. $\dot{\beta}_3 = 1$) while the other

coordinates are kept constant. These vectors are given by

$$\mathbf{b}_1 = \begin{pmatrix} -\eta\frac{L_1^2}{2}\sin(\theta_2+\beta_1) \\ \\ \eta\frac{L_1^2}{2}\cos(\theta_2+\beta_1) \\ \\ -\eta(L_1(\frac{L_1^2}{3}+\frac{L_2L1}{4}\cos\beta_1) \end{pmatrix}, \quad \mathbf{b}_2 = \begin{pmatrix} \eta\frac{L_3^2}{2}\sin(\theta_2+\beta_3) \\ \\ -\eta\frac{L_3^2}{2}\cos(\theta_2+\beta_3) \\ \\ -\eta L_3(\frac{L_3^2}{3}+\frac{L_2L_3}{4}\cos\beta_3) \end{pmatrix}. \tag{5.35}$$

Thanks to the invertibility of the matrix A we obtain the system (4.22), with

$$\mathbf{g}_1(\theta_2,\beta_1,\beta_3) = \begin{pmatrix} 1 \\ 0 \\ -\mathbf{A}^{-1}(\theta_2,\beta_1,\beta_3)\mathbf{b}_1(\theta_2,\beta_1,\beta_3) \end{pmatrix} \tag{5.36}$$

and

$$\mathbf{g}_2(\theta_2,\beta_1,\beta_3) = \begin{pmatrix} 0 \\ 1 \\ -\mathbf{A}^{-1}(\theta_2,\beta_1,\beta_3)\mathbf{b}_2(\theta_2,\beta_1,\beta_3) \end{pmatrix}. \tag{5.37}$$

Appendix C

The $3N \times 3N$ matrix $\mathbf{A}$ appearing in equation (5.12) is given by blocks as

$$\mathbf{A} = \begin{pmatrix} F_{x,\dot{x}} & F_{x,\dot{y}} & F_{x,\dot{\theta}} \\ F_{y,\dot{x}} & F_{y,\dot{y}} & F_{y,\dot{\theta}} \\ T_{\dot{x}} & T_{\dot{y}} & T_{\dot{\theta}} \\ C_{x,\dot{x}} & 0 & C_{x,\dot{\theta}} \\ 0 & C_{y,\dot{y}} & C_{y,\dot{\theta}} \end{pmatrix} \tag{5.38}$$

according to the force, torque and constraint equations (5.10)-(5.11). The F matrices are $1 \times N$ row vectors given component-wise by

$$\begin{array}{ll} (F_{x,\dot{x}})_{1,i} = -l_i(\xi_i \cos^2\theta_i + \eta_i \sin^2\theta_i)\,, & (F_{y,\dot{x}})_{1,i} = -l_i(\xi_i - \eta_i)\sin\theta_i\cos\theta_i\,, \\ (F_{x,\dot{y}})_{1,i} = (F_{y,\dot{x}})_{1,i}\,, & (F_{x,\dot{y}})_{1,i} = -l_i(\xi_i - \eta_i)\sin\theta_i\cos\theta_i\,, \\ (F_{x,\dot{\theta}})_{1,i} = \frac{l_i^2}{2}\eta_i \sin\theta_i\,, & (F_{y,\dot{\theta}})_{1,i} = -\frac{l_i^2}{2}\eta_i\cos\theta_i\,, \end{array}$$

for $i = 1 \cdots N$. Matrices T are $N \times N$ matrices given by

$$\begin{aligned} (T_{\dot{x}})_{ij} &= \eta_j \frac{l_j^2}{2}\sin\theta_j - (x_j - x_i)l_j(\xi_j - \eta_j)\sin\theta_j\cos\theta_j + (y_j - y_i)l_j(\xi_j\cos^2\theta_j + \eta_j\sin^2\theta_j)\,, \\ (T_{\dot{y}})_{ij} &= -\eta_j\frac{l_j^2}{2}\cos\theta_j + (x_j - x_i)l_j(\xi_j\sin^2\theta_j + \eta_j\cos^2\theta_j) - (y_j - y_i)l_j(\xi_j - \eta_j)\sin\theta_j\cos\theta_j\,, \\ (T_{\dot{\theta}})_{ij} &= -\eta_j\frac{l_j^3}{3} - (x_j - x_i)\frac{l_j^2}{2}\eta_j\cos\theta_j - (y_j - y_i)\frac{l_j^2}{2}\eta_j\sin\theta_j \end{aligned}$$

for i, j ranging from 1 to N. Finally, matrices C are $(N-1) \times N$ matrices for which the non-vanishing terms are given by

$$\begin{array}{lll} (C_{x,\dot{x}})_{i,i} = -1\,, & (C_{x,\dot{x}})_{i,i+1} = 1\,, & (C_{x,\dot{\theta}})_{i,i} = l_i\sin\theta_i\,, \\ (C_{y,\dot{y}})_{i,i} = -1\,, & (C_{y,\dot{y}})_{i,i+1} = 1\,, & (C_{x,\dot{\theta}})_{i,i} = -l_i\cos\theta_i\,, \end{array}$$

for i ranging from 1 to $N-1$. For what concerns the vector-fields appearing in equation (5.12), we have

$$\begin{aligned}
\mathbf{F}_0 &= -\kappa(0,0,0,\theta_2-\theta_1,\cdots,\theta_N-\theta_{N-1},0\cdots,0)^t\,,\\
\mathbf{F}_1 &= -M_s(0,0,\sum_{i=1}^{N}\sin\theta_i,\cdots,\sum_{i=k}^{N}\sin\theta_i,\cdots,\sin\theta_N,0\cdots,0)^t\,,\\
\mathbf{F}_2 &= M_s(0,0,\sum_{i=1}^{N}\cos\theta_i,\cdots,\sum_{i=k}^{N}\cos\theta_i,\cdots,\cos\theta_N,0\cdots,0)^t\,.
\end{aligned}$$

Notice that the $2(N-1)$ zeros at the end of the vector-fields correspond to the (differential) constraint equations (5.11)

Bibliography

[1] A.Agrachev, U.Boscain., and D.Barilari. *Introduction to Riemannian and Sub-Riemannian geometry.* pre-print sissa edition, 2014.

[2] A. A. Agrachev. *Non linear and optimal control theory.* Springer Verlag, 2008.

[3] F. Alouges, A. DeSimone, L. Giraldi, and M. Zoppello. Self-propulsion of slender micro-swimmers by curvature control: N-link swimmers. *Journal of Nonlinear Science*, 56:132–141, 2013.

[4] F. Alouges, A. DeSimone, L. Giraldi, and M. Zoppello. Can magnetic multilayers propel artificial micro-swimmers mimicking sperm cells? *Soft Robotics*, 2(3):117–128, 2015.

[5] F. Alouges, A. Desimone, L. Heltai, A. Lefebvre, and B. Merlet. Optimally swimming stokesian robots. *Discrete and Continuous Dynamical Systems - Series B*, 18(5):1189 – 1215, 2010.

[6] F. Alouges, A. DeSimone, and A. Lefebvre. Biological fluid dynamics: Swimming at low reynolds numbers. *Encyclopedia of Complexity and System Science, Springer Verlag*, 2008.

[7] F Alouges, A. DeSimone, and A. Lefebvre. Optimal strokes for low reynolds number swimmers : an example. *Journal of Nonlinear Science*, 18(3):277–302, 2008.

[8] F. Alouges and L. Giraldi. Enhanced controllability of low reynolds number swimmers in the presence of a wall. *Acta Applicandae Mathematicae*, 128(1):153–179, 2012.

[9] P. R. Amestoy, I. S. Duff, J. Koster, and J.-Y. L Excellent. A fully asynchronous multifrontal solver using distributed dynamic scheduling. *SIAM Journal of Matrix Analysis and Applications*, 23(1):15–41, 2001.

[10] P. R. Amestoy, A. Guermouche, J.-Y. L Excellent, and S. Pralet. Hybrid scheduling for the parallel solution of linear systems. *Parallel Computing*, 32(2):136–156, 2006.

[11] M. Arroyo. Reverse engineering the euglenoid movement. *Proc. Nat. Acad. Sci. USA*, 109(44):17874–17879, 2012.

[12] M. Arroyo and A. DeSimone. Shape control of active surfaces inspired by the movement of euglenids. *J. Mech. Phys. Solids*, 62:99–112, 2014.

[13] L. E. Becker, S. A. Koehler, and H. A. Stone. On self-propulsion of micro-machines at low reynolds number: Purcell's three-link swimmer. *J. Fluid Mech.*, 490:15–35, 2003.

[14] J. Betts. Practical methods for optimal control using nonlinear programming. *Advances in design and control*, 2001.

[15] A.M. Bloch. *Non holonomic Mechanics and Control*. Interdishiplinary Applied Mathematics. Springer, 2003.

[16] V. G. Boltyanskii, R. V. Gamkrelidze, and L. S. Pontryagin. Towards a theory of optimal processes. *Dokl. Akad. Nauk SSSR*, 110(1):7–10, 1956.

[17] J. Bonnans, Frédéric, Pierre Martinon, and Vincent Grélard. Bocop - A collection of examples. Technical report, INRIA, 2012. RR-8053.

[18] Alberto Bressan. Impulsive control of lagrangian systems and locomotion in fluids. *Discrete Contin. Dyn. Syst.*, 20(1):1–35, 2008.

[19] Aldo Bressan. On control theory and its applications to certain problems for lagrangian systems. on hyper-impulsive motions for these. ii. some purely mathematical considerations for hyper-impulsive motions. applications to lagrangian systems. *Atti Accad. Naz. Lincei Rend. Cl. Sci. Fis. Mat. Natur.*, 8(1):107–118, 1988.

[20] Aldo Bressan. On the application of control theory to certain problems for lagrangian systems, and hyper-impulsive motion for these. i. some general mathematical considerations on controllizable parameters. *Atti Accad. Naz. Lincei Rend. Cl. Sci. Fis. Mat. Natur.*, 8(1):91–105, 1988.

[21] Aldo Bressan. On control theory and its applications to certain problems for lagrangian systems. on hyper-impulsive motions for these. iii. strengthening of the characterizations performed in parts i and ii, for lagrangian systems. an invariance property. *Atti Accad. Naz. Lincei Rend. Cl. Sci. Fis. Mat. Natur.*, 8(3):461–471, 1990.

[22] F. Cardin and M. Favretti. On nonholonomic and vakonomic dynamics of mechanical systems with nonintegrable constraints. *Journal of Geometry and Physics*, 18(4):295–325, 1996.

[23] F. Cardin and M. Favretti. Hyper-impulsive motion on manifolds. *Dynam. Contin. Discrete Impuls. Systems*, 4(1):1–21, 1998.

[24] T. Chambrion and A. Munnier. Generic controllability of 3d swimmers in a perfect fluid. *SIAM J. Control Optim.*, 50(5):2814–2835, 2011.

[25] A. Cherman, J. Delgado, F. Duda, K.Ehlers, J. Koiller, and R. Montgomery. Low reynolds number swimming in two dimensions. *Hamiltonian Systems and Celestial Mechanics (Pátzcuaro, 1998), 32-62*, World Sci. Monogr. Ser. Math.,6 World Sci. Publ., River Edge, NJ, 2000.

[26] S. Childress. *Mechanics of Swimming and Flying*. Cambridge University Press, 1981.

[27] G. Colmbo and Khai T. Nguyen. On the structure of the minimum time function. *SIAM J. Contr. Optim.*, 48(7):4776–4814, 2010.

[28] G. Colombo and Khai T. Nguyen. On the minimum time function around the origin. *Mathermatics od Control and Related Fields*, 3(1):51–82, 2013.

[29] J.M Coron. *Control and Nonlinearity*. American Mathematical Society, 1956.

[30] T Courcier. Tumbling motion yielding fast displacements of synthetic antiferromagnetic nanoparticles for biological applications. *Appl. Phys. Lett.*, 99, 2011.

[31] Dreyfuss R. et al. Microscopic artificial swimmers. *Nature*, 437:862–865, 2005.

[32] A.W. Feinberg. Muscular thin films for building actuators and powering devices. *Science*, 317:1366, 2007.

[33] B. M. Friedrich, I. H. Riedel-Kruse, J. Howard, and F. Jülicher. High-precision tracking of sperm swimming fine structure provides strong test of resistive force theory. *The Journal of Experiment Biology*, 213:1226–1234, 2010.

[34] E. Gauger and H. Stark. Numerical study of a microscopic artificial swimmer. *Phys. Rev. E*, 74:021907, 2006.

[35] A. Gebremedhin, A. Pothen, and A. Walther. Exploiting sparsity in jacobian computation via coloring and automatic differentiation: a case study in a simulated moving bed process. In C. Bischof et al, editor, *Lecture Notes in Computational Science and Engineering 64*, pages 339–349. Springer, 2008. Proceedings of the Fifth International Conference on Automatic Differentiation (AD2008).

[36] L. Giraldi, P. Martinon, and M. Zoppello. Controllability and optimal strokes for n-link microswimmer. *IEEE 52th Conference on Decision and Control*, December 2013.

[37] L. Giraldi, P. Martinon, and M. Zoppello. Optimal design of the three-link purcell swimmer. *Phys. Rev. E*, 91(2), 2015.

[38] J.M. Godhavn, A Balluchi, L.S.Crawford, and S.s. Sastry. Steering of class of nonholonomic systems with drift terms. *Automatica*, 35:837–847, 1999.

[39] J. Gray and J. Hancock. The propulsion of sea-urchin spermatozoa. *Journal of Experimental Biology*, 1955.

[40] E. Gutman and Y. Or. Simple model of a planar undulating microswimmer. *Phys. Rev. E*, 90:013012, 2014.

[41] J. Happel and H. Brenner. *Low Reynolds Number Hydronynamics with special applications to particulate media*. Prentice-Hall Inc., Englewood Cliffs, N.J., 1965.

[42] S. Hirose. *Biologically inspired robots: snake-like locomotors and manipulators*. Oxford University Press, 1993.

[43] J. G. Houot, J. San Martin, and M. Tucksnac. Existence of solutions for the equations modelling the motion of rigid bodies in an ideal fluid. *J. Funct.Anal*, 259(11):2856–2885, 2010.

[44] T. Iwai. The mechanics and control for multi-particle systems. *J.Phys. A: Math*, 31(16):3849–3865, 1998.

[45] T. Iwai. Geometric mechanics of many-body systems. *Journal of Computatiuonal and Applied Mathematics*, 140(1-2):403–422, 2002.

[46] T. Iwai and Akitomo Tachibana. The geometry and mechanics of multi-particle systems. *Ann. Inst. H. Poincaré Phys. Théor.*, 70(5):525–559, 1999.

[47] F. Jing and S. Alben. Optimization of two- and three-link snakelike locomotion. *Phys. Rev. E*, 87, 2013.

[48] J.Lohéac, J. F.Sched, and M. Tucksnak. Controllability and time optimal control for low reynolds number swimmers. *Acta Appl. Math*, 123:175–200, 2013.

[49] V. Jurdjevic. *Geometric control theory*. Cambridge University Press., 1997.

[50] S.D. Kelly and H. Xiong. Self-propulsion of a free hydrofoil with localized discrete vortex shedding. *Theoretical and Computational Fluid Dynamics*, 24(1):45–50, 2010.

[51] A. Y. Khapalov. Local controllability for a swimming model. *SIAM J. Contr. Optim.*, 46:655–682, 2007.

[52] A. Y. Khapalov. Micromotions of a swimmer in the 3-d incompressible fluid governed by the nonstationary stokes equations. *SIAM J. Math. Anal.*, 45(6):3360–3381, 2013.

[53] S. Kim, C. Laschi, and B. Trimmer. Soft robotics: a bioinspired evolution in robotics. *Trends in Biotechnology*, 31:287–294, 2013.

[54] S. Kobayashi and K. Nomizu. *Foundation of differential geometry*. Interscience publishers, 1963.

[55] V.V. Kozlov and D.A. Onishchenko. The motion in a perfect fluid of a body containing a moving point mass. *Journal of Applied Mathematics and Mechanics*, 67(4):553–564, 2003.

[56] V.V. Kozlov and S.M. Ramodanov. The motion of a variable body in an ideal fluid. *Journal of Applied Mathematics and Mechanics*, 65(4):579–587, 2001.

[57] H. Lamb. *Hydrodynamics*. Cambridge University Press, 1916.

[58] T. Levi-Civita and U. Amaldi. *Lezioni di Meccanica Razionale*. Edizioni Compomat, 2013, reprint of the 1923-1927.

[59] A.D. Marchese, C.D. Onal, and D. Rus. Autonomous soft robotic fish capable of escape maneuvers using fluidic elastomer actuators. *Soft Robotics*, 1:75–87, 2014.

[60] C. Marchioro and M. Pulvirenti. *Mathematical Theory of Incompressible Nonviscous Fluids*, volume 96 XII of *Applied Mathematical Sciences*. Springer Verlag, 1994.

[61] C. M. Marle. *Géométrie des systèmes mécaniques à liaisons actives.* Symplectic Geometry and Mathematical Physics, progr. math., 99 edition, 1991.

[62] E. Marsden, J. E. Kanso, J. C. W. Rowley, and B. Melli-Huber. Locomotion of articulated bodies in a perfect fluid. *Journal of Nonlinear Science*, 15(4):255–289, 2005.

[63] J.E. Marsden. *Lectures on Mechanics*. Cambridge University Press, 1992.

[64] R. Mason and J. Burdick. Propulsion and control of deformable bodies in a ideal fluid. *Proceedings of the 1999 IEEE International conference on Robotics and Automation*, 1999.

[65] A. Munnier and T. Chambrion. Locomotion and control of a self-propelled shape-changing body in a fluid. *Nonlinear Science*, 21(3):325–285, 2011.

[66] J.J. Muskhelishvili N.I., Brandstatter. Some basic problems of the mathematicat theory of elasticity. *Appl.Mech.Rev.*, 7(7):293–294, 1953.

[67] Š. Nečasová, T.Takahashi, and M. Tucksnac. Weak solutions for the motion of a self-propelled deformable structure in a viscous incompressible fluid. *Acta Appl. Math*, 116(3):329–352, 2011.

[68] C. Pommerenke. *Boundary behaviour of conformal maps*. Springer Verlag, 1992.

[69] M. Porez, F. Boyer, and A. Ijspeert. Improved lighthill fish swimming model for bio-inspired robots - modelling, computational aspects and experimental comparisons. *Int. Journal Robotics Res.*, 33:1321–1341, 2014.

[70] E. M. Purcell. Life at low reynolds number. *American Journel of Physics*, 45:3–11, 1977.

[71] F. Rampazzo. On the riemannian structure of a lagrangian system and the problem of adding time-dependent constraints as controls. *European J. Mech. A Solids*, 10(4):405–431, 1991.

[72] B. L. Reinhart. Foliated manifolds with bundle-like metrics. *Ann. of Math. (2)*, 69:119–132, 1959.

[73] I. H. Riedel-Kruse, A. Hilfinger, J. Howard, and F. Jülicher. How molecular motors shape the flagellar beat. *HFSP*, 1:192–208, 2007.

[74] M. Roper. Do magnetic micro-swimmers move like eukaryotic cells? *Proc. Roy. Soc. A*, 464:877–904, 2008.

[75] Y. Sawa. Thermally driven giant bending of liquid crystal elastomer films with hybrid alignment. *Macromolecules*, 43:4362–4369, 2010.

[76] A. Shapere and F. Wilczek. Gauge kinematics of deformable bodies. *Am. J. Phys*, 57(514), 1989.

[77] A. Shapere and F. Wilczek. Geometry of self-propulsion at low reynolds number. *J. Fluid Mech*, 198:557–585, 1989.

[78] B.N. Shashikanth, J.E. Marsden, J. Burdick, and S.D.Kelly. The hamiltonian structure of a two-dimensional rigid circular cylinder interacting dynamically with n point vortices. *Physics of fluids*, 14(3):1214–1227, 2002.

[79] H. Sussamnn. Geometry and optimal control. *Springer-Verlag*, 1998.

[80] D. Tam and A. E. Hosoi. Optimal strokes patterns for purcell's three link swimmer. *Physical Review Letters*, 2007.

[81] G. Taylor. Analysis of the swimming of microscopic organisms. *Proc. R. Soc. Lond. A*, 209:447–461, 1951.

[82] E. Trelat. *Contrôle optimal : théorie and applications.* Vuibert, Collection Mathématiques Concrètes, 2005.

[83] A. Wächter and L.T. Biegler. On the implementation of a primal-dual interior point filter line search algorithm for large-scale nonlinear programming. *Mathematical Programming*, 106(1):25–57, 2006.

[84] A. Walther and A. Griewank. Getting started with adol-c. In U. Naumann and O. Schenk, editors, *Combinatorial Scientific Computing.* Chapman-Hall CRC Computational Science, 2012.